


Joint mAster of Mediterranean Initiatives on renewabLe and sustainAble energy

Palestine Polytechnic University

Deanship of Graduate Studies and Scientific Research

Master Program of Renewable Energy and Sustainability

Electrical Characteristics and Efficiency of Organic Solar Cells with (P3HT: ICBA) Active Layer at Ambient

By

Nader Ahmed Khalil Adawi

Supervisors

Prof. Abdel-Karim Daud
Department of Engineering
Palestine Polytechnic University

Dr. Jamal Ghabboun
Physics department
Bethlehem University

Thesis submitted in partial fulfillment of requirements of the degree
Master of Science in Renewable Energy & Sustainability

May, 2019

The undersigned hereby certify that they have read, examined and recommended to the Deanship of Graduate Studies and Scientific Research at Palestine Polytechnic University and the Faculty of Science at Al-Qdus University the approval of a thesis entitled:

Electrical Characteristics and Efficiency of Organic Solar Cells with (P3HT: ICBA) Active Layer at Ambient

Submitted by

Nader Ahmed Khalil Adawi

In partial fulfillment of the requirements for the degree of Master in Renewable Energy & Sustainability.

Graduate Advisory Committee:

Prof. Abdel-Karim Daud
(Supervisor), Palestine Polytechnic University.
Signature:——————————— Date:———————

Dr. Jamal Ghabboun
(Co-supervisor), Bethlehem University.
Signature:——————————— Date:———————

Dr. Husain Al-Samamra
(Internal committee member), Al-Quds University.
Signature:——————————— Date:———————

Dr. Ishaq Musa
(External committee member), Palestine Technical University-Kadoorie.
Signature:——————————— Date:———————

Thesis Approved by:

Name: Dr. Murad Abu Sbeih	Name: Dr.Wadie Sultan
Dean of Graduate Studies & Scientific Research	Dean of Faculty of Graduate Studies
Palestine Polytechnic University	Al-Quds University
Signature:……...……	Signature:……...……
Date:…..……...……	Date:…..……...……..

Electrical Characteristics and Efficiency of Organic Solar Cells with (P3HT: ICBA) Active Layer at Ambient

By **Nader Ahmed Khalil Adawi**

ABSTRACT

Organic solar cells become one of the highly active research fields in Material Science for renewable energy. Organic photovoltaic systems hold the promise for a cost-effective, lightweight solar energy conversion platform, which could benefit from simple processing of the active layer. Using organic materials such as polymers and fullerene derivatives show great potential being electron donors and acceptors. A combination of narrow band donor polymer and one of the fullerene derivatives provide a possible solution for the production of efficient organic solar cells. One of the best organic active layer is the combination of Poly(3-hexylthiophene-2,5-diyl) with 1',1'',4',4''-tetrahydro-di[1,4] methanonaphthaleno [5,6] fullerene-C60 (P3HT:ICBA). High holes mobility in conjunction with good solubility and partial air stability make regio-regular P3HT electron donor, a reference material of choice for both fundamental and applied research in organic solar cells. Polymers fullerene ICBA organic solar cells are effective acceptors because of their high electron affinity and ability to transport charge effectively.

Simulation of molecular properties of the P3HT and ICBA were carried out to confirm appropriateness of HOMO-LUMO levels with the energy levels of other electrodes used in the solar cell to facilitate charge mobility through junctions of the device. A GAUSSIAN software package was used for the purpose of simulation.

Spin coating was used to deposit the P3HT:ICBA layer on a ITO substrate. Aluminuim electrodes were vapor deposited under vacuum, at different stages with a thermal evaporator and a Keithley set-up was used for Current-Voltage (IV) measurements at ambient.

The success of this research is measured by effectively building and test the cells under ambient with the available modest facilities, while the efficiency is better appreciated through using a glove box with inert gas. Samples were prepared with different P3HT:ICBA blend

ratios. While the maximum efficiency known for the best organic cells is 10% the maximum achieved efficiency in this research is 0.89% for 1:1 (P3HT:ICBA) blend ratio. IV curves were made for the cells with illumination 100 mW/cm^2 at 25 ºC. Solar cell parameters were extracted using Matlab to build our organic solar cell. Moreover, the extracted parameters were used for modeling in Matlab and got the IV and Power-Voltage PV curves at different irradiation.

الخصائص الكهربائية وكفاءة الخلايا الشمسية العضوية باستخدام (P3HT:ICBA) كطبقة فعالة في البيئة المحيطة

نادر أحمد خليل عدوي

ملخص

أصبحت الخلايا الشمسية العضوية واحدة من أهم مجالات البحث النشطة في علوم المواد و الطاقة المتجددة. إن الأنظمة الكهروضوئية العضوية تعمل على تحويل الطاقة الشمسية إلى طاقة كهربائية بسعر مناسب و وزن خفيف ، والتي يمكن أن نستفيد منها من خلال عمليات بسيطة للطبقة الفعالة. إن استخدام المواد العضوية مثل البوليمرات ومشتقات الفوليرين يدل على وجود إمكانات كبيرة لكونها من الجهات المانحة للإلكترون والمستقبلات. مزيج من البوليمر و مشتقات الفوليرين ذو فجوة طاقة ضيقة يوفر حلاً ممكن لإنتاج خلايا شمسية عضوية ذات كفاءة جيدة. واحدة من أفضل الطبقات النشطة العضوية هي مزيج من بوليمر(P3HT) والفوليرين(ICBA)-(P3HT: ICBA) ذو الإمكانية العالية لتشكل الثقوب "القطب الموجب" والذوبان في المذيبات العضوية و استقراره في الهواء يجعل من البوليمر"P3HT" مانح جيد ، وهو مادة مرجعية مفضلة في البحوث الأساسية والتطبيقية في الخلايا الشمسية العضوية. وتعتبر الفوليرين "ICBA" من المستجيبات الفعالة بسبب جذبها العالي للالكترونات وقدرتها على نقل الشحنة بشكل فعال.

تم إجراء محاكاة للخصائص الجزيئية لـ P3HT و ICBA لتأكيد ملاءمة مستويات الطاقة HOMO-LUMO مع مستويات الطاقة للأقطاب الأخرى المستخدمة في الخلية الشمسية لتسهيل حركة الالكترونات من خلال الطبقات المختلفة للخلية الشمسية. تم استخدام حزمة برنامج GAUSSIAN لغرض محاكاة مستويات الطاقة للمادة العضوية.

تم استخدام الحركة الدورانية لوضع الطبقة الفعالة P3HT: ICBA على ITO. تم ترسيب الأقطاب الكهربائية من الالمنيوم تحت فراغ في مراحل مختلفة باستخدام مبخر حراري ، وتم استخدام مجموعة Keithley لقياسات الجهد و التيار(IV) في جو المختبر.

يتمثل نجاحنا في هذا البحث من خلال بناء واختبار الخلايا تحت المحيط بفاعلية مع المعدات و الادوات المتاحة ، بينما يتم قياس الكفاءة بشكل أفضل من خلال استخدام صندوق القفازات مع غاز خامل. تم تحضير العينات بنسب مختلفة من (P3HT: ICBA). أفضل كفاءة للخلايا الشمسية العضوية وصلت إلى حوالي 10 ٪ الحد الأقصى للكفاءة الذي حققناه في هذا البحث هو 0.89٪ لنسبة مزيج 1:1 (P3HT: ICBA). تم عمل القياسات الخاصة بالمنحنيات (IV) للخلايا على شدة أشعاع 100 ملي واط / سم^2 عند درجة حرارة 25 درجة مئوية ، ثم تم استخراج المتغيرات الخاصة لخلايانا الشمسية العضوية باستخدام برنامج ماتلاب. علاوة على ذلك ، تم استخدام المتغيرات المستخرجة لعمل نموذج للخلية الشمسية العضوية في برنامج ماتلاب وتم الحصول على منحنيات IV و PV عند اشعاعات مختلفة.

DECLARATION

I declare that the Master Thesis entitled **"Electrical Characteristics and Efficiency of Organic Solar Cells with (P3HT: ICBA) Active Layer at Ambient"** is my own original work, and herby certify that unless stated, all work contained within this thesis is my own independent research and has not been submitted for the award of any other degree at any institution, except where due acknowledgement is made in the text.

Nader Ahmed Khalil Adawi

Signature:———————————— Date:————————————

STATEMENT OF PERMISSION TO USE

In presenting this thesis in partial fulfillment of the requirements for the joint Master's degree in Renewable Energy & Sustainability at Palestine Polytechnic University and Al-Quds University, I agree that the library shall make it available to borrowers under rules of the library.

Brief quotations from this thesis are allowable without special permission, provided that accurate acknowledgement of the source is made.

Permission for extensive quotation from, reproduction, or publication of this thesis may be granted by my main supervisors, or in his absence, by the Dean of Graduate Studies and Scientific Research when, in the opinion of either, the proposed use of the material is for scholarly purposes.

Any coping or use of the material in this thesis for financial gain shall not be allowed without my written permission.

Student Name: Nader Ahmed Khalil Adawi

Signature:_____ Date:_____

DEDICATION

To my family, especially, to my father, to my mother, the reason of what I become and reached today.

To my brothers.

To my sister.

To my sweetie.

Thank you for your support

ACKNOWLEDGEMENT

First I wish to express my gratitude to the Almighty Allah for providing the grant to make this thesis possible.

I would like to thank **JAMILA Project-544339-TEMPUS-1-2013-1-IT-TEMPUS-JPCR** funded by the European Union which was administrated by Sapienza University of Rome and partner Universities for their support in launching this program, provided infrastructure and opportunities for scientific visits.

I express my gratitude and appreciations to project coordinator Prof. Sameer Hanna and to my supervisor Prof. Abdel-Karim Daud who helped and support me through all stages of my studies.

Special thanks are extended to my co-supervisor Dr. Jamal Ghabboun who introduced me to the topic and for helping me through all stages of my Master Thesis and for giving me the chance to use all available equipment and materials in the Physics laboratory at Bethlehem University.

I wish to express my thanks to employees at the Physics and Chemistry Laboratories at Bethlehem University Mr. Ahmad Atiyah and Tanas Khoury. Many thanks go to Mrs. Maryam Faroun from the Nanolab Research Laboratory at Al-Quds University who assisted me in using chemicals and equipment.

Special thanks go to Dr. Ishaq Musa and Dr. Hussien Shanak from Palestine Technical University for their advices and for providing us with the P3HT material. I like also to thank Dr. Abdallah AlSaid and Prof. Edward Sader from the Physics department at BirZeit University for providing us with Al filament for thermal evaporation.

Finally, I am so grateful to my family and friends, who stood beside me and encouraged me constantly.

Table of Content

List of Tables

List of Figures

List of Abbreviations and Symbols

AC	Alternating Current
AM	Air Mass
A-Si	Amorphous Silicon Solar Cell
BHJ	Bulk Heterojunction
BIPV	Building-Integrated Photovoltaics
C	Carbon
CdTe	Cadmium Telluride
CH_4	Methane
CIGS	Copper Indium Gallium Selenide
CZTS	Copper Zinc Tin Sulphide
DC	Direct Current
DFT	Density Functional Theory
DSC	Dye Sensitized Cell
DSSC	Dye Sensitized Solar Cell
e	The elementary charge
E	Energy
EA	Electron Affinity
E_g	Band-gap Energy
E_v	The potential energy
eV	Electron-Volts
FF	Fill Factor
GaAs	Gallium Arsenide
GaInP	Gallium Indium Phosphorous
$\hat{H}$	The Hamiltonian operator
ħ	The reduced Planck constant
HF	Hartree Fock
HOMO	Highest Occupied Molecular Orbital
I	Current
I_0	Intensity of incident light
I_v	Intensity of transmitted light

I_D	Diode current
I_L	The generated current during illumination
I_{mpp}	The current at the maximum power point
IP	Ionization Potential
IPCE	Incident Photon to Current Efficiency
I_{ph}	Irradiation current or photo generated current
IR	Infra-Red light
I_r	Irradiance (light intensity)
I_s	Saturation current of the diode
I_{SC}	Short Circuit Current
I_{sh}	Leakage current in shunt resistance
ITO	Indium Tin Oxide
IV	Current-Voltage
J	Joule
J_{SC}	Short Circuit Current density
K	Kelvin
LCAO	Linear Combinations of the single-Atom Orbitals
LUMO	Lowest Unoccupied Molecular Orbital
M	The electron mass
MJ	Multi-junction
N	Diode ideality factor
Nm	Nanometers
NRL	Nanotechnology Research Laboratory
OPV	Organic Photovoltaic
OSC	Organic solar cell
PCE	Power Conversion Efficiency
PM3	Parametric Method Number 3
P_{mpp}	The power at the maximum power point
PV	Photovoltaic
QE	Quantum Efficiency
Rpm	Revolutions per minute
R_s	Series Resistance.
R_{sh}	Shunt Resistance

Si	Silicon
SMU	Source Measure Units
SQ	Shockley-Queisser limit
T	Temperature
T_A	Absorber temperature “Hot temperature”
T_C	Cold temperature
T_S	Sun temperature
Tg	Glass transition temperature
UV	Ultra-Violet light
V	Voltage
Vis	Visible light
V_{mpp}	The voltage at the maximum power point
V_{OC}	Open Circuit Voltage
V_t	Thermal voltage
VTE	Vacuum Thermal Evaporation
W	Watt
X	Gaseous State
π	Pi Bond
π-system	Conjugated Systems
σ	Sigma Bond
Ψ	Probability Distribution
d	Thickness of the medium
α	Constant which depends upon wavelength and absorbing medium
∇	The Laplacian operator
°C	Celsius
η	Efficiency
η_{SC}	Total efficiency of ideal solar cell

Chapter 1

Introduction

The huge demand of energy is a fact .Human cannot live nowadays without it. Fossil fuels are the major energy source that are being used in the world today. However, the over-consumption can lead to serious environmental issues such as air pollution and global warming through greenhouse effects. Fossil fuels release carbon dioxide, nitrogen dioxide, sulfur dioxide, carbon monoxide and other gases, their sources are limited and they are depleting at a faster rate and will not available in the future. So we need to use energy sources that have no effect on the environment and be sustainable that towered us to renewable energy like sun , wind , geothermal ,hydroelectric, biomass and other renewable sources.

The amount of energy that the Earth receives from the sun is enormous: 1.75×10^{17} W per day (1.51×10^{22} J per day). As the world energy consumption in 2003 amounted to 4.4×10^{20} J per year, Earth receives enough energy to fulfill the yearly world demand of energy in less than an hour. Not all of that energy reaches the Earth's surface due to absorption and scattering, however, the photovoltaic conversion of solar energy remains an important challenge. The inorganic solar cells have a record power conversion efficiency of close to 39% [1], while commercially available solar panels have a significantly lower efficiency of around 15–20%. Another approach to making solar cells is to use organic materials, such as conjugated polymers. Solar cells based on thin polymer films are particularly attractive because of their ease of processing, mechanical flexibility, and potential for low cost fabrication of large areas. Additionally, their material properties can be tailored by modifying their chemical makeup, resulting in greater customization than traditional solar cells allow. Although significant progress has been made, the efficiency of converting solar energy into electrical power obtained with organic solar cells still does not warrant commercialization [2]. The most efficient devices have an efficiency of 5-11%. To improve the efficiency of organic solar cells it is, therefore, crucial to understand the limits their performance.

1.1 Photovoltaic

It's the direct conversion of light into electrical energy (voltage and electrical current) by means of solar cells. The conversion process is based on the photoelectric effect discovered by Alexander Bequerel in 1839. The photoelectric effect describes the release of positive and negative charge carriers in a solid state when light strikes its surface [3].

A solar cell is a device that converts light into electricity. They are also commonly called 'photovoltaic cells' after photovoltaic effect, and also to differentiate them from solar thermal devices. The photovoltaic effect is a process that occurs in some semiconducting materials. At the most basic level, the semiconductor absorbs a photon, exciting an electron which can then be extracted into an electrical circuit by built-in and applied electric voltage and current.

Quantum theory describes the differences between conductors (metals) and semiconductors using energy-band diagrams such as those shown in figure 1.1. Electrons have energies that must fit within certain allowable energy bands. The top energy band is called the conduction band, and the electrons within this region which contribute to current flow. The conduction band for metals is partially filled, , which allows them to carry electric current easily, but for semiconductors at absolute zero temperature, the conduction band is empty, which makes them insulators [4].

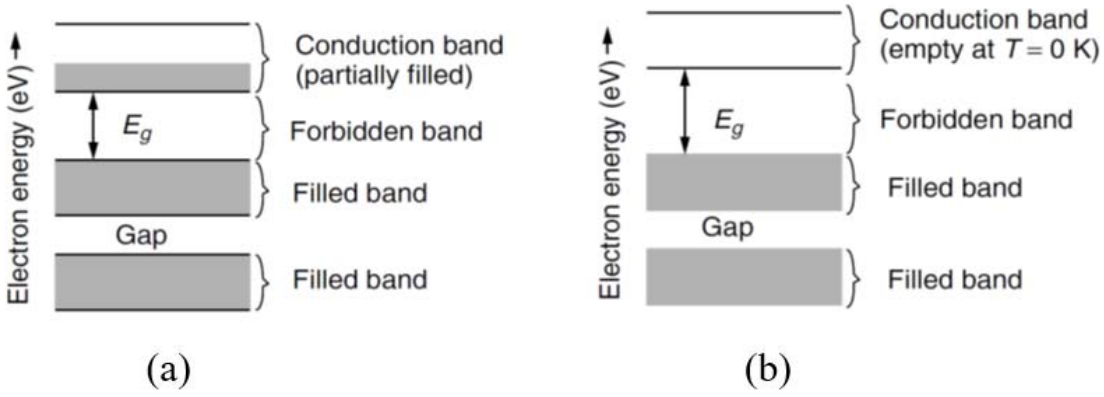

Figure 1.1: Energy bands for (a) metals and (b) semiconductor [4]

The gaps between allowable energy bands are called forbidden bands, the most important of which is the gap separating the conduction band from the highest filled band below it. The energy that an electron must acquire to jump across the forbidden band to the conduction band is called the band-gap energy, designated E_g. The units for band-gap energy are usually electron-volts (eV), where one electron-volt is the energy that an electron acquires when its voltage is increased by 1 V ($1\ eV = 1.6 \times 10^{-19}$ J).

One of the most famous semiconductors materials is silicon. It is in the fourth column of the periodic table, which is referred to as Group IV as shown in figure 1.2. Germanium is another Group IV element, and is used as well as a semiconductor in some electronics [4].

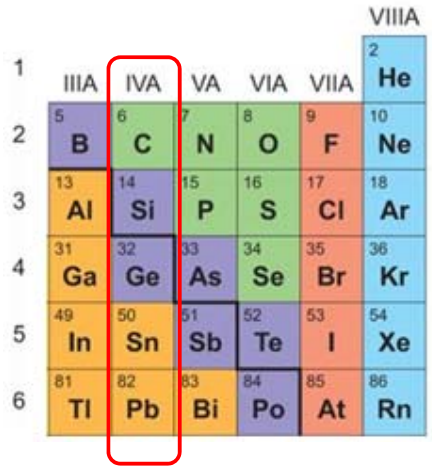

Figure 1.2: Part of periodic table

Silicon has 14 protons in its nucleus, and so it has 14 orbital electrons as well. As shown in figure 1.3, its outer orbit contains four valence electrons, it is tetravalent. Those valence electrons are the only ones that matter in electronics, so it is common to draw silicon as if it has a +4 charge on its nucleus and four tightly held valence electrons.

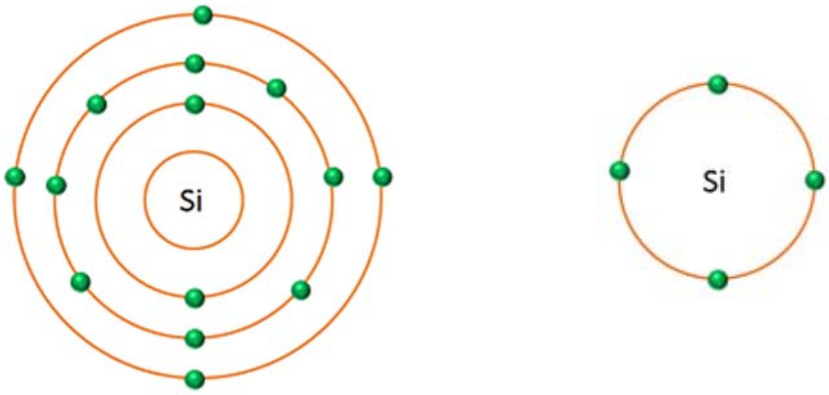

Figure 1.3: Silicon atom

The band-gap E_g for silicon is 1.12 eV, which means an electron needs to acquire that much energy to free itself from the electrostatic force that ties it to its own nucleus to jump into the conduction band.

1.2 Solar Cells Classification

The solar cells is devices based on the photovoltaic phenomena, These cells classify into three main groups:

A. **Silicon** solar cells is the solar cells based on silicon, this type is available commercially.
B. **Semiconductor compounds** solar cells, it is made from a compound of two materials usually group number three and group number five from periodic table (III-V), this type is available in laboratory.
C. **Emerging (Novel Materials)** solar cells, it is made from new materials like organic materials.

Figure 1.4 shows the classification of the solar cells and table 1.1 shows the efficiencies for each type and the commercial availability [5].

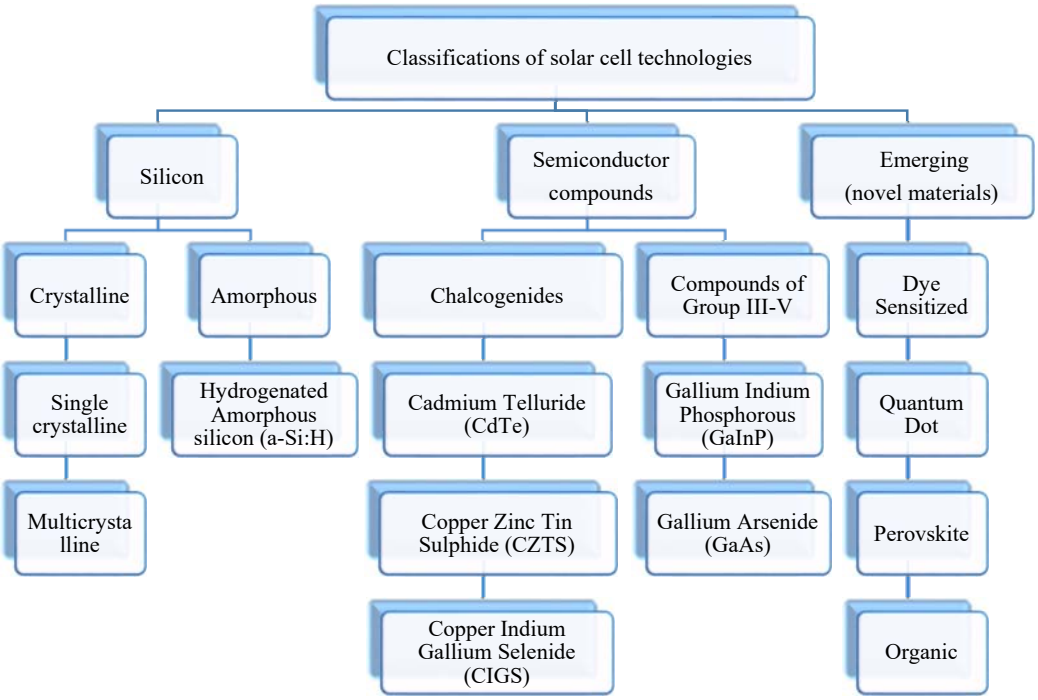

Figure 1.4: The classification of solar cells [5]

Table 1.1: Solar cells efficiencies [5, 6].

Type	Class	Commercial η %	Lab η %
Mono crystalline	**Silicon**	**21.5**	**26.7**
Multi crystalline	**Silicon**	**12.0**	**22.3**
Amorphous Silicon	**Silicon**	**-**	**10.2**
Cadmium Telluride	**Compound**	**17.0**	**21.0**
Copper Zinc Tin Sulphide	**Compound**	**-**	**10.0**
Copper Indium Gallium Selenide	**Compound**	**-**	**21.7**
Gallium Indium Phosphorous	**Compound**	**-**	**21.4**
Gallium Arsenide	**Compound**	**-**	**25.1**
Multijunctions	**compound**	**-**	**38.8**
Dye Sensitized	**Emerging**	**-**	**11.9**
Quantum Dot	**Emerging**	**-**	**8.0**
Perovskite	**Emerging**	**-**	**20.9**
Organic	**Emerging**	**-**	**11.2**

1.3 Organic Solar Cell

Organic solar cell or organic photovoltaic (OSC or OPV) is a photovoltaic device like other solar cells. The material used to absorb the solar light in organic solar cells, is an organic material such as a conjugated polymer. The basic principle behind both the organic solar cell and other forms of solar cells is the same which is based on the transformation of the energy in the form of electromagnetic radiation (light) into electrical energy (a current and a voltage). This energy conversion is possible with the use of semiconductors. The fact that polymers can behave as semiconductors is a discovery which Alan J. Heeger, Alan MacDiarmid and Hideki Shirakawa received the Nobel Prize in Chemistry for in the year 2000 [7]. This discovery of conjugated polymers being able to transfer electrons upon doping with iodine made it possible to prepare solar cells from polymers and thereby a new research area was born. Organic solar cells have for a long time lagged behind traditional solar cells on both performance and stability. However, they have always had a potential advantage; that is their ability to be produced from solution. This means that they can be printed or coated, instead of using expensive vacuum deposition as for the first generation silicon solar cells.

Today, performances of 11.2% have been demonstrated for organic solar cells. [6] .In addition, large scale production of polymer solar cells is today to some extent a reality, as demonstrated by for example the free OPV initiative [8].figure 1.5 show free OPV.

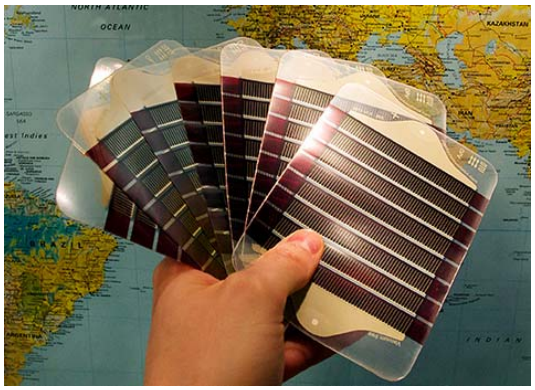

Figure 1.5: Free OPV

Organic solar cell is a type of flexible solar cell (also called "plastic solar cells"). Organic solar cells are lightweight (which is important for small autonomous sensors), potentially disposable and inexpensive to fabricate (sometimes using printed electronics), flexible, customizable on the molecular level and potentially have less adverse environmental impact. Organic solar cells also have the potential to exhibit transparency, suggesting applications in windows, walls.

1.4 Research Statement

Organic solar cell have many advantages over inorganic solar cell, but until now organic solar cell are not used in a commercial way because of efficiency which is still low if compared to the commercially known inorganic solar cell.

My approach to reach objectives of this research will focus on the followings:

1- Simulation of HOMO-LUMO energies of P3HT (Poly(3-hexylthiophene-2,5-diyl) and ICBA (1',1'',4',4''-tetrahydro-di[1,4] methanonaphthaleno fullerene-C60) where the combination of this polymer/molecule will be used as active layer responsible to produce electron-hole pair resulting in a current upon exposure to light.
2- Building the solar organic device with thermally evaporated Alumimuim electrodes
3- Testing and building a model for the constructed solar cells.
4- Achieve a stable efficiency for organic solar cell at ambient

Chapter 2

Basic Concept in Organic Solar Cells

2.1 Organic Solar Cell - Organic Photovoltaic (OPV)

Organic solar cell is one type of solar cells based on photovoltaic phenomena (direct conversion of light to electrical energy). The semiconductor in these cells is the organic semiconductor and this is the naming reason.

Organic electronics have significant potential where organic semiconductor materials can be deposited on flexible substrates using low-cost processing techniques, such as roll-to-roll solution printing or vacuum deposition [9, 10]. Moreover, manufacturing technology for flexible electronics is already established in the OLED industry where the fundamental issues, including molecular design, thin-film deposition or device encapsulation, have already been confronted [11]. This development could boost fabrication of organic photovoltaic in the laboratory and in industrial environment.

The organic solar cell have many advantages over inorganic solar cell, but until now organic solar cell are not used in a commercial way because the efficiency is still low comparing with the inorganic solar cell. As shown in table 2.1.

Table 2.1: Organic cells VS Inorganic cells [12]

	Organic Cells	Inorganic Cells
Production	Cheap by high-throughput roll-to-roll printing	Expensive
Environmental impact during manufacturing	Low	High
Materials per m^2	A few grams	Huge amount
Color	Color and (semi-)transparency	Blue or black
Toxicity	Non-toxicity	Toxicity
Efficiency	5% - 10 %	15% - 20 %
Using	Not commercially	Commercially
Temperature coefficient	Positive	Negative
Low-light performance	Good	Not good
Weight	Low weight	Heavy weight
Flexibility	Flexible	Not flexible
Application	Easy integration	Difficult integration

To use the organic solar cells commercially, efficiency should be achieved with more than 10% (PCE>10%). At this efficiency production of organic cells will be useful and compete with the inorganic cells.

2.1.1 History of OPV

Organic solar cell research has developed during the last three decades, especially in the last decade it has attracted scientific and economic interest triggered by a rapid increase in power conversion efficiencies. This was achieved by the introduction of new materials, improved materials engineering, and more sophisticated device structures. Table 2.2 gives a history for the events that lead to invention of solar cells [13].

Table 2.2: A brief history for OPV.

1839	• Becquerel observed the photoelectrochemical process.
1906	• Pochettino studied the photoconductivity of anthracene.
1958	• Kearns and Calvin worked with magnesium phthalocyanines (MgPh), measuring a photovoltage of 200 mV.
1964	• Delacote observed a rectifying effect when magnesium phthalocyanines (CuPh) was placed between two different metalelectrodes.
1986	• Tang published the first heterojunction PV device.
1991	• Hiramoto made the first dye/dye bulk heterojunction PV by co-sublimation.
1993	• Sariciftci made the first polymer/C60 heterojunction device.
1994	• Yu made the first bulk polymer/C60 heterojunction PV.
1995	• Yu / Hall made the first bulk polymer/polymer heterojunction PV.
2000	• Peters / van Hal used oligomer-C60 dyads/triads as the active material in PV cells.
2001	• Schmidt-Mende made a self-organised liquid crystalline solar cell of hexabenzocoronene and perylene.
2001	• Ramos used double-cable polymers in PV cells.
2006	• First time in Solar Cell Efficiency Tables (Version 28) with 3% efficiency
2017	• The last Solar Cell Efficiency Tables (Version 50) maximum efficiency 11%

Today, solar power conversion efficiencies in excess of 11% have been accomplished in laboratory. Though efficiencies of these organic solar cells have not yet reached those of their inorganic counterparts (the commercially efficiency 16% and the research's efficiency with more than 22%); the perspective of cheap production drives the development of organic photovoltaic devices further in a dynamic way.

After these achievements, the amount of publications rose nearly exponentially in the last decade [14, 15], also pushed by several spin-offs and established companies turning focus on this topic. The reason for this boom is found in the expected high potential of organic semiconductors. Figure 2.1 show (a) Number of research about organic solar cells in the

database, and in (b) Development of the maximum power-conversion efficiency for organic solar cells on the laboratory scale during the last decade.

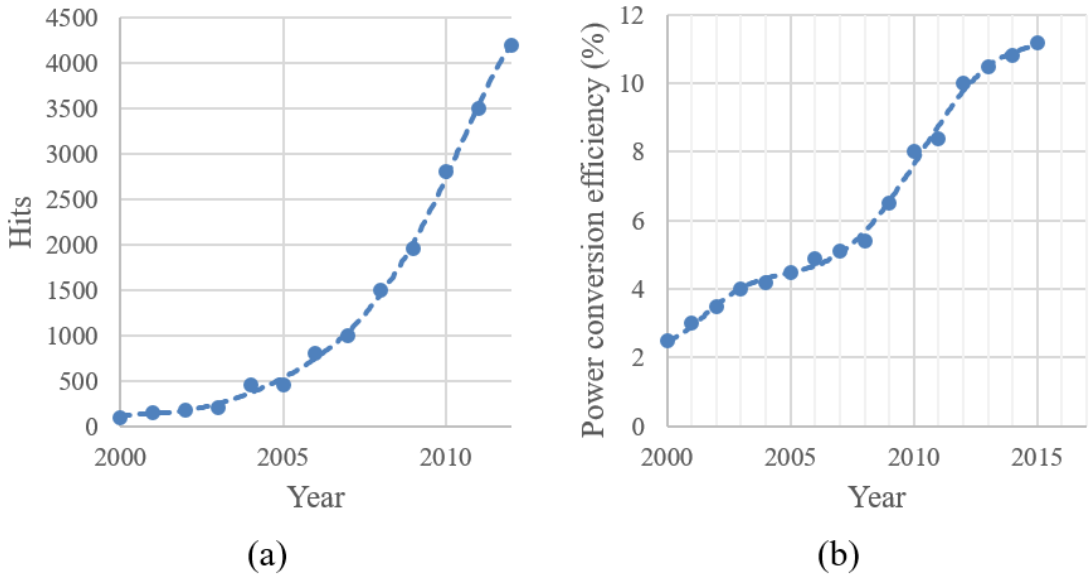

Figure 2.1: (a) Hits of a search in the database. (b) Development of the efficiency of OSC

The first time, the organic solar cell enters the "Solar Cell Efficiency Tables" was in 2006 (Version number 28) and the efficiency was 3.0%±0.01. Whereas the last publication for "Solar Cell Efficiency Tables (Version number 50)" was in 30-may-2017 with a recorded efficiency of 11.2%±0.3.

2.1.2 Types of OPV

The organic solar cells can be classified based on the active layer to three types:

A. Single Layer OPV

Single layer OPV cells are the simplest of the OPVs. They are made by one layer of organic semiconductor between two metallic conductors. A typical layer of indium tin oxide (ITO) with high work function and a metal layer of low work function such as Al, Mg or Ca, is shown in the figure 2.2.

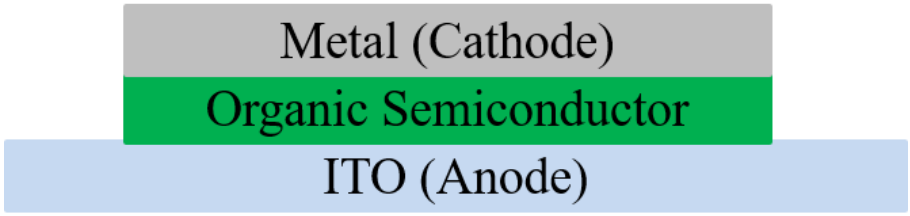

Figure 2.2: Single layer OPV

The difference of the work functions between the two conductors sets up an electric field in the organic layer. When it absorbs light, electrons will be excited to the LUMO and leave holes in the HOMO forming excitons. The potential created by the different work functions of conductors helps to separate the exciton pairs, pulling electrons to the positive electrode and holes to the negative electrode. But they have problems [16]:

1. Low power conversion efficiencies (<0.1%).

2. The field between the two electrodes is seldom sufficient to break up the excitons. The electrons recombine with the holes before reaching the electrodes.

B. Bi-layer OPV

This type is built from two layers of organic semiconductor, the first one is donor and the second is acceptor formed between two electrodes. The ITO is the anode and the metal is the cathode as shown in figure 2.3, the donor and acceptor are small molecules. This structure is also called a planar donor-acceptor hetero-junction.

The ionization energy of an atom or molecule describes the amount of energy required to remove an electron from the atom or molecule in the gaseous state. X + energy → X+ + e-. The different affinities between the two layers generate a potential that can break up the excitons. As well known that exciton dissociation is efficient at the interface between materials with different electron affinity EA and ionization potential IP. The layer with higher electron affinity and ionization potential is called the acceptor, and the other layer is called the donor

in other word EA and IP of the electron acceptor should be higher than those of the donor. This structure is also called a planar donor-acceptor heterojunction. [17].

The main problem with this type is that the diffusion length of the excitons in the organic materials (order of 10 nm) is small compared to the practical thickness to absorb enough photons for power conversion (100 nm). At such a large thickness, only a small fraction of the excitons can reach the heterojunction interface.

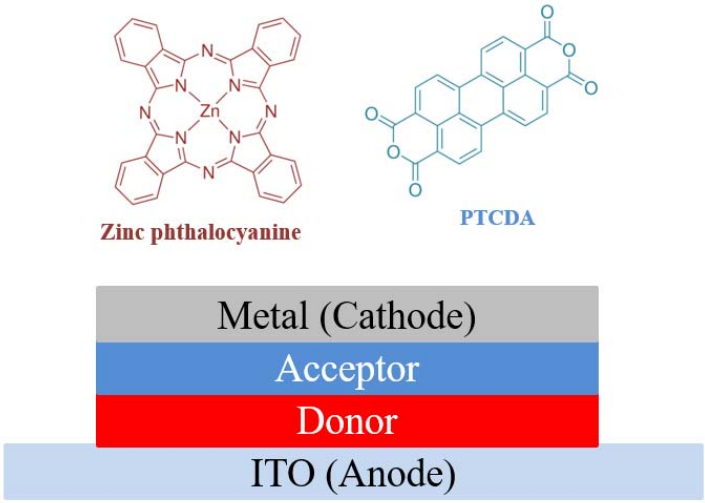

Figure 2.3: Bi-layer OPV [18]

C. Bulk Heterojunction (BHJ) OPV

These cells are similar to the bi-layer cells but the donor and the acceptor layers are mixed to form a blend layer sandwiched between the electrodes as shown in figure 2.4. This form was invented in the 1990s. The junction is formed by mixing donor and acceptor materials in a solution then forming the active layer by spin coating of the mixture on the substrate. The resulting film represents a nanoscale network of donors and acceptors. The phase separation within the film is about 10-20 nm which is comparable to the exciton diffusion length [18].

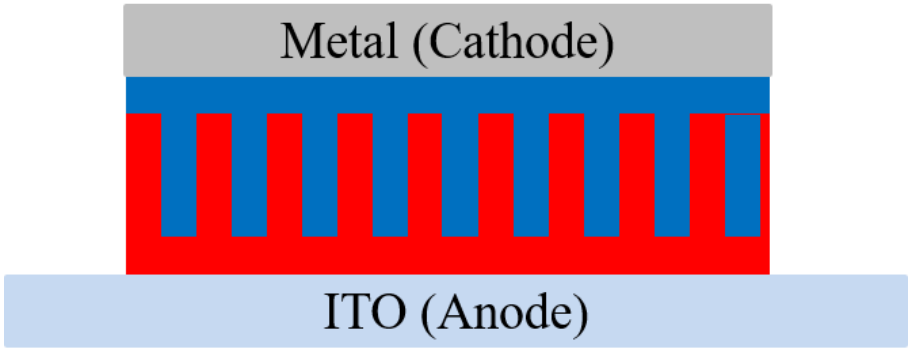

Figure 2.4: Ideal structure of BHJ cells [19]

The bulk heterojunction can be divided into three types:

I. Polymer-Polymer, in this type both the donor and acceptor are polymers, figure 2.5 shows the layers.

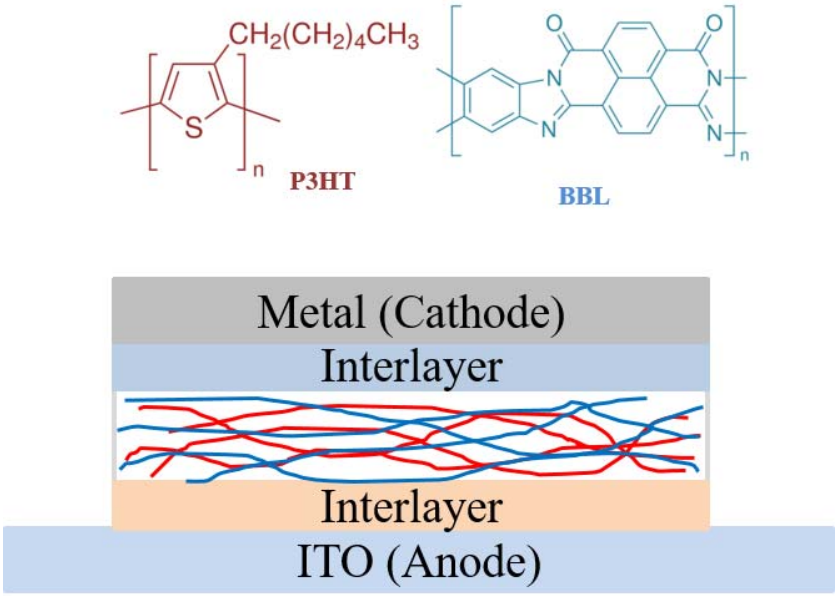

Figure 2.5: BHJ OPV (donor polymer – acceptor polymer) [20]

II. Polymer-Molecule, the maximum efficiency of organic solar cell is obtained from this type of OPV. (The acceptor molecule has is the fullerene). As shown in figure 2.6.

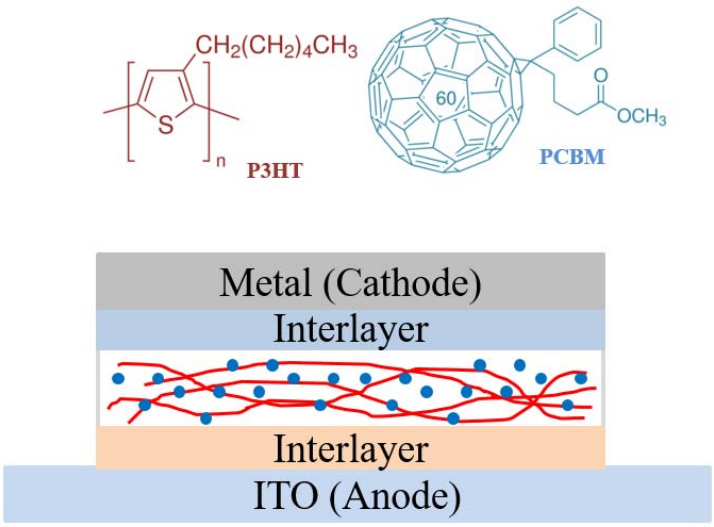

Figure 2.6: BHJ OPV (donor polymer – acceptor small molecule) [20]

III. Co-Polymer, it is a polymer derived from more than one species of monomer. Block copolymer-based devices demonstrate efficient photo conversion well beyond devices composed of homo polymer blends. 3% efficiencies were achieved without the use of a fullerene acceptor. Conjugated block copolymers thus may enhance performance through control of donor–acceptor interfaces [21]. As shown in figure 2.7.

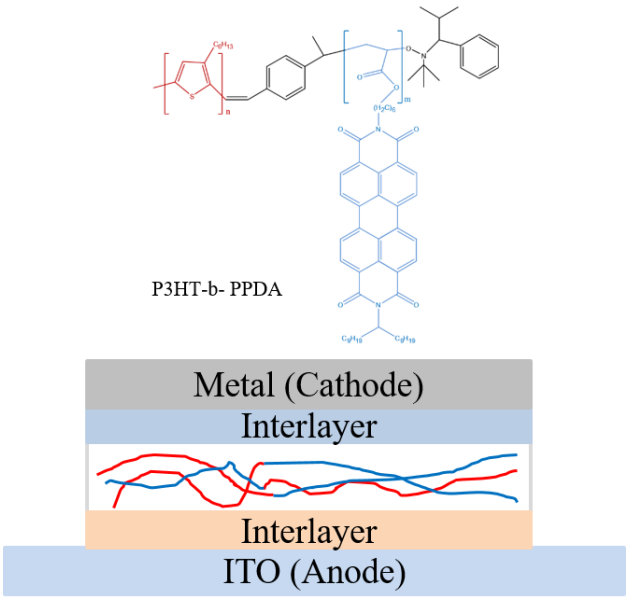

Figure 2.7: BHJ OPV (Block Co-polymer)

Table 2.3: Organic cells VS Inorganic cells **[6, 20, 22-25].**

Type		Donor	Acceptor	Efficiency	Invention
Single Layer		One layer		<0.1%	1964
Bi-layer (Heterojunction)		Molecule or Polymer	Molecule or Polymer	≈5%	1986
Bulk Heterojunction	Polymer-Polymer	Polymer	Polymer	≈6%	1995
	Polymer-Fullerene	Polymer	Molecule	≈11%	1990
	Co-polymer	Co-polymer		≈3%	2006

2.2 Basic Working Principles

The process of converting light into electric current in an organic photovoltaic cell is accomplished by four consecutive steps, as shown in figure 2.8:

1. Absorption of a photon leading to the formation of an excited state, the electron-hole pair (exciton).

2. Exciton diffusion to a region at the same level.

3. The charge separation occurs in opposite directions.

4. Finally the charge transport to the anode (holes) and cathode (electrons), to supply a direct current for the consumer load [18].

The potential energy stored within one pair of separated positive and negative charges is equivalent to the difference in their respective quasi-Fermi levels, or in other words it corresponds to the difference in the electrochemical potentials [26]. The larger the quasi-Fermi level splitting remains during charge transport through the interfaces at the contacts, the larger will be the voltage.

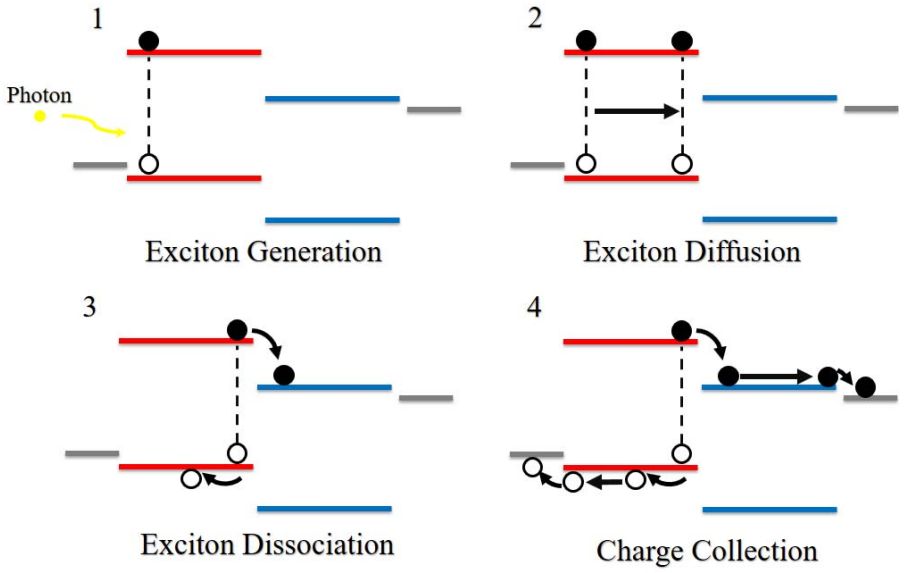

Figure 2.8: OPV Basic Working Principles [18]

2.3 Materials of OPV

The materials used in OPV cells are classified as organic semiconductors due to their capability to absorb light and conduct electricity either within molecules or conjugated polymers. Figure 2.9 shows some donor while figure 2.10 show some acceptor ones.

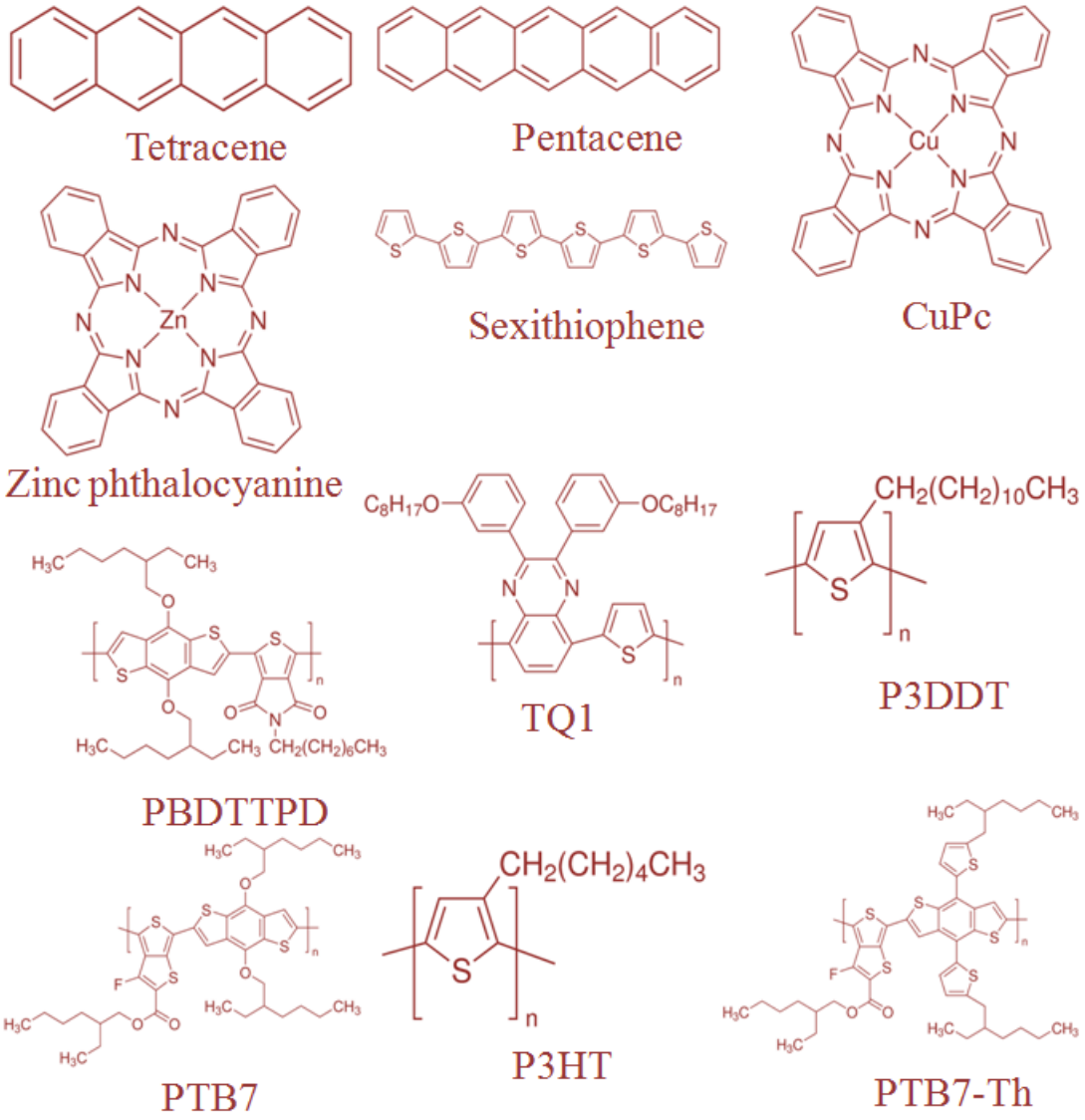

Figure 2.9: Organic semiconductores used as donor [20, 27]

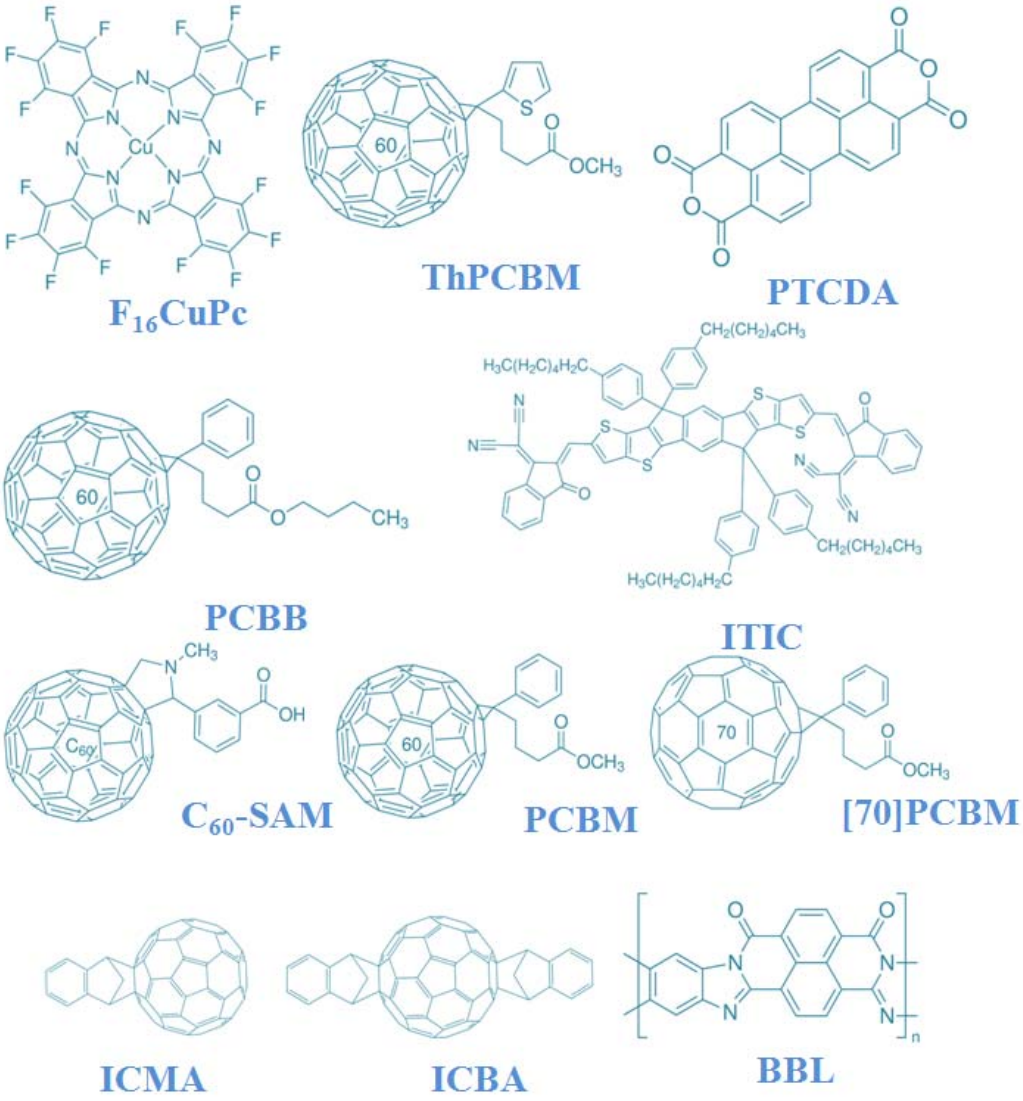

Figure 2.10: Organic semiconductores used as acceptor [20, 27]

2.4 Solar Cell Characterizations

The solar cell in the dark acts as a simple diode, and the equivalent electric circuit that approximates it is shown in figure 2.11 which comprises:

1. A diode with I_D current (current in the dark reverse bias).
2. A current source that corresponds to photocurrent I_L generated during illumination.
3. R_s series resistance.
4. R_{sh} shunt resistance with I_{sh} leakage current through resistance as a result of defects in the films.

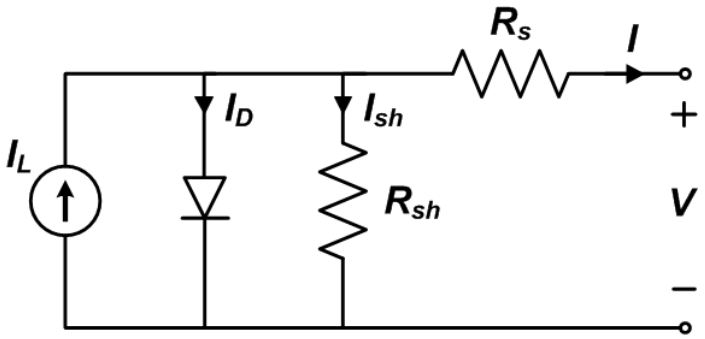

Figure 2.11: Equivalent circuit for OPV [28]

For good performance, R_s should be low and R_{sh} high. When light shines the cell the current-voltage (IV) curve becomes a superposition of the dark IV with the light generated current, and the curve is shifted down to the fourth quadrant, as shown in figure 2.12 [29].

The low performance of organic cells is attributed to the following two factors:

1. Inefficient photo-induced charge generation due to low exciton diffusion length compared to the optical absorption length.
2. Poor collection efficiency due to low carrier mobilities ($10^{-3}cm^2/Vs$). However, carrier mobilities approaching those of amorphous silicon have been achieved in certain organic semiconductors. The progress in this field will depend on materials improvements and innovative engineering.

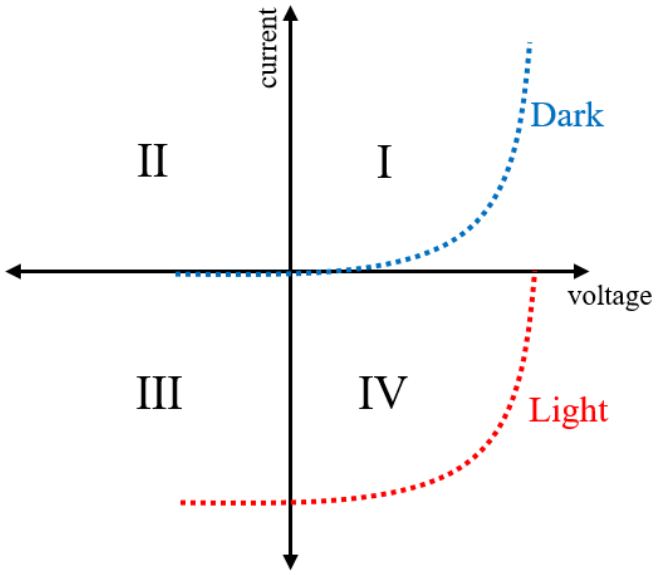

Figure 2.12: Dark and light IV curves for an OPV

To understand the dark and light IV curve of the organic cell, we need to familiarize with some parameters related to the electrical characteristics of the cell, Short Circuit Current (I_{SC}), Short Circuit Current density (J_{SC}), Open Circuit Voltage (V_{OC}), Fill Factor (FF) and efficiency (η). As shown in figure 2.14.

Short Circuit Current (I_{SC} or J_{SC})

It is the current through the cell when the voltage across it is zero (short circuited V = 0). The short-circuit current is due to the generation and collection of light-generated carriers. For an ideal solar cell, the I_{SC} and the light-generated current should be identical, the I_{SC} is the largest current that can be drawn from the cell. I_{SC} depends on the following factors:

1. The active material area to normalize, one can use current density (J_{SC} in mA/cm^2).
2. Light or photons intensity. J_{SC} is directly proportional to the light intensity.
3. The spectrum of the incident light: and the active cell excitation region
4. The optical properties (absorption and reflection).
5. The collection probability which depends on the surface passivity and the minority carrier lifetime in the base.

Open Circuit Voltage (V_{OC})

It is the electrical potential difference between the two terminals when there is no external load current flow between the terminals (when $I_{external}$ =0). The voltage is given the symbol V_{OC}. The V_{OC} of solar cells are often measured under particular conditions (illumination, temperature, etc.). V_{OC} can be increased as shown in figure 2.13 through increasing the polymer ionization potential; the band gap and decreasing the driving force for hole transfer and decreasing the driving force for the electron transfer.

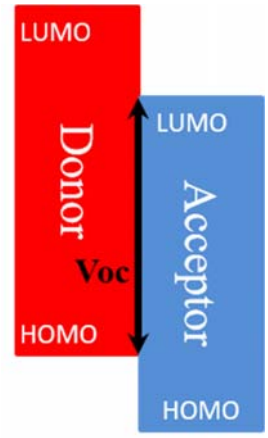

Figure 2.13: Open circuit voltage V_{OC} for OPV [30]

The open circuit voltage of a conjugated polymer:PCBM solar cell can be estimated by [31]:

$$V_{oc} = \frac{1}{e}\left(|E_{Donor}HOMO| - |E_{Acceptor}LUMO|\right) - 0.3 \qquad (2.1)$$

Where

e: The elementary charge and using –4.3 eV for the PCBM (LUMO) energy.

0.3: Is an empirical factor.

Illuminated Current (I_L)

It is the light generated current inside the cell. At short circuit conditions the externally measured current I_{SC} and is equal to I_L and can be used interchangeably. However for high series resistance (> 10 Ωcm^2) I_{SC} becomes less than I_L and using it in the cell equation is incorrect.

Fill Factor (FF)

It is a parameter that determines the maximum power from a cell in conjunction with V_{OC} and I_{SC}. It is defined as the ratio of the maximum power from the cell over the product of V_{OC} and I_{SC}. Graphically, the FF is a measure of the "squareness" of the cell and it is represented as the area of the largest rectangle that fit in the IV curve. The FF values for OPV are reached 65-75% [32]. Figure 2.24 illustrates the concept.

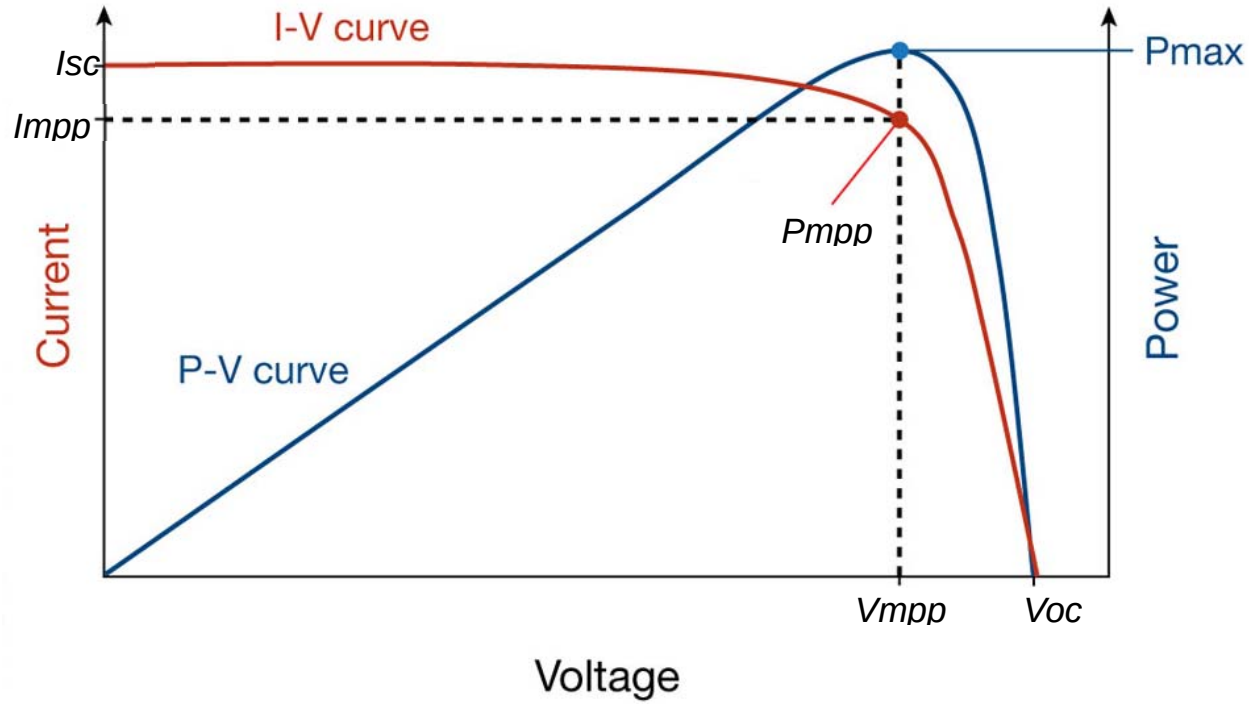

Figure 2.14: IV curve and maximum power point [33]

The overall power conversion efficiency PCE (η) is calculated according to the following equations:

$$\eta = \frac{P_{out}}{P_{in}} = \frac{FF(V_{oc}I_{sc})}{P_{in}} \quad (2.2)$$

$$FF = \frac{V_{mpp}I_{mpp}}{V_{oc}I_{sc}} \quad (2.3)$$

Where

η: Efficiency.

P_{out}: The maximum output electrical power of the device under illumination.

P_{in}: The light intensity incident on the device.

FF: The available power at the maximum power point.

V_{oc}: Open circuit voltage.

I_{sc}: Short circuit current.

V_{mpp}: The voltage at the maximum power point.

I_{mpp} : The current at the maximum power point.

Organic solar cells based on polymer: fullerene bulk hetero junctions, the magnitude of I_{SC}, V_{OC}, and FF depends on parameters such as:

1- Light intensity [34].
2- Temperature [35, 36].
3- Composition of the components [37].
4- Thickness of the active layer [38].

5- The choice of electrodes used [39, 40].
6- The solid state morphology of the film [41].
7- Dimensions, internal construction and active area.
8- Material properties (optical, electrical and energy levels).
9- Anti-reflective coating, and surface texture.

Efficiency (η)

Efficiency is the most commonly used parameter to compare the performance of cells. It is defined as the ratio of energy output from the cell to the input energy from the sun.

In addition to reflecting the performance of the cell itself, the efficiency depends on the spectrum and intensity of the incident sunlight and the temperature of the cell. Therefore, conditions under which efficiency is measured must be carefully controlled in order to when comparing different cells.

Two solar cells have the same V_{OC} and I_{SC} but different efficiency. The one which has a higher FF will have higher efficiency [42], as shown in figure 2.15.

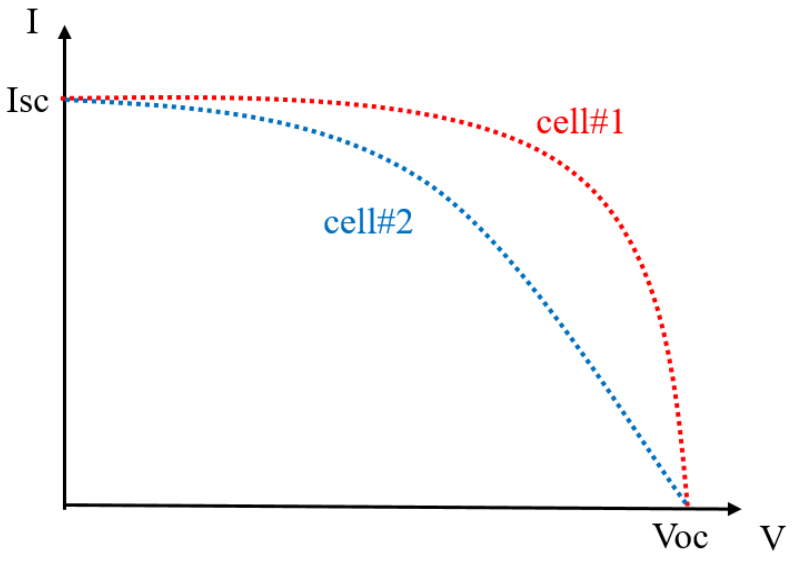

Figure 2.15: Two cells have the same V_{OC} and J_{SC}, but different in FF

2.5 Photovoltaic limitation

It is very important to understand, why a solar cell cannot convert 100% of the incident light into electricity. Different efficiency limits can be formulated, each taking different effects into account.

2.5.1 The thermodynamic limit

The most general efficiency limit is the thermodynamic efficiency limit, the solar cell is seen as a thermodynamic heat engine, it has Carnot efficiency and absorber efficiency. By combining these two efficiencies the total efficiency of the ideal solar cell as following equation [4] [43]:

$$\eta_{SC} = \left(1 - \frac{T_A^4}{T_S^4}\right)\left(1 - \frac{T_C}{T_A}\right) \tag{2.4}$$

Where

η_{SC}: Total efficiency of ideal solar cell.

T_A: Absorber temperature “Hot temperature”.

T_S: Sun temperature.

T_C: Cold temperature.

By assuming that the surrounding temperature T_C = 300 K, and the sun temperature T_S = 5,800 K, the maximum efficiency reach 85% when absorber temperature T_A = 2,478 K, see figure 2.16.

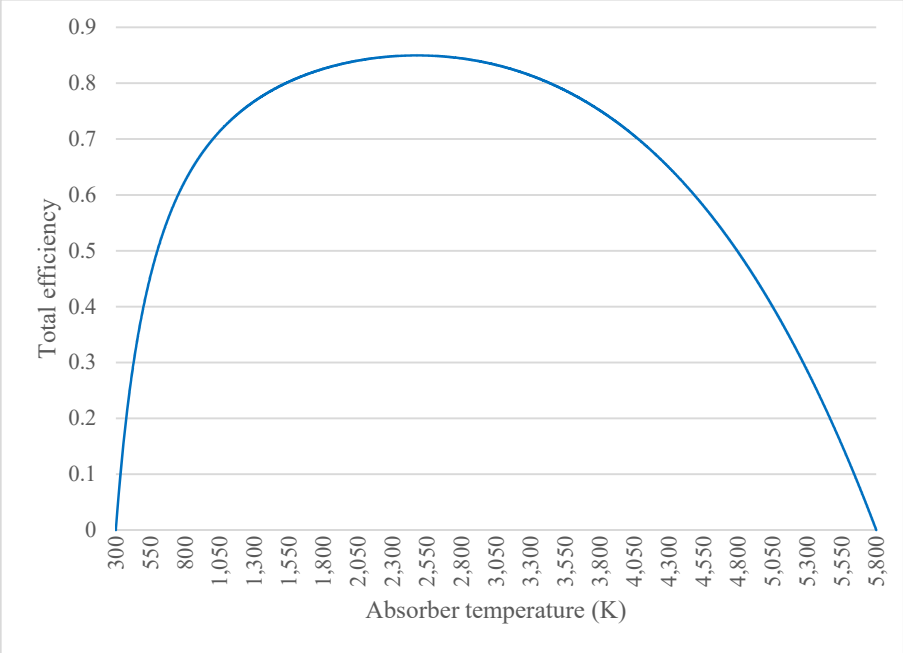

Figure 2.16: Solar cell efficiency η_{SC} [43]

2.5.2 The Shockley-Queisser Limit

This limit is usually referred to the Shockley-Queisser (SQ) limit, its theoretical limit for single-junction solar cells. It was first calculated in 1961 by William Shockley and Hans Queisser, where the formulate of this limit is based purely on physical assumptions and without using empirically determined constants [43]. Which does not exhibit extrinsic losses caused by series resistances or by reflection and transmission of light due to detrimental properties of the surface or overly thin absorbers. We consider only physical ("intrinsic") losses, which are unavoidable [4].

Spectral mismatch, for the generation of electron–hole pairs was assumed that photons with an energy below the energy band gap do not interact with the solar cell while photons with an energy above the band gap are converted into electron-hole pairs with a quantum efficiency of 100%. Shockley and Queisser calculated the efficiency limit for a single junction solar cell [44].

Shockley and Queisser calculated the maximum efficiency for a single-bandgap semiconductor as a function of the bandgap approximating the sun as a black body at cell temperature T_C = 300 K. Henry refined the data using the air mass AM1.5 spectrum. The maximum efficiency at 1 sun is around 30 % and increases to 36 % for a concentration factor of 1,000 (AM1.5d). AM1.5g gives a value of 33 %. The ideal bandgap is between 1.1 and 1.6 eV. Lower bandgaps lead to a decrease in η due to high thermalization losses resulting in a low V_{OC}, as shown in figure 2.17 [4].

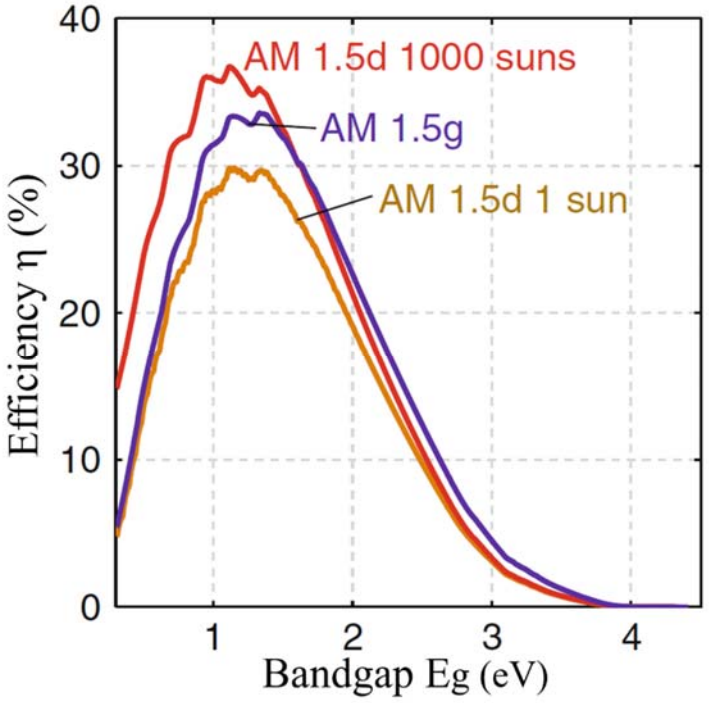

Figure 2.17: Maximum efficiency of a single-gap absorber as a function of the bandgap E_g

Other Losses could be due optical losses, solar cell collection losses and the voltage. Figure 2.18 shows the major losses of photovoltaic.

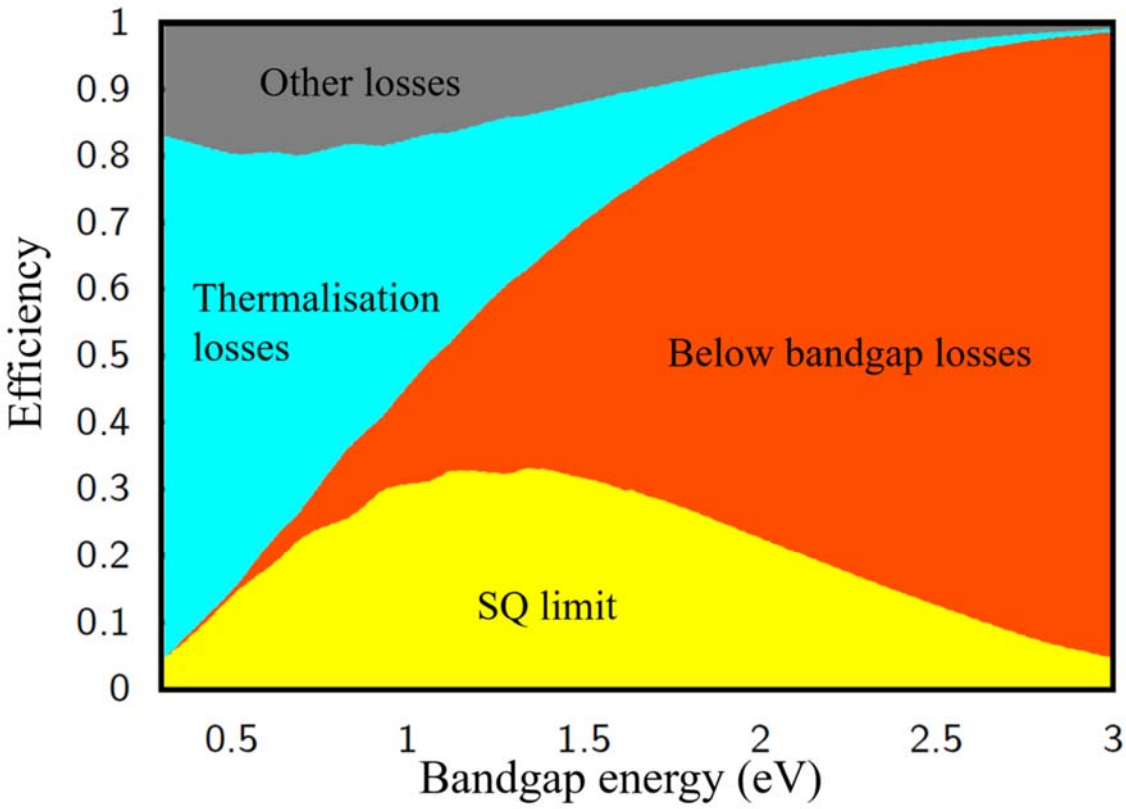

Figure 2.18: Major losses of photovoltaic [43]

2.6 Design Rules for Solar Cells

After showing the OPV's functionality, their efficiency and limitation. There are three design rules:

1. **Band gap energy**, until increase the efficiency we should find materials with bandgap 1.4 eV, and the bandgap between the LUMO of acceptor and HOMO of the donor to be chosen as maximum as possible to increase the V_{OC}. As explained in section 2.4.

2. **Spectral utilisation**, is mainly determined by the choice of materials from which the solar cell is made of, the material should absorb wavelength with peak irradiation.

3. **Light trapping**, in an ideal solar cell, all light that is incident on the solar cell should be absorbed in the absorber layer. The intensity of light decreases exponentially as it travels through an absorptive medium. This is described by the Lambert-Beer law equation (2.5) [43]:

$$I_v = I_0 e^{-\alpha d} \tag{2.5}$$

Where

I_v: Intensity of transmitted light.

I_0: Intensity of incident light.

α: Constant which depends upon wavelength and absorbing medium.

d: Thickness of the medium.

From the Lambert-Beer law, it follows that at the side, at which the light is entering the film, more light is absorbed in reference to the back side.

Ideally, we would like to absorb a 100% of the incident light on a solar cell. Such an absorber is called optically thick and has a transmissivity very close to 0. As we can see from the Lambert-Beer law, this can be achieved by either absorbers with a large thickness d or with very large absorption coefficients α.

2.7 Manufacturing

One of the advantage of the organic solar cell its low cost of production. The field of organic solar cells profited well from the development of light emitting diodes based on similar technologies, which have entered the market recently. The manufacturing method of organic photovoltaic can be divided into two techniques used in research and industrial [45]:

1. Wet solution processing: spin coating, ink jet, screen print, roll to roll printing (gravure print), slot-die coating, and knife over edge coating.

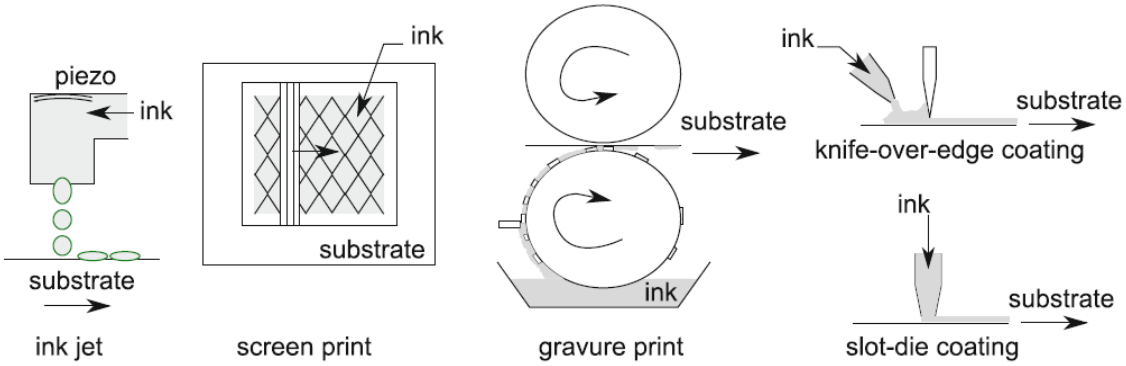

Figure 2.19: Wet solution processing [4]

2. Dry thermal evaporation: vacuum evaporation (for small molecules).

2.8 Applications

Organic photovoltaic is economically viable based on its low production cost in comparison to traditional silicon based photovoltaic materials. Aside from its production cost, the most obvious and useful advantages of this material is its flexibility and light weight. Traditional silicon cells (wafers) are extremely fragile and brittle, and therefore require expensive and/or heavy environmental shielding. This reduces the possible applications of these cells down to rigid structures.

With that in mind, the organic photovoltaic take advantage of lightweight and flexibility that can be easily integrated with any application or device. The following points, show some of OPV applications:

1. Building integration

   Building-integrated photovoltaics (BIPV) is a key example of an application of solar cells. Increasingly conventional solar cells are being incorporated into the construction of new buildings as a source of electrical power and existing buildings are retrofitted with solar cell technology.

2. Power generation

   Organic photovoltaic being used for larger scale power generation.

3. Education

   Using modules of OPV in primary school education and university teaching. The modules are not fragile, toxic, or unwieldy, rather they are affordable, flexible, comes in many forms, and can be designed to facilitate certain learning goals.

4. Small devices

   Incorporating organic solar cells into consumer products (gadgets) allows for a design freedom not possible with conventional solar cell technologies.

5. Clothing integration

   OPV it can easily integrated with clothes and use to charging or heating. As shown in figure 2.20.

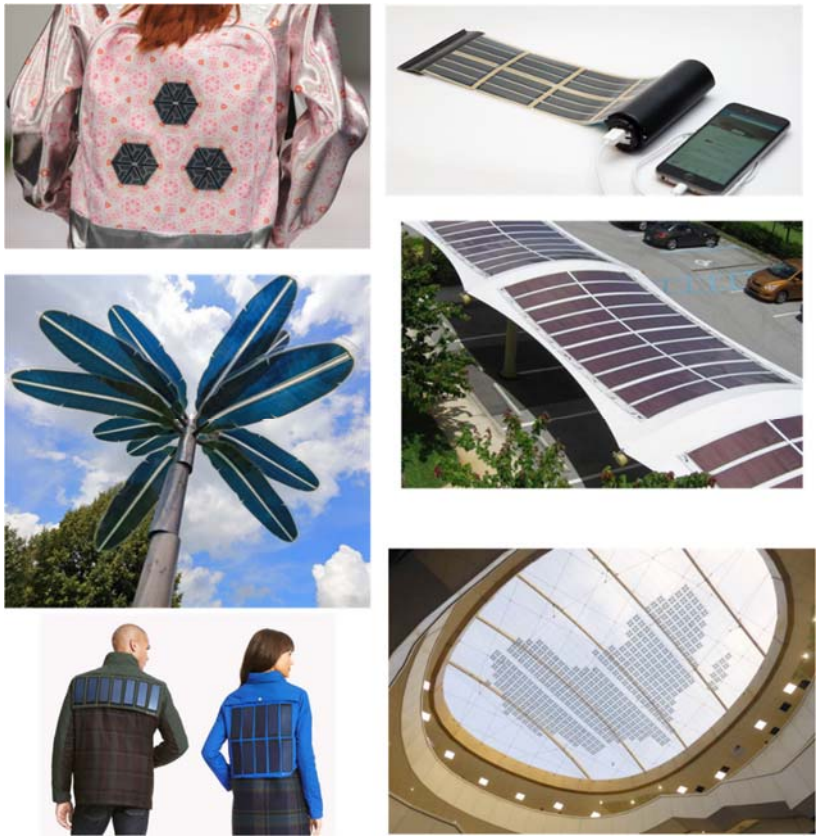

Figure 2.20: OPV applications

Chapter 3

Computational Chemistry

Chemistry is the science dealing with construction, transformation and properties of molecules. Theoretical chemistry is the subfield where mathematical methods are combined with fundamental laws of physics to study processes of chemical relevance [46].

Computational chemistry is rapidly emerging as a subfield of theoretical chemistry, where the primary focus is on solving chemically related problems by calculations.

As computer programs evolve, they become easier to use. Modern programs often communicate with the user in terms of a graphical interface, and many methods and procedures have become essential: we can draw the molecule, we can also do the calculation. This effectively means that you no longer have to be a highly trained theoretician to run even quite sophisticated calculations.

There is many software deal with computational chemistry such: Gaussian, GAMESS, NWChem, ORCA (Quantum Chemistry Program), Spartan and PSI. These programs base on quantum mechanics and elementary mathematics, especially linear algebra, vector, differential and integral calculus.

3.1 Computational Chemistry Methods

The quantum mechanics is the basic of computational chemistry and the methods that use in the computational chemistry is to solve Schrödinger equation. Equation 3.1 is the general form of Schrödinger equation [47].

$$\hat{H}\Psi = E\Psi \qquad (3.1)$$

Where $\hat{H}$: the Hamiltonian operator.

Ψ : the total wavefunction, which depends on the position of all nuclei and electrons.

E : the system's energy.

Hamiltonian ($\hat{H}$) consists of three terms: one for the kinetic energy of the electrons, one for the attraction between the nuclei and the electrons and the third for the repulsion between electrons.

The Schrödinger equation, sometimes called the Schrödinger wave equation, is a partial differential equation. It uses the concept of energy conservation (Kinetic Energy + Potential Energy = Total Energy) to obtain information about the behavior of an electron bound to a nucleus. It does this by allowing an electron's wave function, Ψ, to be calculated. Solving the Schrödinger equation gives us Ψ. With these we get the quantum numbers and the shapes and orientations of orbitals that characterize electrons in an atom or molecule. The Schrödinger equation gives exact solutions only for nuclei with one electron: H, He^{+}, Li^{+2}, Be^{+3}, B^{+4}, C^{+5}, etc. In mathematical language, we say that analytic solutions for Ψ are possible only for one-electron systems. One-electron systems are often described as hydrogenic - meaning "like hydrogen". For all other atoms, ions, and molecules, no analytic solutions for Ψ are possible; approximation methods of calculation, such as the orbital approximation and variation theorem, are then utilized [48].

The equation can be written in any suitable coordinate system, such as Cartesian coordinates (x,y,z). For hydrogenic atoms, spherical polar coordinates are more suitable, equation 3.2 shows (Kinetic energy + potential energy = total energy) [48].

$$\frac{-\hbar^2}{2m}\nabla^2\Psi(r) + V(r)\Psi(r) = E_v\Psi(r) \qquad (3.2)$$

Where $\hbar$: the reduced Planck constant.

m : the electron mass.

∇ : the Laplacian operator.

Ψ : the wave function.

V : the potential energy.

E_v : the energy eigenvalue.

(r) : denotes the quantities are functions of spherical polar coordinates (r, θ, φ).

There are many methods used to solve the Schrödinger equation such as: Semiempirical methods, HF (Hartree Fock), DFT (Density Functional Theory), and other. Figure 3.1 illustrate the accuracy of the methods relative to number of atoms.

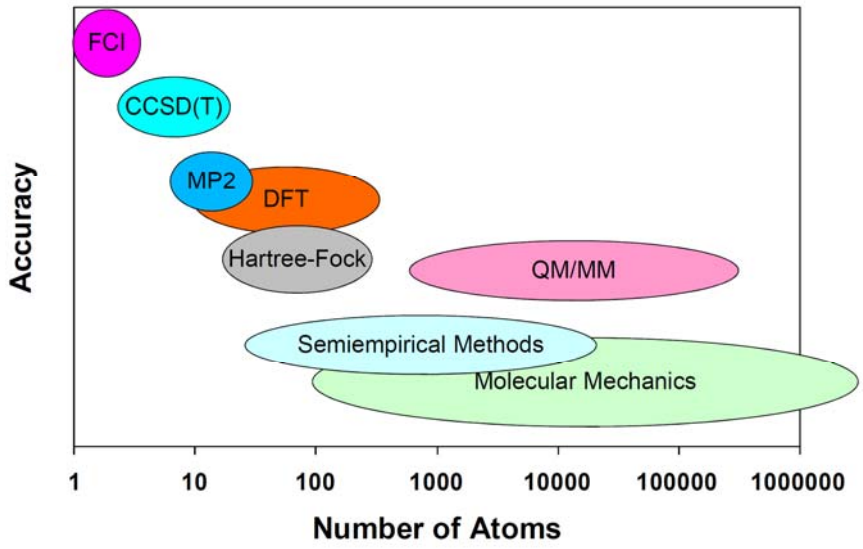

Figure 3.1: Computational chemistry methods (number of atoms VS accuracy) [49]

3.1.1 HF (Hartree Fock)

The Hartree-Fock method is one of the methods used in computational chemistry that seeks to approximately solve the electronic Schrödinger equation, and it assumes that the wave function can be approximated by a single Slater determinant made up of one spin orbital per electron. Since the energy expression is symmetric, the variational theorem holds, and so we

know that the Slater determinant with the lowest energy is as close as we can get to the true wave function for the assumed functional form of a single Slater determinant. The Hartree-Fock method determines the set of spin orbitals which minimize the energy and give us this "best single determinant" [50].

3.1.2 DFT (Density Functional Theory)

Density functional theory (DFT) is a computational quantum mechanical modeling method used to investigate the electronic structure (principally the ground state) of many-body systems, in particular atoms, molecules, and the condensed phases, it become one of the most widely used methods and the most popular and versatile methods available in computational chemistry [51].Using this theory, the properties of a many-electron system can be determined by using functional, functions of another function, which in this case is the spatially dependent electron density. Hence the name density functional theory comes from the use of functional of the electron density.

DFT was not considered accurate enough for calculations in quantum chemistry until the 1990s, when the approximations used in the theory were greatly refined to better model the exchange and correlation interactions. Computational costs are relatively low when compared to traditional methods, such as exchange only Hartree-Fock theory and its descendants that include electron correlation.

DFT calculation adds an additional step to each major phase of a Hartree-Fock calculation. This step is a numerical integration of the functional (or various derivatives of the functional). The accuracy of DFT calculations also depends on the number of points used in the numerical integration.

3.1.3 Basis Sets

One way to improve the overall quality of the results is to choose mathematical expressions which best shape in the space which a given electron is allowed to move.

The choice of the basis set is generally done by using a combination of Gaussian functions (primitives). The larger is the number of primitives and the more articulated is their convolution is the better basis set. This requires significant work of optimization of the coefficients with which the primitives sum up together. Such a procedure is called contraction [52].

The most popular QM packages offer the possibility of using predefined basis sets. Is (6-31++G*) provides information on the mathematical generation of the various atomic orbitals.

First number: the core orbitals are derived from a single contraction of six primitives.

Second number: the number of primitives first contraction valence shell orbital.

Third number: the number of primitives second contraction valence shell orbital.

The symbols (++) indicate that diffusion functions are added to increase the flexibility of the orbital far from the nucleus.

The sign (*) indicates the presence of polarization functions. These functions provide additional mathematical flexibility, which accounts for peculiar structural features.

3.2 Gaussian Software

Gaussian is a general purpose computational chemistry software package initially released in 1970 by John Pople and his research group at Carnegie Mellon University as Gaussian 70. Originally available through the Quantum Chemistry Program Exchange, it was later licensed out of Carnegie Mellon University, and since 1987 has been developed and licensed by Gaussian, Inc. [53].

Gaussian quickly became a popular and widely used electronic structure program. Prof. Pople and his students and post-docs were among those who pushed the development of the package, including cutting-edge research in quantum chemistry and other fields [54].

Since 1970 the Gaussian has been continuously updated starting with Gaussian 70, Gaussian 76, Gaussian 80, Gaussian 82, Gaussian 86, Gaussian 88, Gaussian 90, Gaussian 92, Gaussian 92/DFT, Gaussian 94, Gaussian 98, Gaussian 03, Gaussian 09 and the current version of the program is Gaussian 16. The Gaussian one of the most powerful computational chemistry software.

Through Gaussian we can calculate : Dipole, Electron density, Hyper polarization, Hyperfine coupling constant, Ionization potential, Molecular surfaces, Molecular volume, Mullikan charges, Polarizability, RMS force, SCF energy, Spin density.

Gaussian dose these calculation through various methods as: Semiempirical methods (Austin Model 1 “AM1”, Parametric Method Number 3 “PM3”), HF (Hartree Fock), DFT (Density Functional Theory), and other. Figure 3.2 show how Gaussian work to find the approximate solution using DFT.

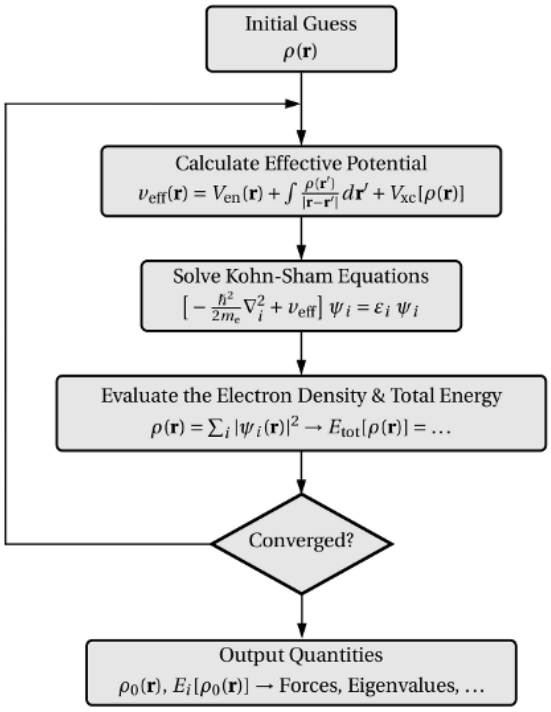

Figure 3.2: How Gaussian work (Gaussian algorithm)

It is the Gaussian software that was used to carry out the molecular properties polymers being used in my research.

3.3 Gaussian Calculation and Results

The Gaussian 09 was used as a tool to help us to select our donor and acceptor and Chem3D 16 software was used to build our polymers and molecules, then send the input file to Gaussian through Chem3D 16 to make calculation for molecular surfaces to get the HOMO (Highest Occupied Molecular Orbital) – LOMO (Lowest Unoccupied Molecular Orbital) energy.

Calculations were done by using DFT/B3LYP/6-31+G method because this it gives the most accurate results [55-57]. Figures (3.3 and 3.4) show the graphical results of Gaussian for the used materials in this research. The graphical results display the structures and the location of electrons in HOMO and LUMO levels for polymers (P3HT) and molecule (ICBA).

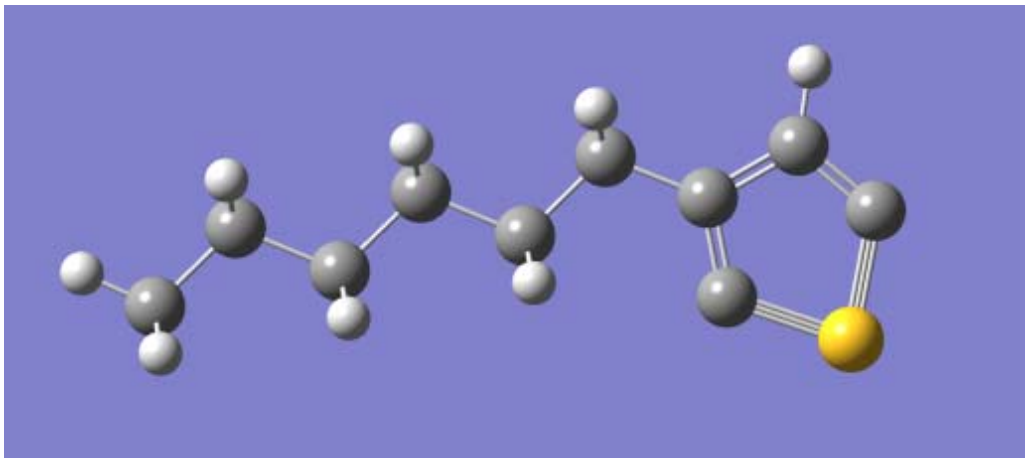

(a)

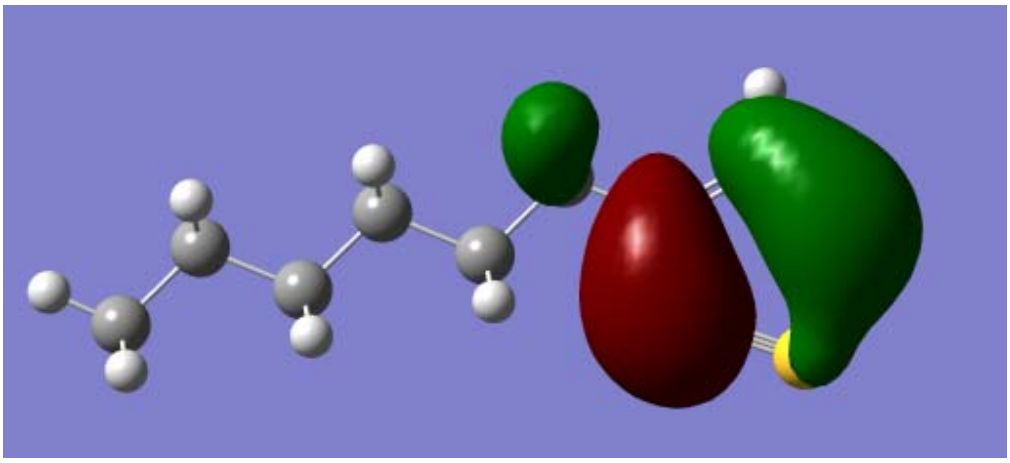

(b)

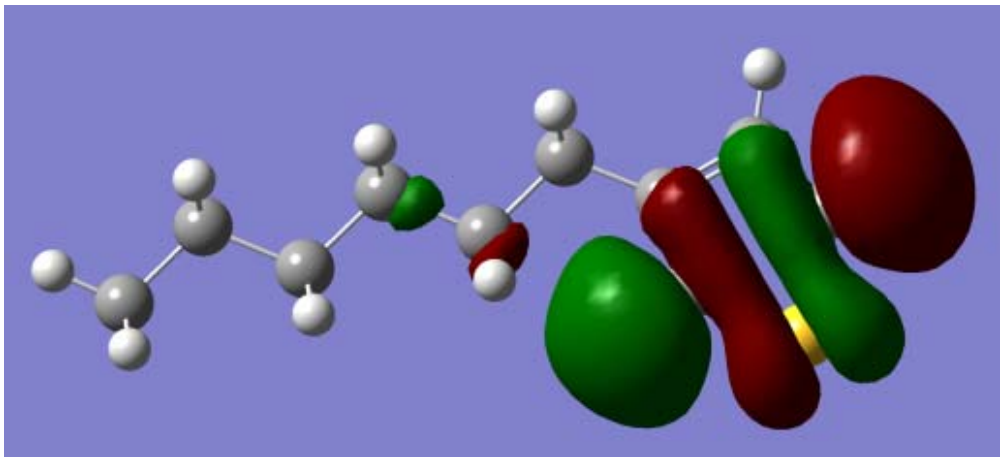

(c)

Figure 3.3: P3HT (a) structure, (b) HOMO, (c) LUMO

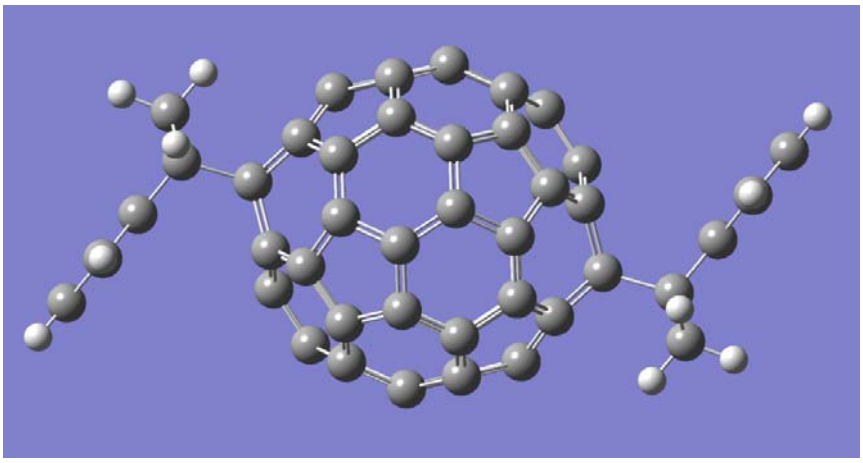

(a)

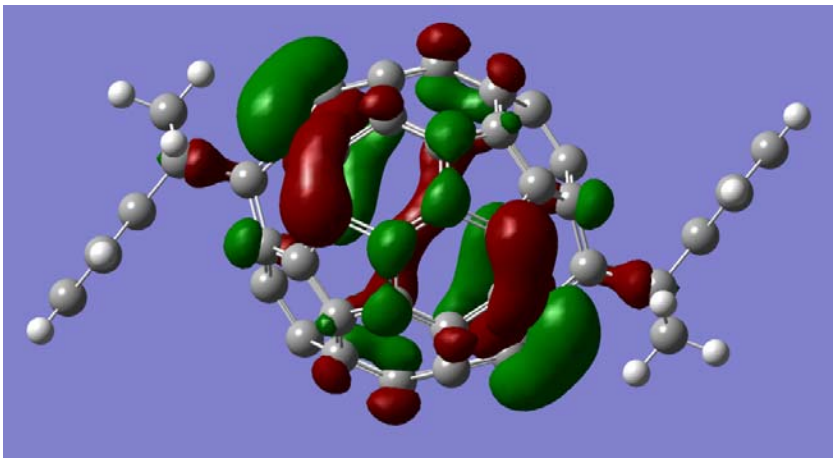

(b)

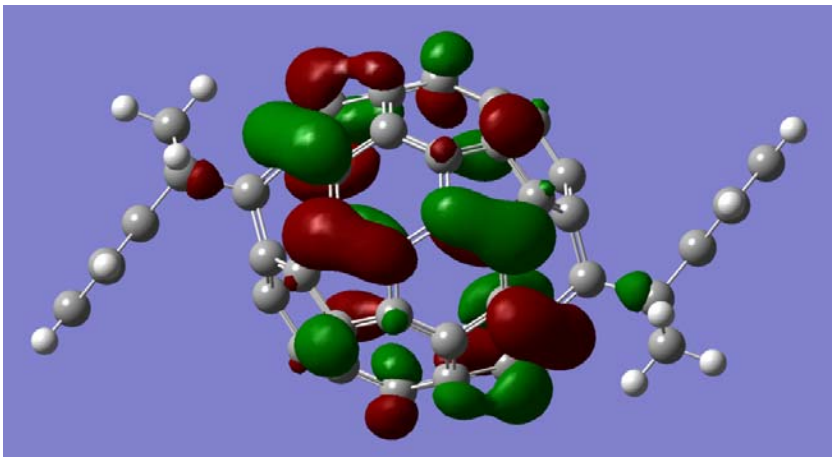

(c)

Figure 3.4: ICBA (a) structure, (b) HOMO, (c) LUMO

The tables (3.1 and 3.2) summaries the result of Gaussian software and show the energy of HOMO and LUMO for P3HT, PCBM, ICBA in atomic unit (a.u, 1 a.u= 27.211eV).

Table 3.1: HOMO, LUMO Energy.

	HOMO a.u	LUMO a.u	HOMO eV	LUMO eV	Band gap eV
P3HT	0.236	0.133	6.416	3.623	2.793
ICBA	0.197	0.138	5.348	3.748	1.600

Table 3.2: Number of π bond, molecular weight and linear formula.

	π Bond	MW g/mol	Linear Formula
P3HT	2	168.097	$C_{10}H_{14}S$
ICBA	34	952.125	$C_{78}H_{16}$

Table 3.1 and figure 3.5 shows the electrons that can easily jump from the P3HT LUMO to ICBA LUMO because the energy level of ICBA is less than the LUMO of P3HT which means that P3HT and ICBA are suitable to each other. The Voc of (P3HT:ICBA) as described in the equation 2.1 is around 2 volt, it is high voltage for a solar cell.

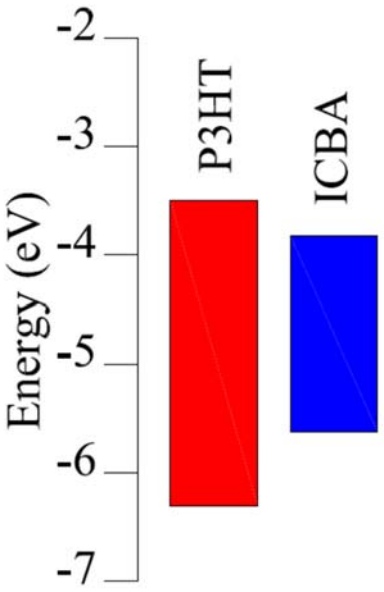

Figure 3.5: P3HT,PCBM and ICBA energy level

Chapter 4

P3HT: ICBA Cell Architecture and Fabrication

In this section we elaborate about the fabrication of P3HT: ICBA organic solar cell "P3HT: Poly(3-hexylthiophene-2,5-diyl); ICBA: 1′,1″,4′,4″- Tetrahydro di[1,4] methanonaphthaleno [1,2:2′,3′,56,60:2″,3″] [5,6] fullerene-C60, C60 derivative , indene-C60 bisadduct ". It is a BHJ Polymer-Fullerene.

4.1 BHJ Cell Architecture

The BHJ cells consist of layers as shown in figure 4.1. These are mainly; an ITO (Indium Tin Oxide) coated glass substrate, with aluminum electrodes directly deposited on it, followed by a PEDOT:PSS layer, covered by the organic active layer, over which lies an aluminum cathode.

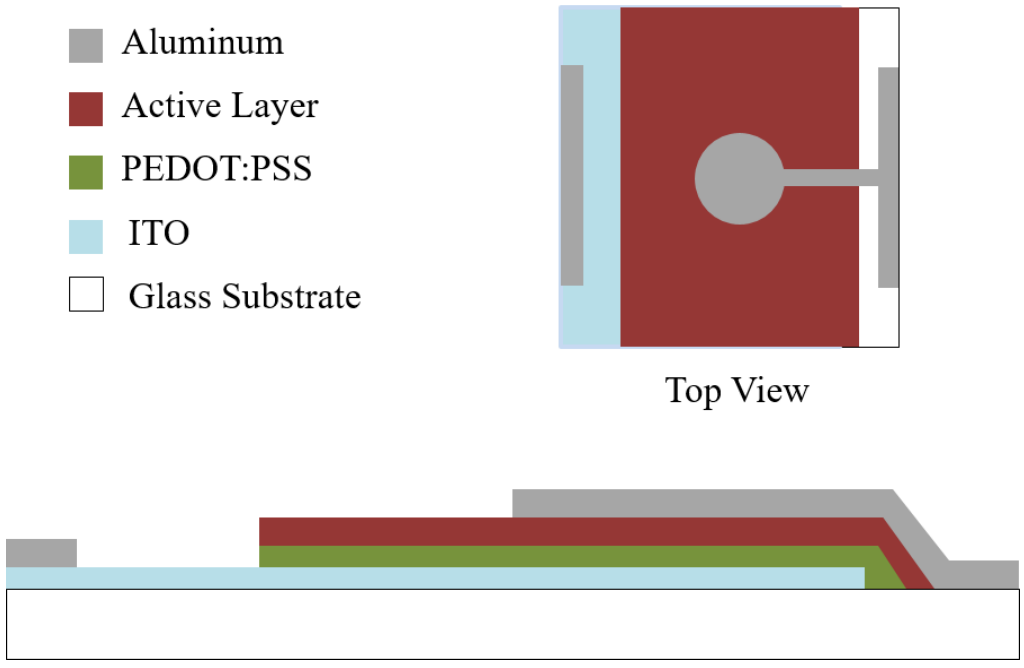

Figure 4.1: BHJ cell architecture

The layer of the solar cell are described by the following:

A. Substrate: a glass substrate coated with ITO layer. As shown in figure 4.1.

B. Electrodes: are deposited directly on the substrate and their function is to collect the excitons within their lifetimes. A high work function anode and low work function cathode are used and this difference creates a built-in electric field within the solar cell that determines the V_{OC} of the cell [18], Aluminum electrodes are used for building devices.

C. PEDOT: PSS [Poly 3, 4-EthyleneDiOxyThiophene: Poly-Styrene Sulfonate], as shown in figure 4.2, is a mixture of two ionomers. The PSS component is made up of sodium polystyrene sulfonate and carries negative charge. The PEDOT is a conjugated polymer and carries positive charges. Together they form a macromolecular salt. Being used as a transparent conductive polymer with high ductility. The compound improves the surface quality of the ITO layer, i.e. reducing the probability of shorts, and facilitates the hole injection/ extraction.

The PEDOT:PSS is widely used in various organic optoelectronic devices. High electrical conductivity and good oxidation resistance of such polymers make it suitable for electromagnetic shielding and noise suppression. Thus, the polymer film was found to possess high transparency throughout the visible light spectrum [58].

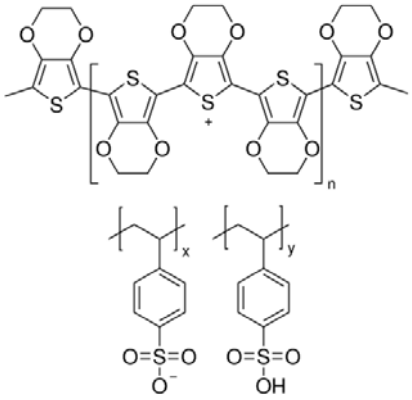

Figure 4.2: PEDOT:PSS

PEDOT:PSS was purchased from SIGMA-ALDRICH factory code (655201-5G), with conductivity > 200 S/cm stored in cold.

D. The active layer (P3HT: ICBA)

One of the most efficient materials used in the cells are P3HT and ICBA. P3HT is the most used donor in organic solar cells research. P3HT has a reported efficiency of more than 5%.

P3HT is a member of the Polythiophene conducting polymer family. The excitation of the π-orbital electron gives the photovoltaic effect in the blend. Polythiophenes represent an important class of conjugated polymers, because they meet the essential requirements of process ability, adequate charge transport properties, and the possibility of structural modifications. Due to the poor solubility of un-substituted polythiophene in organic solvents, a hexyl-chain is added in the 3 position, rendering it asymmetrical.

The 3-hexylthiophene monomers (figure 4.3a) can be coupled with different orientations with respect to the side chain. Polymerization leads to regiorandom (RRa) and regioregular (RR-P3HT), as shown in figure 3.4b, 3.4c. RRa-P3HT has no practical use with low crystallinity. On the other hand RR-P3HT features a high crystallinity because of the π-π stacking of thiophene rings resulting in a good hole mobility up to 10^{-2} $cm^2V^{-1}s^{-1}$ [59].

These polymers was used in our work because of their relatively short excitation diffusion length (10~20 nm). This type of active layer has shown impressive progress in terms of power conversion efficiency. [22]

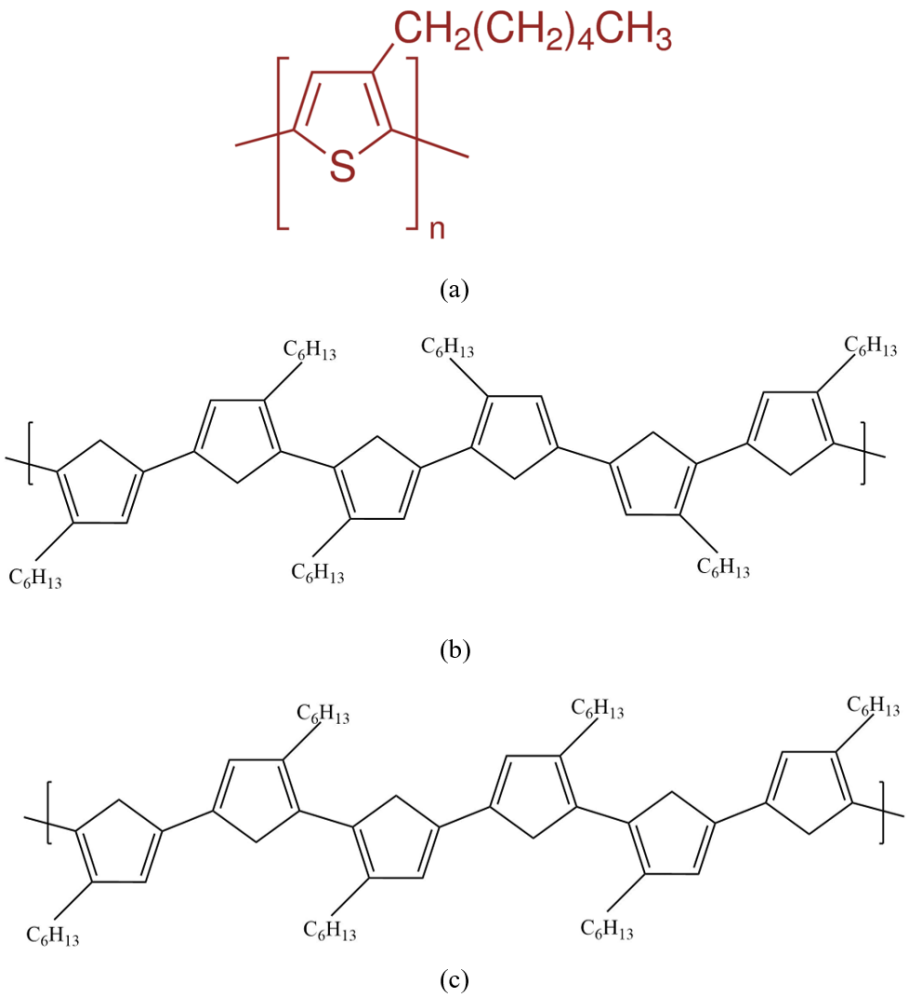

Figure 4.3: (a) P3HT structure (monomer), (b) RRa P3HT,(c) RR P3HT

P3HT was brought from Dr. Hussien Shanak "SIGMA-ALDRICH factory code (445703-1G)", table 4.2 shows the properties.

Table 4.1: P3HT properties.

Form	Solid
Molwt	**Average Mw 50,000-100,000**
Solubility	**chlorobenzene: soluble**
	dichlorobenzene: soluble
MP	**238 ºC**
Orbital energy	**HOMO 5 eV**
	LUMO 3 eV

ICBA is a fullerene derivative, because of the high hole mobility it plays the role as an ideal electron acceptor for many reasons. First, is the spherical shape and the favorable electron affinity with good electron mobility of 0.1 $cm^2 V^{-1}s^{-1}$. Second, it has an energetically deep-lying LUMO, which endows the molecule with high electron affinity relative to many potential organic donors. Third, it is designed to increase the open circuit voltage of solar cells, for example increase the V_{oc} for P3HT solar cells around 0.17 eV due to the higher lying LUMO level in order to significantly increase the power conversion efficiency. [60] [61]. The problem is that this molecule has a low solubility in organic solvents. To solve this problem fullerenes are typically substituted with soluble side chains and ICBA have two side chains. The ICBA: ($C_{78}H_{16}$) is chosen for its high crystallization and charge mobility. Table 4.2 shows its properties, Figure 4.4 shows structure of ICBA, Figure 4.5 shows the HOMO and the LUMO for different donors relative to the fullerene acceptors.

Figure 4.4: ICBA structure

ICBA was purchased from SIGMA-ALDRICH factory code (753955-250MG), table 4.3 show the properties.

Table 4.2: ICBA properties.

Form	Solid
Empirical Formula	$C_{78}H_{16}$
Molwt	952.96
MP	253-260 °C
Orbital energy	LUMO 3.67 eV (CV)

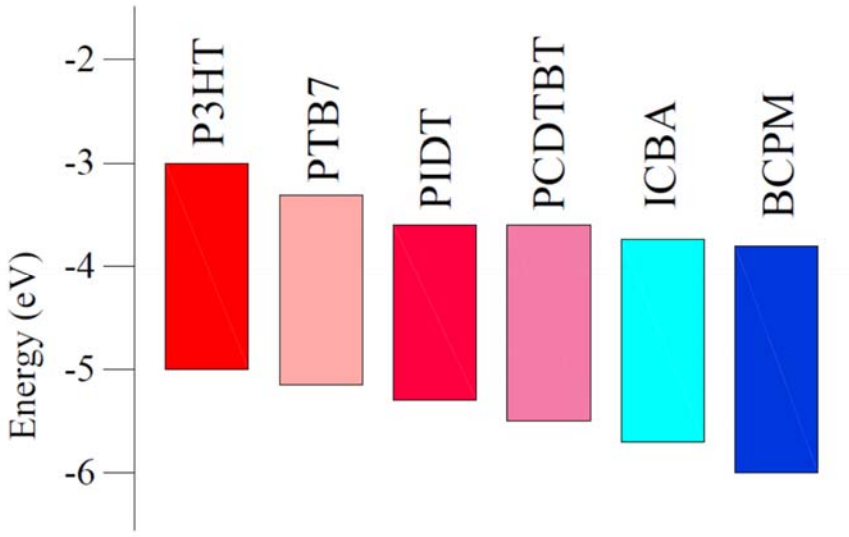

Figure 4.5: HOMO and LUMO energy of some donors to ICBA and PCBM

4.2 Cell Fabrication Procedure

Cell preparation was conducted at Bethlehem University in the Physics Laboratory and at the Chemistry Laboratory where the thermal vacuum evaporator and the spin coater are used. Two micro-manipulators and Keithley 2601 have been borrowed from the Nanotechnology Research Laboratory (NRL) at Al-Quds University.

4.2.1 ITO Substrate Preparation

Twenty eight substrates of ITO was taken off from a plate, then each substrate was masked with scotch except for the last 5 mm as shown in figure 4.7. Zn powder was then spread over the unmasked part and rubbed with a cotton swab dipped in HCl to wipe out the ITO. Then the substrate was washed with water and the mask was rapidly removed.

ITO glass substrate was washed and cleaned by sonicator (ultrasonic): first in de-ionized water 3 times, 15 minutes each. Then it was rinsed in acetone bath for 15 minutes, and in isopropyl bath for 15 minutes. Finally, the sample was dried at 110 ºC in oven for two minute. Results are shown in figures 4.6 and 4.7 before and after etching.

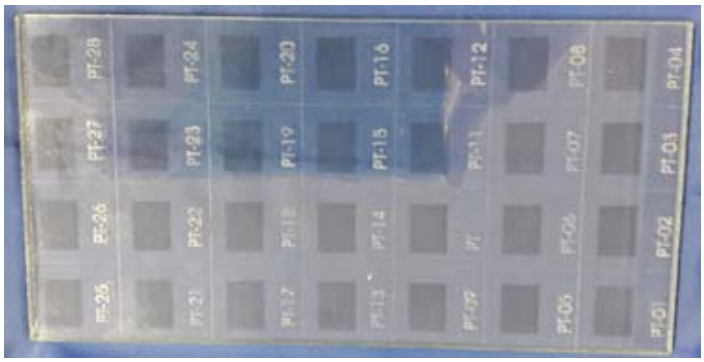

Figure 4.6: ITO plate with 28 substrates

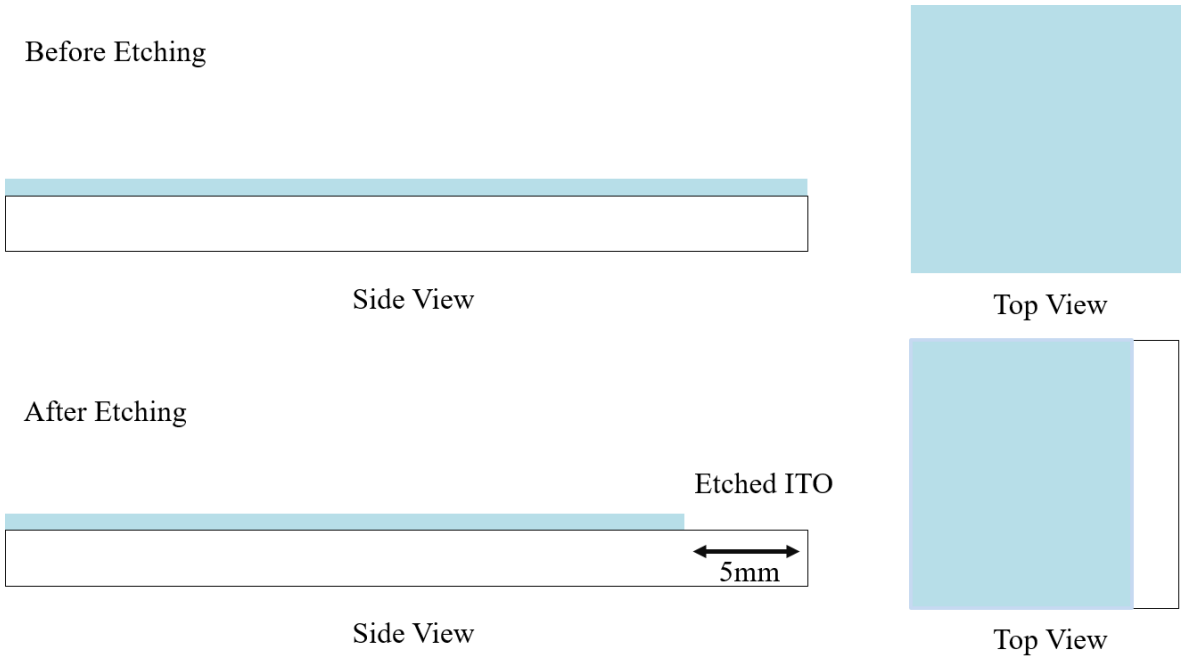

Figure 4.7: steps of ITO substrate etching with Zn powder

Figure 4.8: Sonicator at Bethlehem University

4.2.2 Al Electrodes Deposition

Depositing of Al electrodes with certain thickness was done using Vacuum Thermal Evaporation (VTE). The technique involves heating the Al electrodes materials in vacuum at 10^{-6} torr. The substrate was placed several centimeters away from the source so that the evaporated material can directly be deposited to the substrate, as shown in figure 4.9.

The method is useful for depositing many layers of different materials without chemical interaction between the layers. However, there are sometimes problems with making uniform thickness over large-area substrates. In addition, the deposited materials on the chamber's wall can contaminate later depositions. This method can create holes in the film due to shadowing, which can increase the series-resistance and may create short circuits. When evaporation is performed in poor vacuum or close to atmospheric pressure, the resulting deposition is generally non-uniform and tends not to be a continuous or smooth film. Rather, the deposition will appear fuzzy.

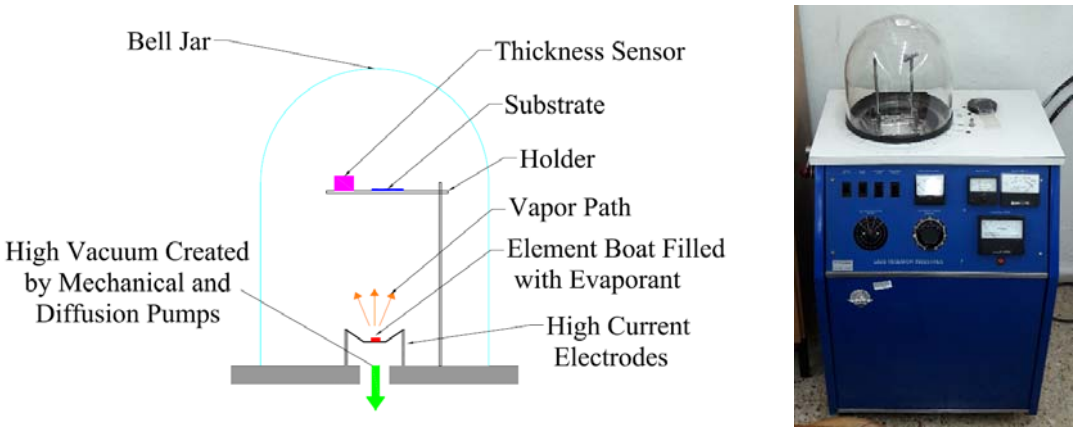

Figure 4.9: (a)Thermal evaporator process, (b)Thermal Vacuum evaporator

To deposit the electrodes by thermal evaporation, the substrate was covered by a scotch except for few millimeters from both sides as shown in figure 4.10.The deposited electrodes was around 100 nm thickness.

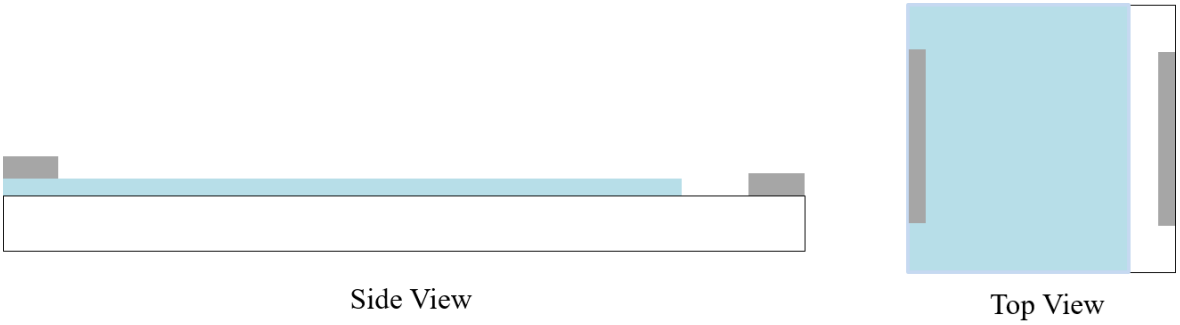

Figure 4.10: Aluminum electrodes deposited substrate

Aluminum started melting at a current value of around 12A and evaporation starts at 15A. The pressure before the melting was $9x10^{-6}$torr, but during evaporation it dropped to $1.5x10^{-5}$torr. The typical pressures for the VTE are 10^{-6} to 10^{-8} torr [62]. Figure 4.11 shows aluminum evaporation using VTE.

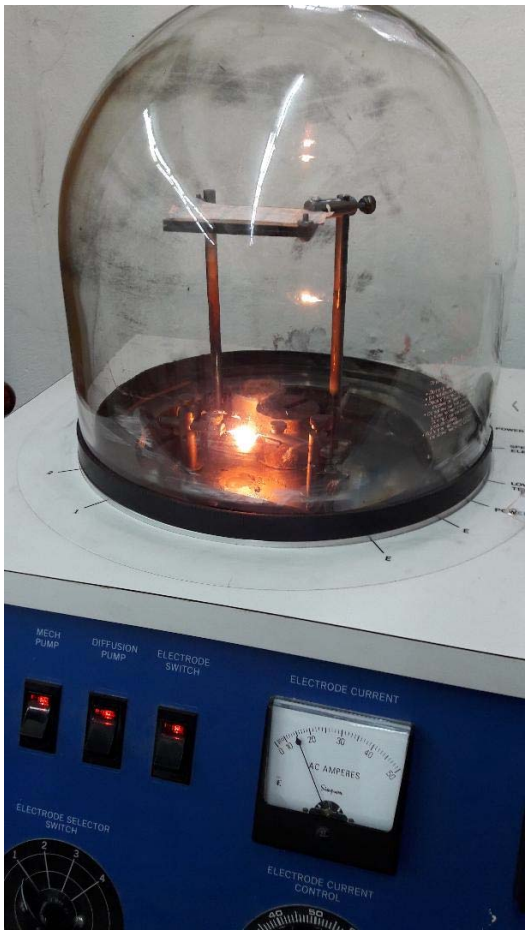

Figure 4.11: Photo of the evaporator during aluminum deposition

After the deposition the substrate was washed for 15 min in iso-propanol path, then dried in oven for two minutes and finally put in UV-ozone for 15 min.

4.2.3 PEDOT:PSS Deposition

Many methods can be used to deposit the active layer on the cell. That includes spraying; spin coating; vaporization; (screen, stamping, gravure and ink-jet) printing; roll to roll and slot-die coating [30]. The spin coater was used to deposit the PEDOT:PSS and the active layer. Spin coating is the method applied to standard flat wafers. It involves the acceleration of a liquid puddle on a rotating substrate. The coating material is deposited at the center of the substrate either manually or by a robotic arm. The coating involves a balance between the rotational centrifugal forces controlled by the spin speed and forces determined by solvent

viscosity. Some parameters involved in spin coating are solution viscosity, solid content, angular speed, and spin time. Figure 4.12 shows our homemade spin coater made by me, and controlled through a program developed by me as well.

Thermal Annealing of sample is done after the deposition of PEDOT:PSS layer and before depositing the active layer that should be annealed too. Thermal annealing is used to optimize the material's morphology. Annealing helps the polymer chains to reorganize, and the fullerene molecules to diffuse freely into the composite and reorder [63].It helps the blend to get a better organized structure, with the P3HT forming long thin fibers while ICBA becomes more homogeneous. Annealing heats the active layer to a temperature greater than the Tg (glass transition temperature)[1] of the material. For P3HT, Tg reported value is 110°C [64]. At room temperature the crystallization of the two components is inhibited by their presence together. Thermal annealing helps the creation of crystalline structure [65].

Figure 4.12: Home made spin Coater designed by me

This mixture of PEDOT:PSS was filtered using a 0.45 μm filter before deposition on the substrate by spin coating at 4000 rpm for 60 sec, to take off all impurities with dimensions >0.45 μm [66].

[1] Glass transition temperature (Tg) when the polymer is cooled below this temperature, it becomes hard and brittle, like glass.

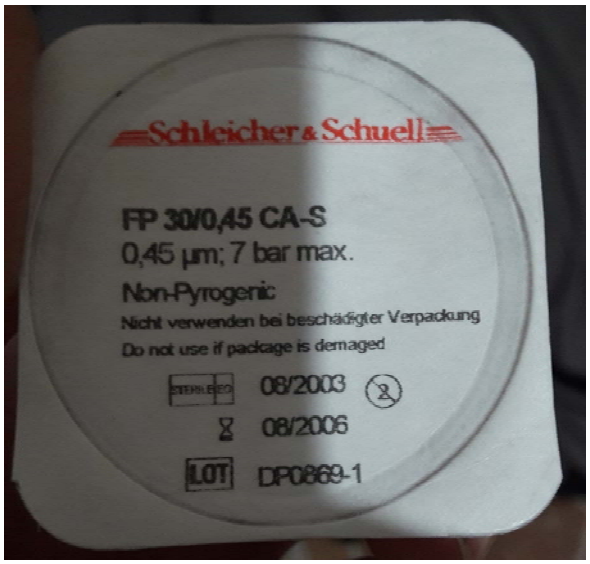

Figure 4.13: 0.45µm filter

The thickness of this layer is around 40 µm. After that electrodes are rapidly cleaned using a cotton swab dipped in de-ionized water. This layer was dried (annealed) at 150 °C for 5 min, as shown in figure 2.14.

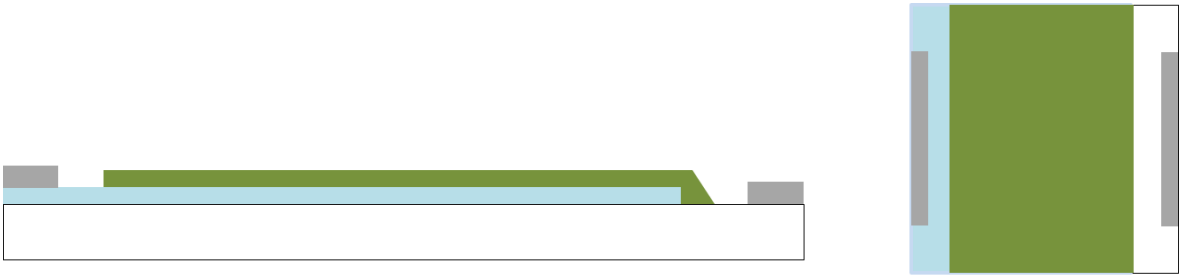

Figure 4.14: PEDOT:PSS deposited layer

4.2.4 Preparing the Active Layer Blends and Depositions

Different concentrations was prepared of the active layer components using spin coater, to optimize the best possible blend that may affect the cells efficiency. The active material was solved in an organic solvent (dichlorobenzene).

For blend preparation, 34mg of P3HT solved in 2ml of dichlorobenzene and 34mg of ICBA in 2ml dichlorobenzene, then each mixture was immersed in water bath at 70 ºC with stirrer for 30 min after that we mixed the active layer blend with different ratio. Table 4.3 shows the ratio of each blend mixed with stirrer for 5 min then cooled down and kept overnight in hotplate at 30 ºC [66]. Figure 4.16 shows the different ratios of the active layer tubes.

Table 4.3: Blends with different P3HT: ICBA Ratio.

P3HT:ICBA Ratio	P3HT mix. (µl)	ICBA mix. (µl)	Total (ml)
1:1	100	100	0.2
1:2	100	200	0.3
1:3	100	300	0.4
2:1	200	100	0.3
3:1	300	100	0.4

Figure 4.15: ICBA, P3HT blend

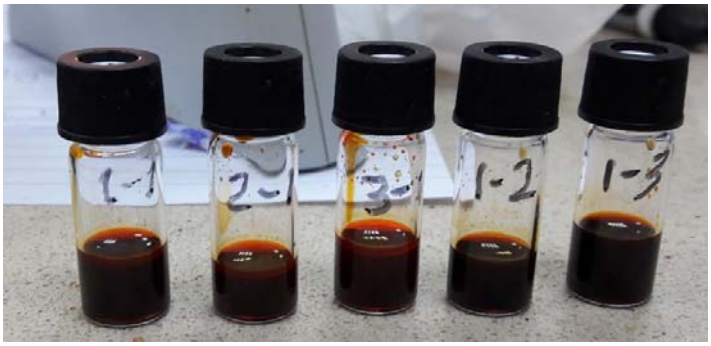

Figure 4.16: Active layer preparation

A total of 5 cells were made using different active layer components mixing ratios and spining at different speeds. Thickness of the active layer at 500 rpm for 60 sec is estimated to

be around 100 nm [66]. To compare the efficiency dependence on blend ratio, table 4.4 shows the blend ratio and spin speed for each cell.

Table 4.4: Blend ratio and spin speed for each cell.

Cell #	Blend	Spin Speed (rpm)
1	1:1	500
2	2:1	500
3	3:1	500
4	1:2	500
5	1:3	500

The blend material was filtered using 0.45µm filter before spin coating. After that rapidly immersed in water. Electrodes were swabbed dipped in dichlorobenzene, then the film was annealed at 110 °C for 2 min [66, 67] [68]. Figure 4.17 shows active layer deposition.

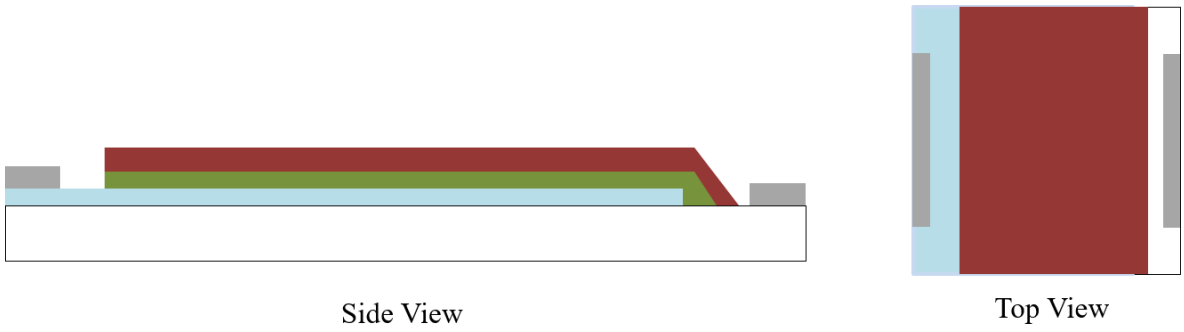

Figure 4.17: Active layer deposition

4.2.5 Al Electrode Deposition

The cell was completed by thermally evaporating the aluminum using a mask. For aluminum, the melting current was about 18A, and evaporation was done at 20A. The pressure before melting was about $9x10^{-6}$torr. The resulting thickness of the deposited electrode is about 100nm. The cell active area was 0.28 cm^2. Figure 4.18 shows a schematic of the cell and figure 4.19 shows one of the prepared cells.

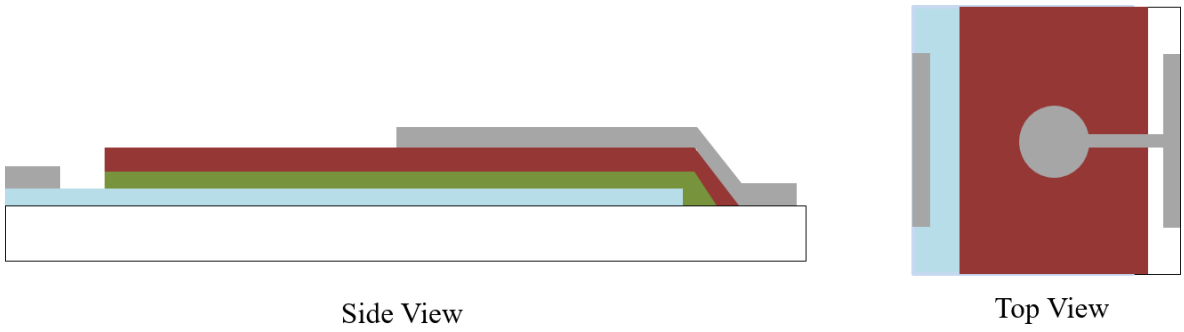

Figure 4.18: Aluminum electrodes deposition

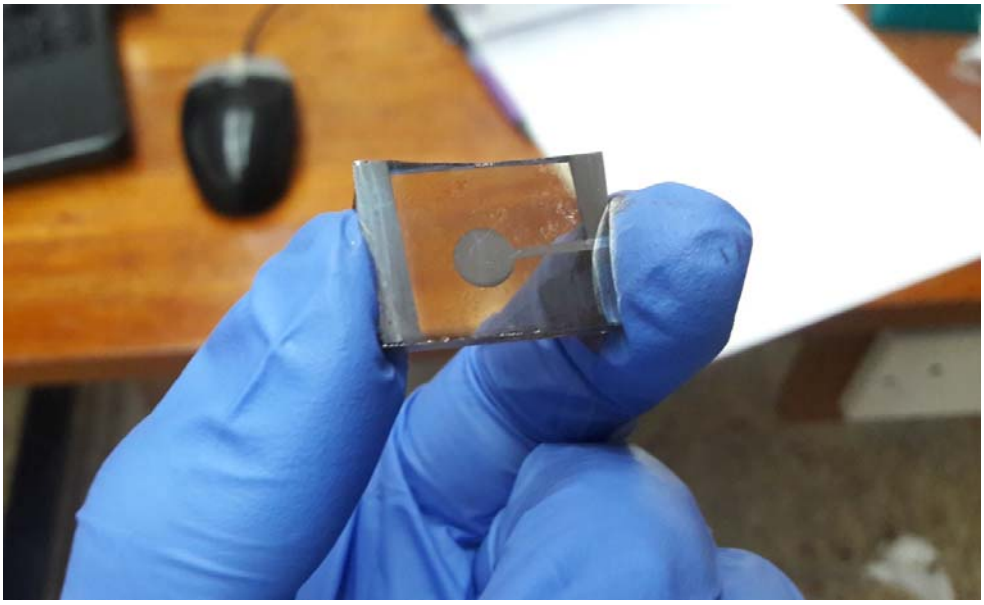

Figure 4.19: One of the prepared cells with all layers

4.3 Testing and Measurements

In this section, a review is given about the basic testing instruments used:

1. **Micro-manipulator:** it is a mechanical probe, which allow the precise positioning of thin needles on the surface of a semiconductor device in three dimensions x,y and z, it is used to connect small devices under test. Figure 4.20, shows the two micro manipulator probes that have been used for IV measurements.

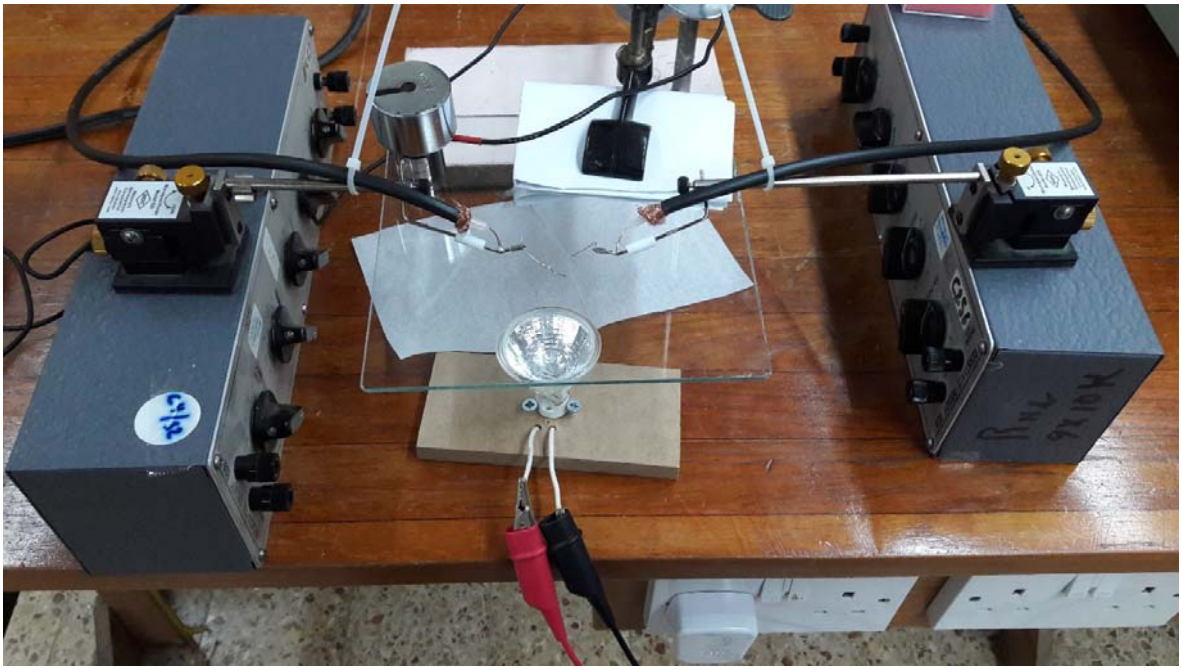

Figure 4.20: The Four Probe Station at NRL, Al-Quds University

2. **Keithley 2601:** Source measure units (SMUs) are an all-in-one solution for current voltage (I/V) characterization with the combined functionality of a precision power supply, high precision DMM, and electronic load. Keithley pioneered the development of individual, compact, bench-top SMU instruments and is the leading supplier of these instruments today.

   SourceMeter instruments offer electronic component and semiconductor device manufacturers a scalable, high throughput, highly cost-effective solution for precision DC, pulse, and low frequency AC source measure testing. Building on the tightly integrated source-measure technology originally developed for Keithleys SourceMeter line, Series 2600 instruments provide from two to four times the test speed of competitive solutions in I-V functional test applications. They also offer higher source-measure channel density and a significantly lower cost of ownership than competing products. The analog-to-digital converters provide simultaneous I and V measurements in less than 100µs (10,000 readings/s) and source-measure sweep speeds of less than 200µs per point (5,500 points/s). This high speed source-measure capability, plus advanced automation features and time-

saving software tools make Series 2600 SourceMeter instruments an ideal solution for I-V testing of a wide range of devices [69].

Figure 4.21: Keithley 2601 at NRL, Al-Quds University

They are ideal for solar cell testing because:

• They have the ability to act as a sink.

• They can act as a high precision electronic load.

• They provide the industry's widest dynamic range and have high and low current capability.

3. **Radiation Meter (LAMBDA Li-185):** It's a portable meter used to measure the quantum sun radiation and photons, provide accurate radiation measurements across a wide variety of applications. This radiometer was used to test light source radiation for IV measurements.

Figure 4.22: Li-185 at Physics Lab, Bethlehem University

4.3.1 Standard Testing Conditions (STC)

STC provides the same testing condition to all types of solar cells, modules and array so that manufactures and customers can make comparison.

The standard conditions are 100 mW/cm^2 of irradiance at a temperature 25ºC and Air Mass (AM) of 1.5 which is a measure of how much atmosphere sunlight must travel through to reach the earth`s surface. This is denoted as AM (x), where x is the inverse of the cosine of the zenith angle of the sun. AM describes the spectrum of radiation not the intensity [70]. AM of 1.5 indicates 1.5 times the thickness of atmosphere. In other words, AM 1.5 indicates the sun shines about 30º from the horizon. The higher the air mass, the larger the radiation amount absorbed by the sky [42].

4.3.2 Testing

Current-Voltage (IV) characteristics: IV test measures the open-circuit-voltage (V_{OC}) and the short current (I_{SC}), to calculate the Fill Factor (FF) and efficiency (η) based on an input power measured by Li-185. In our case the Cryogenic Four-Probe Station was used with two

probes from which connection is established between the cells and Keithley 2601(SMU) to measure the IV characteristics in both light and dark conditions.

4.3.3 Connection

Using 4-wire connection in the following figures (4.23-4.25)

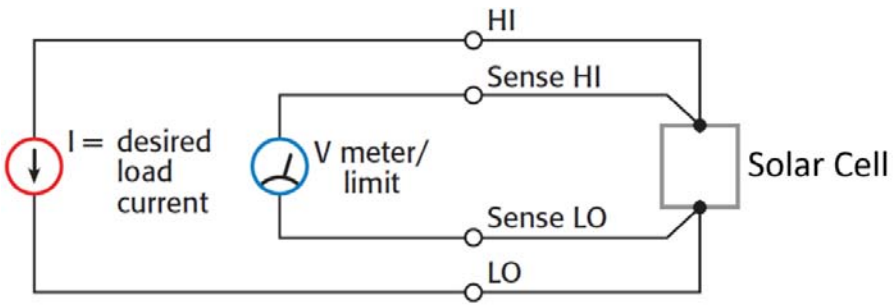

Figure 4.23: Standard 4-wire connection to Keithley SMU

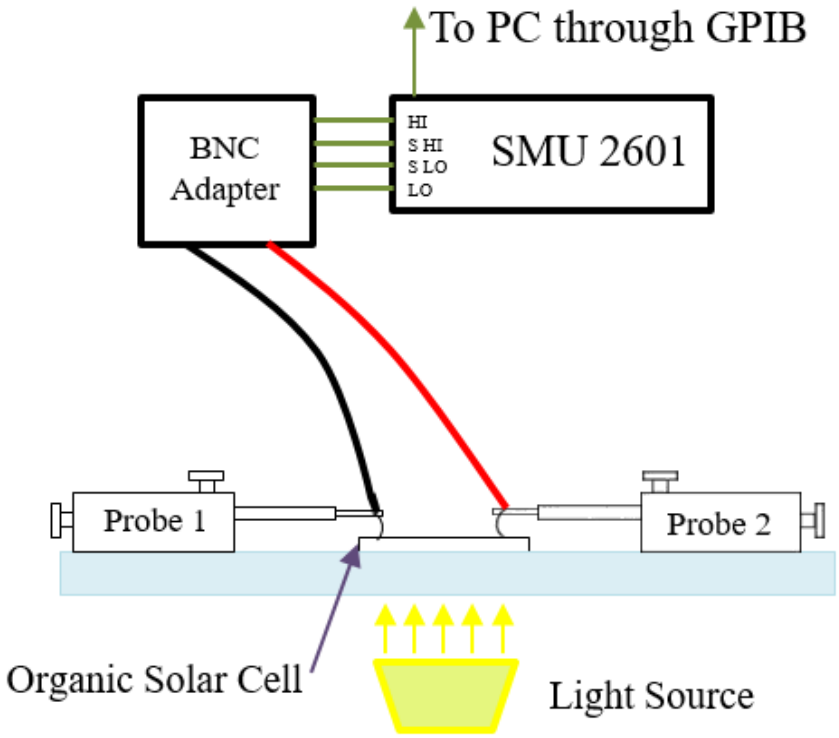

Figure 4.24: Full connection to test solar cell

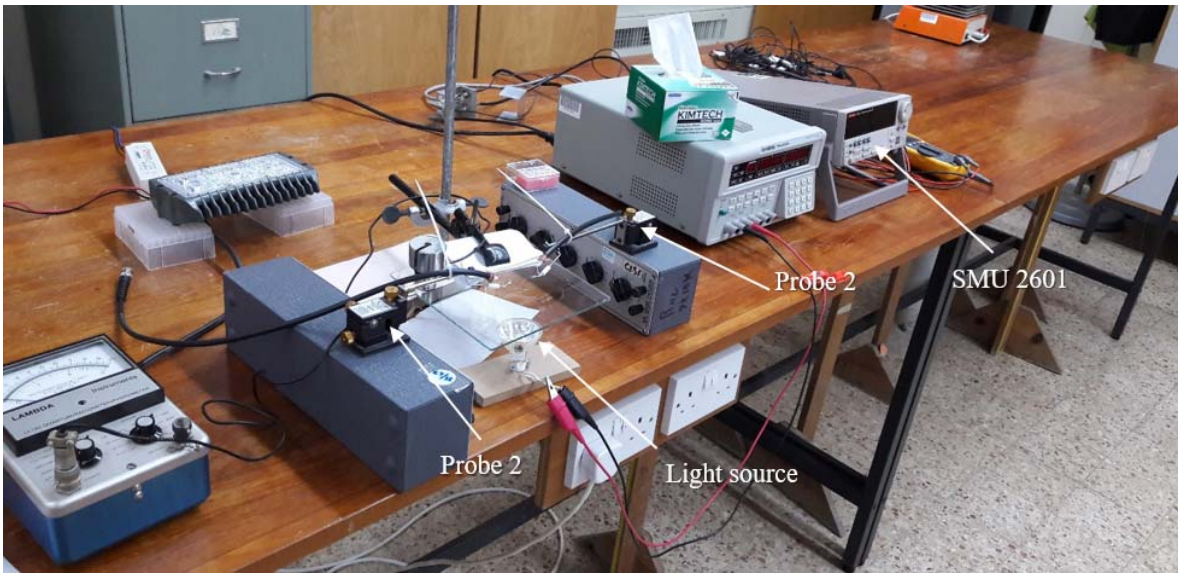

Figure 4.25: Solar cell testing setup at Physics Lab, Bethlehem University

Chapter 5

Results and Analysis

In this chapter the results and the best obtained efficiency with the best active layer blend ratio (P3HT:ICBA) are presented . That include IV measurements using the four probe station and Keithley 2601 to conclude about the effects of blend ratio on the efficiency.

5.1 IV - Characteristics

Table 5.1 summarizes IV characteristics and efficiency dependence on blend ratio. The input power for all setups was 100 mW/cm^2 and the active area is around 0.25 cm^2 for all cells. The table shows the parameters that affect the efficiency of the cells. The measurements that got from Keithley 2601 was processed using Origin Lab 2019 software using fitting "Nonlinear Implicit Curve Fit "with Solar Cell IV function. Full data in Appendix A.

Table 5.1: IV measurements

Cell #	I_{SC} (mA)	J_{SC} (mA/cm^2)	V_{OC} (V)	I_{max} (mA)	J_{max} (mA/cm^2)	V_{max} (V)	FF	η
1:1	0.2827	1.3965185	0.84808	0.26372	1.302320	0.68	0.74772	0.89%
2:1	0.3467	1.4114571	0.09001	0.170378	0.693439	0.04405	0.24043	0.03%
3:1	0.0523	0.2128938	0.44837	0.03894	0.158484	0.3655	0.60684	0.06%
1:2	0.0022	0.0087491	0.43389	0.001249	0.004868	0.22868	0.29329	0.0011%
1:3	0.3455	1.3470955	0.09001	0.170378	0.664241	0.04405	0.24131	0.03%

Figures 5.1, 5.2 show the IV and PV curves for our cells. Some of these curves are similar to a typical solar cell as for the 1:1 and 3:1 blends. Other blends like 2:1 and 1:3 do not show this typical behavior in their IV curves. This could be due to some parameters such as irradiation current (I_{ph}), saturation current of the diode (I_s), diode ideality factor (N), thermal voltage (V_t), series resistor (R_s) and parallel resistor (R_{sh}). These blends of 2:1 and 1:3 blends have high short circuit current I_{SC} but they have very low open circuit voltage V_{OC} that depends on the mentioned parameters. IV for 1:2 blend it has very low I_{SC} and V_{OC} and dose not behave like a solar cell.

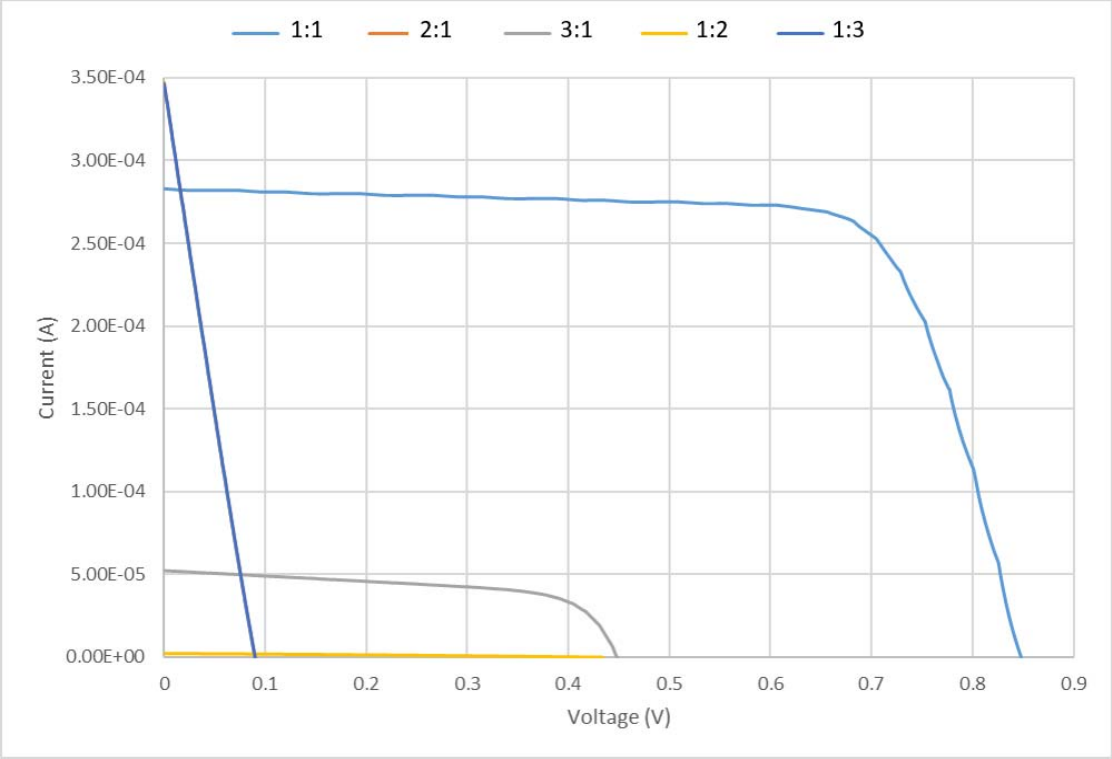

Figure 5.1: IV curves of solar cell

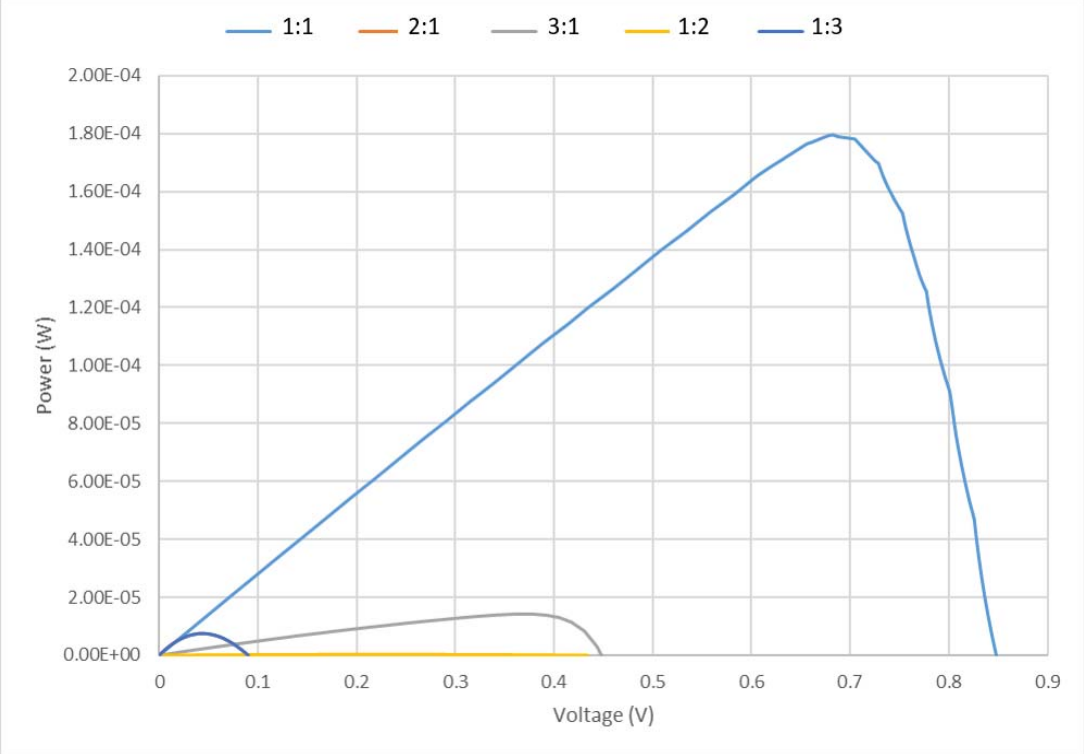

Figure 5.2: PV curves of solar cell

5.2 Influence of the Active Layer Blend Ratio on Efficiency

The highest efficiency η from our data in table 5.1 was achieved at 1:1 blend ratio with 0.89%. This efficiency is considered very low since experiment was done at ambient and not in gloves box with controlled atmosphere, followed by 3:1, 2:1 and 1:3 blend ratios and finally 1:2 is the lowest. For the IV curves, the 2:1 has the highest current most of the time but it falls earlier (decreases) compared to other blends. From the 1:1 IV curve, the maximum power achieved at around 0.68 V. Figure 5.3 shows the efficiency versus the blend ratios.

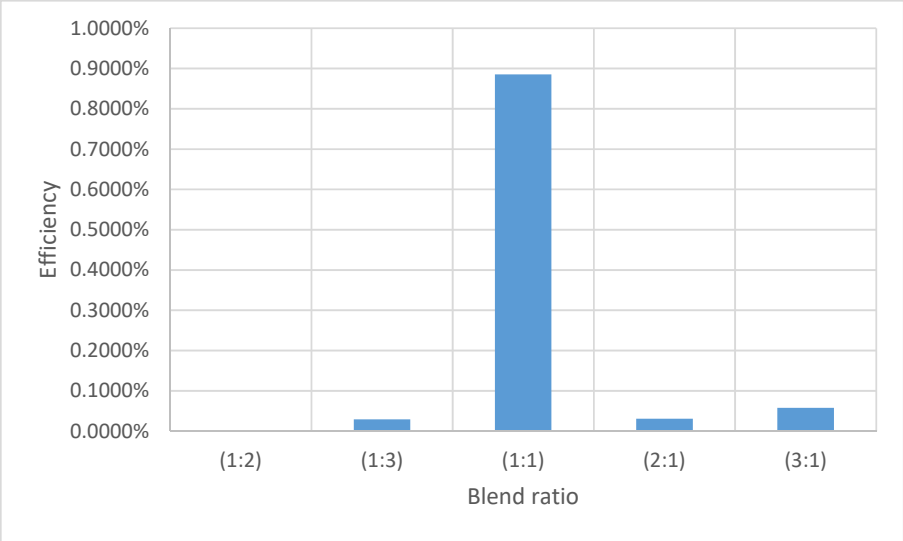

Figure 5.3: Efficiency versus the blend ratio

Chapter 6

Solar Cell Modeling

6.1 Modeling

Modelling is obtaining related data about how something will act without really trying it in real life. Modelling is using models either statically or over time, to build up data as a basis for making technical decisions using software without do it experimentally [71].

First there is difference between modeling and simulation. Modelling is meaningful abstraction of reality, follow-on in the proper necessity of a conceptualization and fundamental assumptions and constraints. Simulation is execution of a model over time. In other words, conceptualization (modelling) and implementation (simulation) are two activities that are jointly dependent, but can be conducted by separate individuals.

Modelling and simulation has helped to reduce expenses, enhance the feature of products and systems.

6.1.1 Features of Simulation:

- Simulation is cheaper and safer than done experimentally.
- As compared to the conventional experiments, simulations can be more realistic because it permits free formation of surroundings parameters that are obtained in the active application area of the final product.
- As compared to real time, execution of simulation is faster.
- Set up of a coherent synthetic environment is permitted by simulation which allows addition of simulated systems in the premature analysis phase through mixed virtual systems with virtual check surrounding to first prototypical elements for concluded system. If managed perfectly, the surrounding can be migrated from the growth and test domain to the domain of training and learning in resulting life cycle phases for the systems.

6.1.2 Steps of Modelling

the modelling can be divide into four basic steps as follows [71]:

- Monitor: Conceptual model of ground profile and job objectives are developed.
- Measure: Theoretical model is developed which is used to explain the main processes running in the problem.
- Describe: Mathematical explanation of these processes are developed and to get a perfect solution verification is done.
- Verify: Under the light of experimental physical reality, results of mathematical expression is interpreted. Confirm the suggestion, get additional measurements, enhance the complexity or precision of the mathematical result, or modify your conceptual understanding until you have complete understanding of the physical actuality.

6.2 Mathematical Modelling

The mathematical model method that we can take out a complex physical actuality to suitable mathematical reality on which designing of system is based. Development of suitable mathematical expression is done in numerical modelling. Mathematical modelling is a group of mathematical expressions that show the variation of a system from one state to another state (differential equations) and dependence of one variable to the other variable (state equations). The use of mathematical words to describe the performance of a system is mathematical modelling. Performance of photovoltaic system [72] is also illustrated by mathematical modelling. Number of different parameters (series and shunt resistance, ideality factor, reverse saturation current, open circuit voltage, short circuit current, fill factor, photo-generated current, efficiency) of photovoltaic system can be calculated by mathematical modelling.

6.2.1 Types of Mathematical Modelling

These can divided into either numerical models or analytical models.

1. Numerical Modelling

It is one of the type of mathematical modelling in which numerical time stepping method is used to obtain model response over time. Results are presented in the form of graph or table.

2. Analytical Modelling

Modelling having a closed form results called analytical modelling. In closed form results, mathematical analytic functions are used to present the response to the equations that describe variation in a system.

6.3 Organic Solar Cell (P3HT:ICBA) Modelling

One of the important characteristics of organic materials is their extremely small mobility, which makes modelling of their electrical properties difficult. Another problem in the electrical modelling of organic thin film devices was the lack of unique and precise electrical parameters for very thin layers of materials and occasionally lack of any information.

First: Organic Solar Cell Equivalent Circuit

The single diode equivalent circuit was used as shown in figure 6.1.

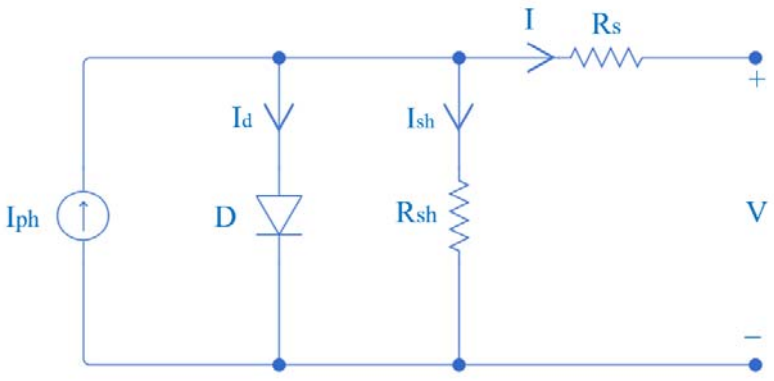

Figure 6.1: Single diode equivalent circuit

Second: Equation that Describe the Equivalent Circuit

Equation 6.1 describe the output current [73].

$$I = I_{ph} - I_s\left(e^{\left(\frac{(V+IR_s)}{(N\,V_t)}\right)} - 1\right) - \frac{(V + IR_s)}{R_{sh}} \quad (6.1)$$

Where:

I_{ph} : Irradiation current or photo generated current.

I_s : Saturation current of the diode.

N : Diode ideality factor.

V_t : Thermal voltage.

R_s : Series resistor.

R_{sh} : Parallel resistor.

Third: Solar Cell Parameters Extraction

There many methods for extraction the solar cell parameter, the method that was used will describe and compare the result with other methods. The MATLAB was used for optimization function fminsearch to fit IV output curves for the parameter of solar cell to data. The optimization function fminsearch use Nelder-Mead simplex algorithm. This algorithm uses a simplex of n + 1 points for n-dimensional vectors x. The algorithm first makes a simplex around the initial guess x_0 by adding 5% of each component $x_0(i)$ to x_0, and using these n vectors as elements of the simplex in addition to x_0. (It uses 0.00025 as component *i* if $x_0(i)$ = 0.) Then, the algorithm modifies the simplex repeatedly according to the following procedure [74].

Let $x(i)$ denote the list of points in the current simplex, $i = 1,...,n+1$.

1. Order the points in the simplex from lowest function value $f(x(1))$ to highest $f(x(n+1))$. At each step in the iteration, the algorithm discards the current worst point $x(n+1)$, and accepts another point into the simplex. [Or, in the case of step 7 below, it changes all n points with values above $f(x(1))$].
2. Generate the *reflected* point

   $$r = 2m - x(n+1),$$

   where

   $$m = \Sigma x(i)/n,\ i = 1...n, \quad \text{and calculate } f(r).$$

3. If $f(x(1)) \leq f(r) < f(x(n))$, accept r and terminate this iteration. **Reflect**
4. If $f(r) < f(x(1))$, calculate the expansion point s

   $$s = m + 2(m - x(n+1)), \text{ and calculate } f(s).$$

   a. If $f(s) < f(r)$, accept s and terminate the iteration. **Expand**

   b. Otherwise, accept r and terminate the iteration. **Reflect**
5. If $f(r) \geq f(x(n))$, perform a *contraction* between m and the better of $x(n+1)$ and r:

   a. If $f(r) < f(x(n+1))$ (i.e., r is better than $x(n+1)$), calculate

      $$c = m + (r - m)/2$$

      and calculate $f(c)$. If $f(c) < f(r)$, accept c and terminate the iteration. **Contract outside** Otherwise, continue with Step 7 (Shrink).

   b. If $f(r) \geq f(x(n+1))$, calculate

      $$cc = m + (x(n+1) - m)/2$$

      and calculate $f(cc)$. If $f(cc) < f(x(n+1))$, accept cc and terminate the iteration. **Contract inside** Otherwise, continue with Step 7 (Shrink).
6. Calculate the n points

   $$v(i) = x(1) + (x(i) - x(1))/2$$

   and calculate $f(v(i))$, $i = 2,...,n+1$. The simplex at the next iteration is $x(1)$, $v(2),...,v(n+1)$. **Shrink.** As shown in figure 6.2.

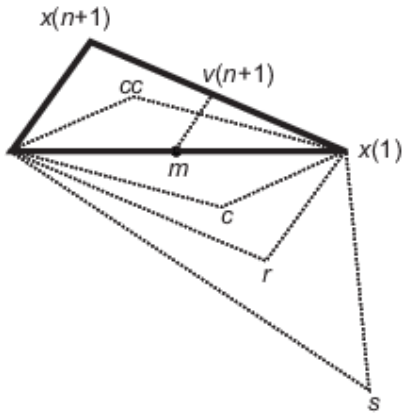

Figure 6.2: How Nelder-Mead algorithm work

For more details about Nelder-Mead method see appendix C.

The fminsearch[2] optimization applied in MATLAB using solar cell parameter tuning that fit the IV curve of the model with the measured data when the model finish display the extracted value of solar cell parameter (I_{ph}, I_s, R_s, R_{sh}, N) as shown in figure 6.3

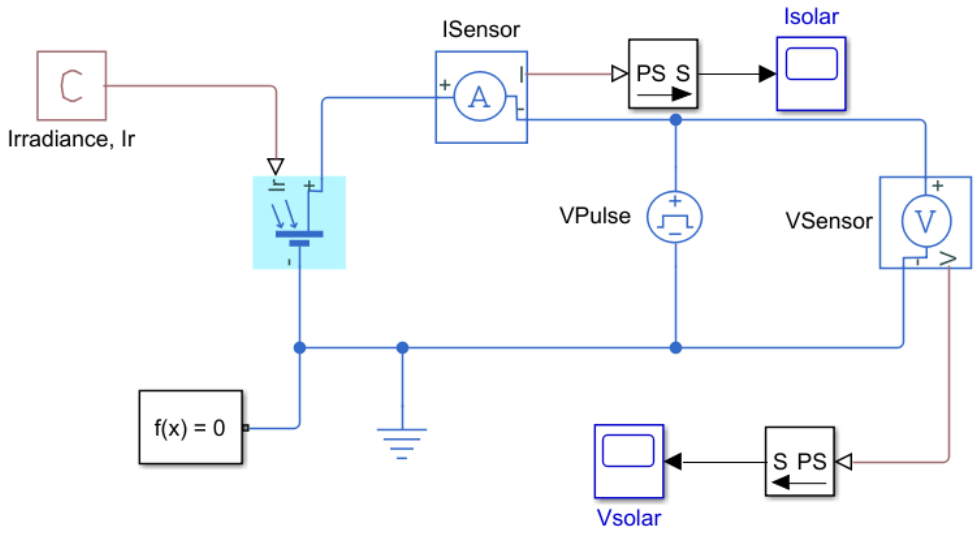

Figure 6.3: Solar cell Parameter tuning model

[2] Fminsearch: is one of optimization function in Matlab

This model needs initial value for the parameter to start optimization the value can be set as the following:

$$I_{ph} = I_{sc} \tag{6.2}$$

$$I_s = \frac{I_{ph}}{e^{(V_{oc}/0.025xN)} - 1} \tag{6.3}$$

R_s, R_{sh} : are estimated from the linear slope at the open circuit voltage (Voc) and the short circuit current (Isc) regions,respectively as shown in figure 6.4 [75].

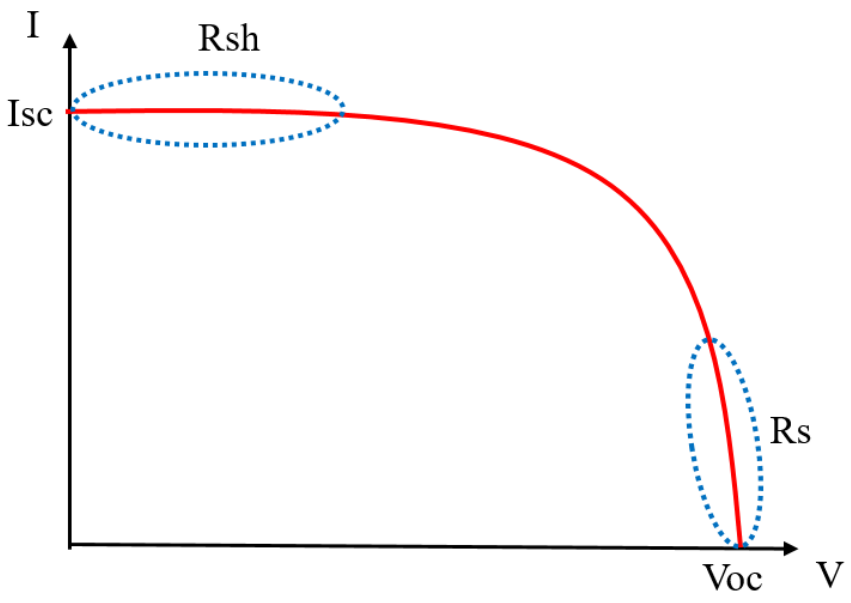

Figure 6.4: IV curve constant voltage and constant current regions

Before using this method for our data we must approve it. So some data was taken from published paper " Parameter identification for solar cell models using harmony search-based algorithms " in this paper there a measured data for IV and value for solar cell parameter using different method.

The optimization started with initial value:

I_s = $3x10^{-07}$ A

I_{ph} = 0.76 A

N = 1.5

R_s = 0.11Ω

R_{sh} = 46 Ω

After optimization the following value was got, figure 6.4 shows the IV measured data vs the model:

I_s = 2.95873x10^{-07} A

I_{ph} = 0.760948 A

N = 1.51318

R_s = 0.0383452 Ω

R_{sh} = 55.6059 Ω

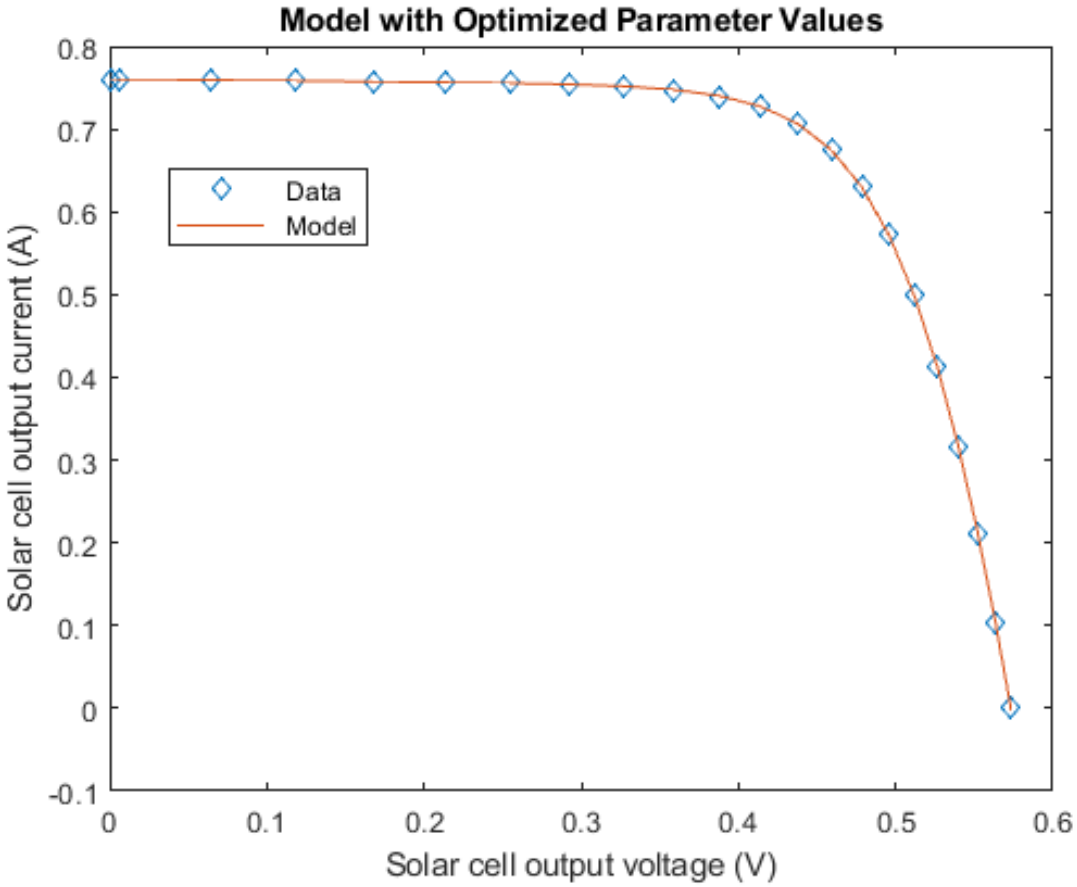

Figure 6.5: MATLAB curve for the extracted parameter

By comparing results with data from the same mentioned paper [76], it is found that our results are of the same range with other algorithms, so the method is approved and can be used it. Results are shown in table 6.1.

Table 6.1: Comparison between many algorithms with Nelder-Mead method (NM).

Item	HS	GGHS	IGHS	SA	PS	GA	CPSO	NM
Rs (Ω)	0.03663	0.03631	0.03613	0.0345	0.0313	0.0299	0.0354	0.038345
Rsh (Ω)	53.5946	53.0647	53.2845	43.1034	64.1026	42.3729	59.012	55.6059
Iph (A)	0.7607	0.76092	0.76077	0.762	0.7617	0.7619	0.7607	0.760948
Isd (μA)	0.30495	0.3262	0.34351	0.4798	0.998	0.8087	0.4	0.29587
N	1.47538	1.48217	1.4874	1.5172	1.6	1.5751	1.5033	1.51318

The measured data (IV curve) applied with the same process in MATLAB, the following parameter were got as shown in table 6.2, the table shows different values of extracted parameters for each active layer ratio. The best solar cell which has very small R_s value and very high value R_{sh}. In the following results the most efficient cell doesn't has the smallest value of R_s and highest value of R_{sh} because the cells best values have very small open circuit voltage.

Table 6.2: Extracted parameters for the solar cells.

Ratio	Is (A)	Iph (A)	N	R_s (Ω)	R_{sh} (Ω)
1:1	1.08E-12	0.00028	1.699787	195.5447	551680.3
2:1	2.77E-24	0.000465	1.353978	67.17241	189.9345
3:1	7.38E-12	5.20E-05	1.127785	1.13E-07	34377.41
1:2	2.80E-08	2.29E-06	5.693788	0.023784	239468.2
1:3	9.74E-15	0.000478	2.529305	72.84437	185.619

The modeling including curves that compare between the measured data and model based on the extracted parameters as shown in figure 6.6 – figure 6.10.

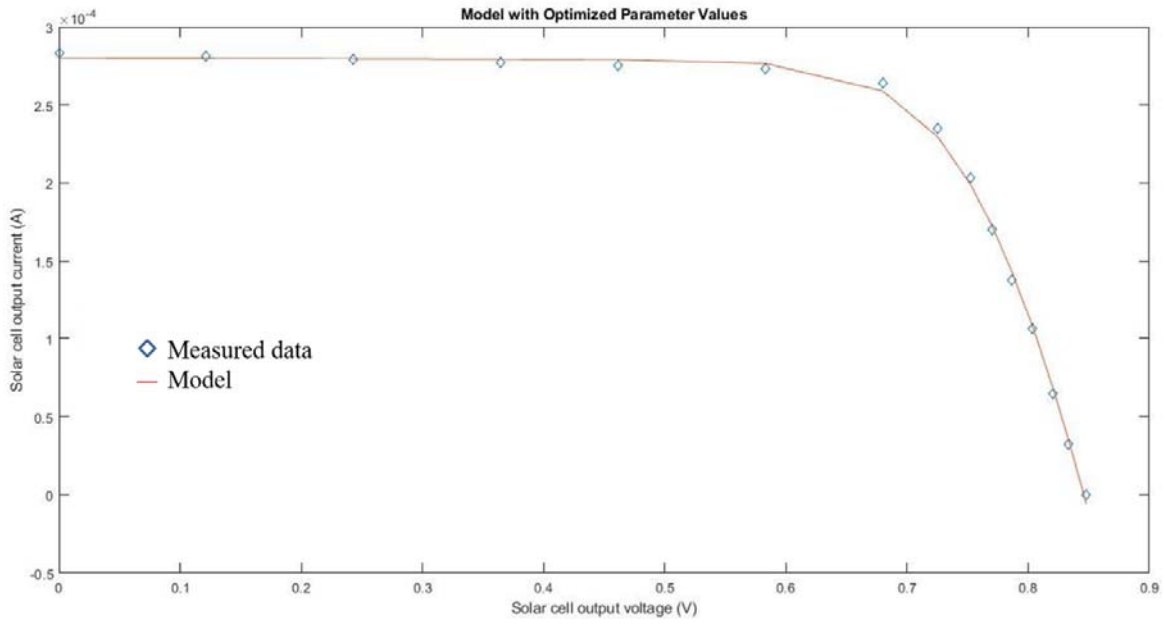

Figure 6.6: MATLAB curve for the extracted parameter for 1:1

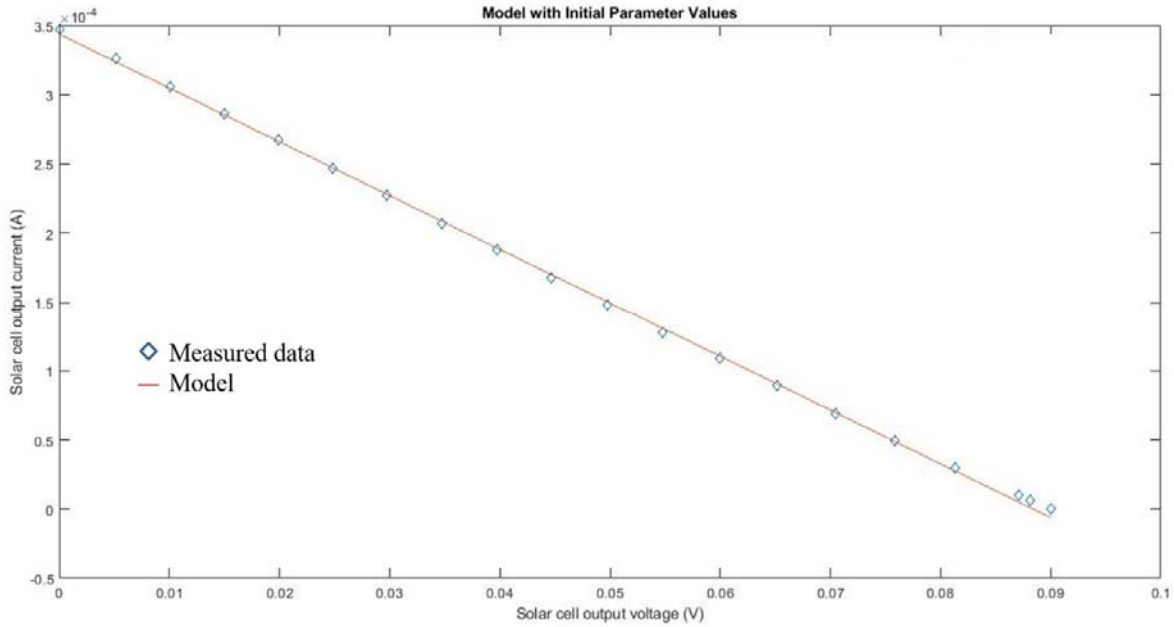

Figure 6.7: MATLAB curve for the extracted parameter for 2:1

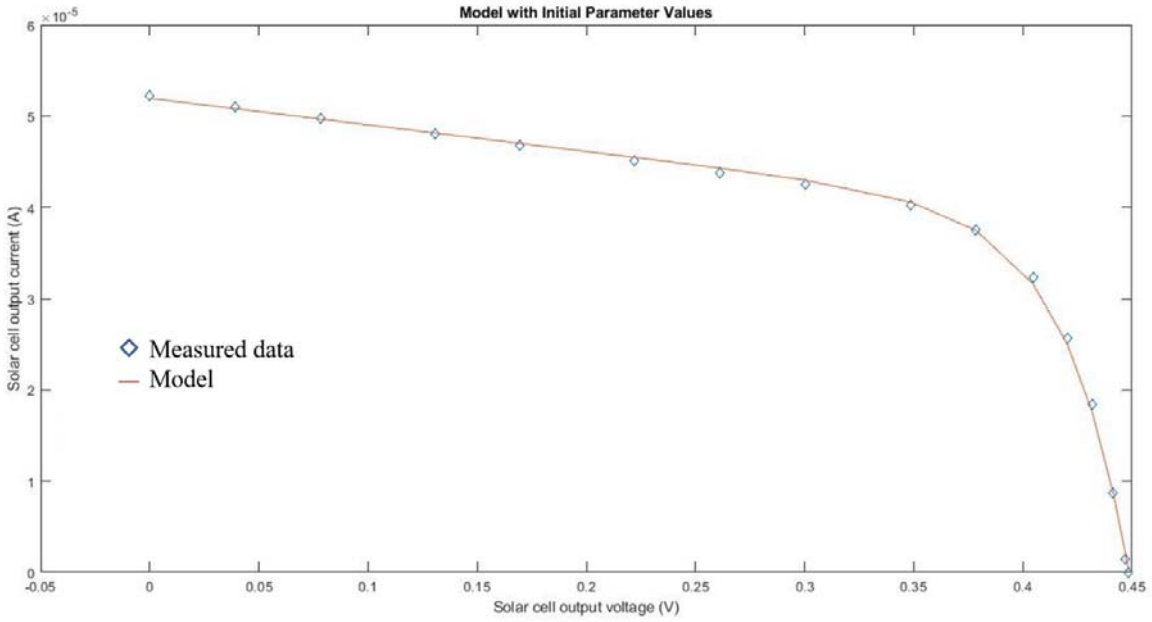

Figure 6.8: MATLAB curve for the extracted parameter for 3:1

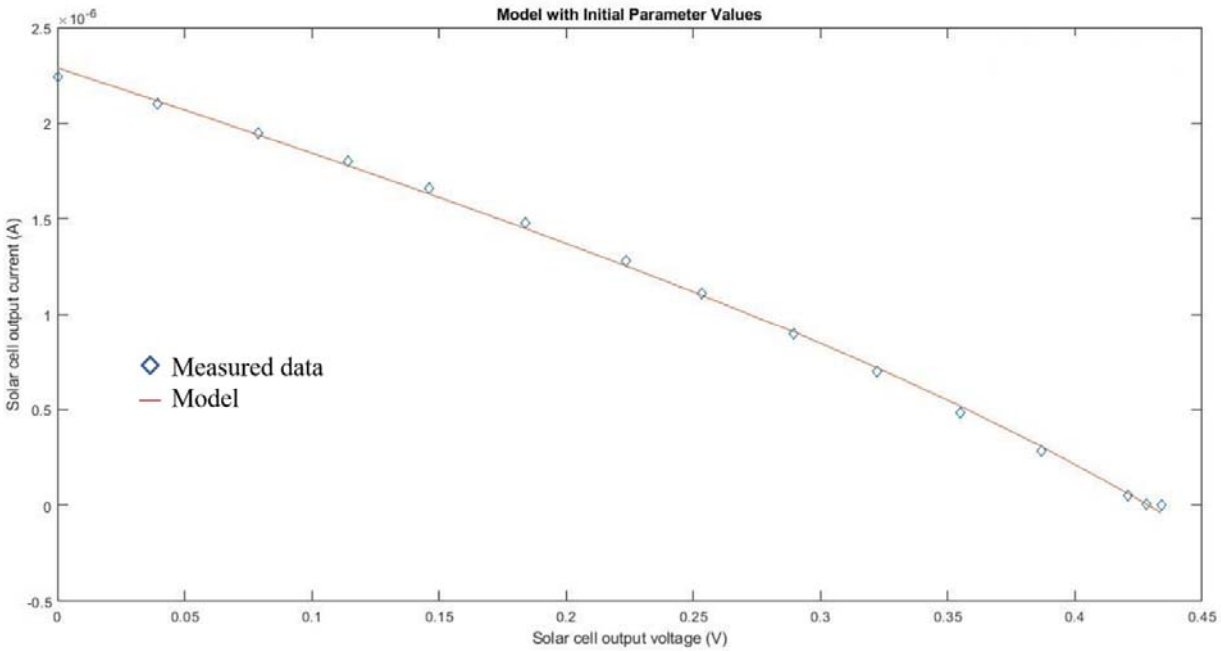

Figure 6.9: MATLAB curve for the extracted parameter for 1:2

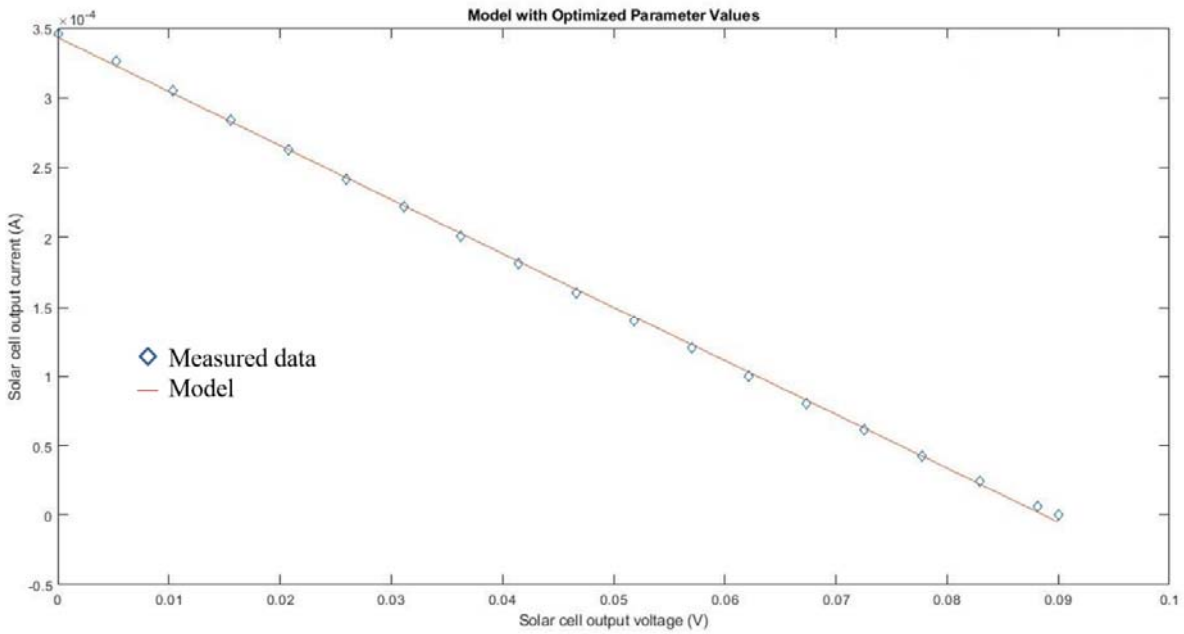

Figure 6.10: MATLAB curve for the extracted parameter for 1:3

Forth: Simulation

For simulation, the MATLAB was used also which is a high performance technical computing language. Because of quality of MATLAB a system of number of numerical equations used for electrical simulating of bilayer organic solar cell are solved easily and in better way as compared to other programming languages.

Our simulation model was built to simulate models using Simulink. Our model contains irradiation source, variable load, ammeter, voltmeter, power meter and solar cell block. This block built base on the equivalent circuit for solar cell a parallel combination of a current source, diode and a parallel resistor R_{sh}, which are connected in series with a resistance R_s. Our load start from zero ohm to infinite ohm and storage the values in workspaces as shown in figure 6.6.

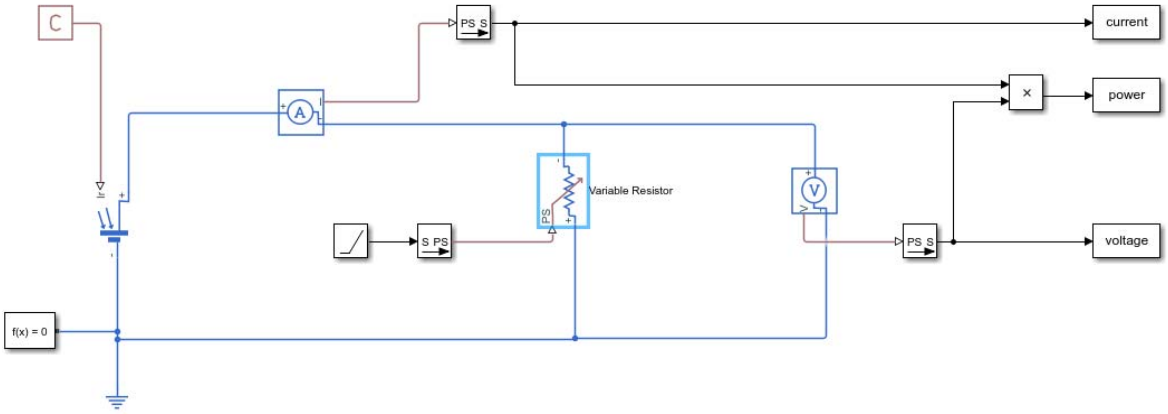

Figure 6.11: Our Simulink model

After that we simulated our model for the (1:1) ratio sample at different irradiation (400 W/m^2, 600 W/m^2, 800 W/m^2. 1000 W/m^2) got the following curves as shown in figure 6.12 current voltage curve and figure 6.13 power voltage curve.

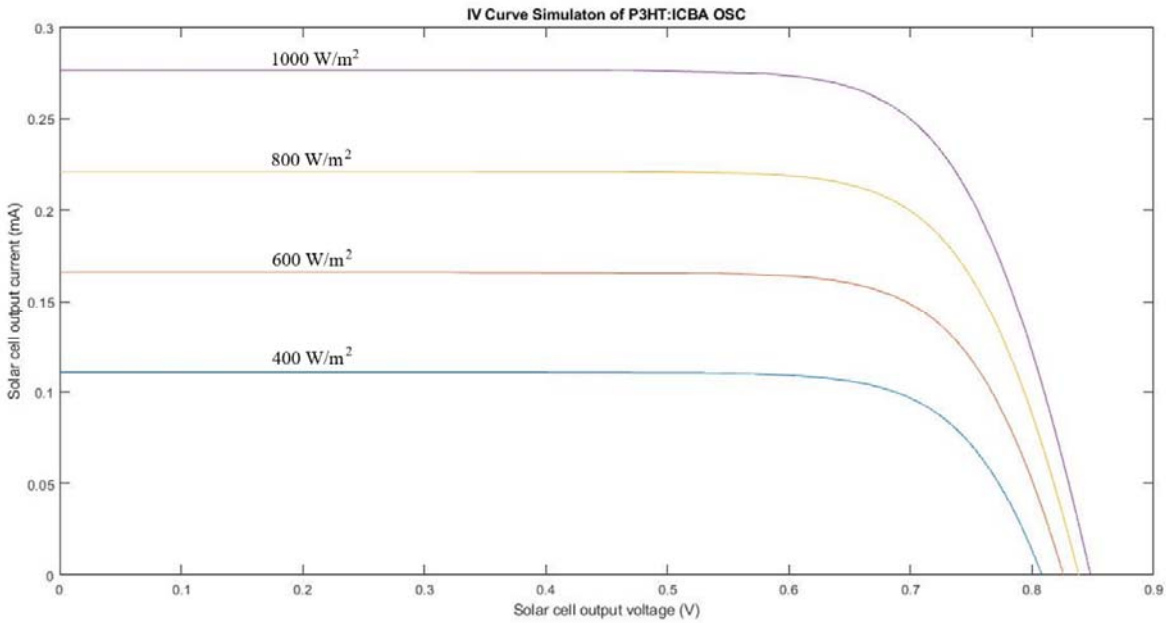

Figure 6.12: IV curve of simulation for 1:1

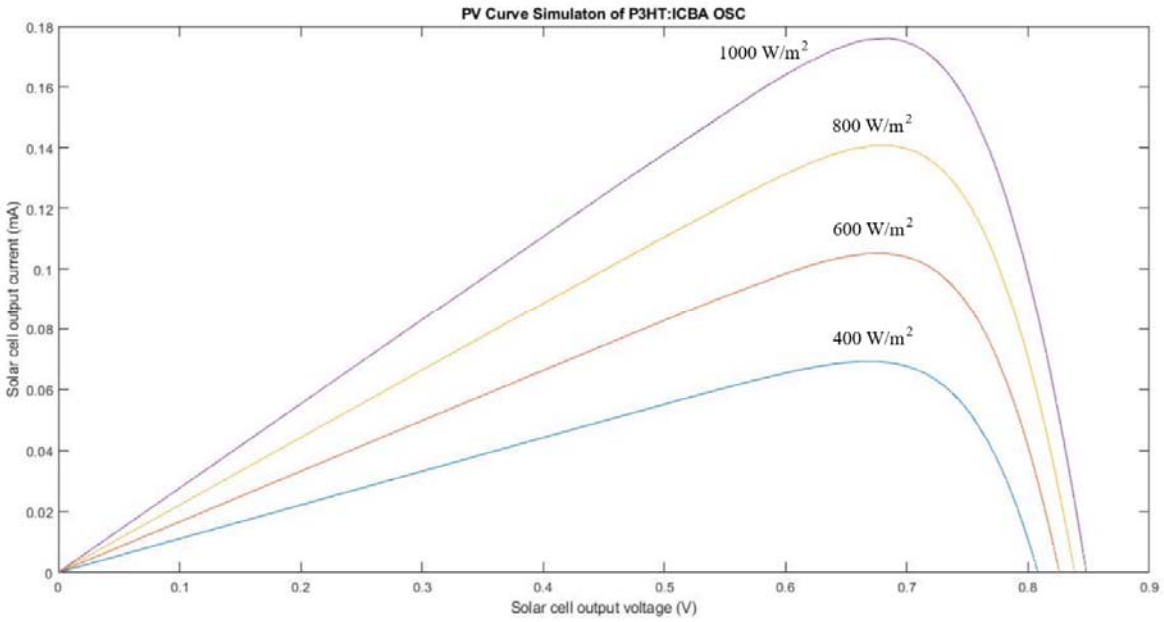

Figure 6.13: PV curve of simulation for 1:1

Chapter 7

Conclusions and Recommendations

7.1 Summary of Conclusions

In this thesis, different OPV cells have been built and tested. Different parameters affecting the efficiency are investigated in the blend ratio. The conclusion is summarized in the following, referring to the parameters involved in building the solar cell.

Study of the effect of the active layer ratio between the acceptor and the donor on efficiency revealed that the best ratio was achieved for the 1:1 blend with a percentage of around 0.89% of conversion efficiency. Our data could have measurements errors or a result of the process of coating that could have affected the actual ratio due to the difference in viscosity.

The active layer thickness, according to [77] and many researches the best value is around 100nm. This thickness is expected as it is comparable to the range of the polymers short excitation diffusion length.

In what concern the input power effect on the efficiency, an ideal fixed band structure in the photovoltaic material affects the output current in a way to be proportional to the incident radiation intensity and while voltage should not depend on that intensity. This could be due to the band structure changes as a result of the variation in the number of exitons created due to the radiation. This is besides the effect of temperature. In other words, the efficiency should not suffer if the band structure is not dependent on the intensity of the incident light. From our measurement, it seems the effect of intensity on the band structure is not significant because we achieved efficiencies comparable to near optimum conditions. Still we cannot exclude the effect. Certainly it will make better results if compared with different incident intensities.

Gold (Au), silver (Ag) and non-pure aluminum (Al) for organic solar cell electrodes, using these materials through thermal vacuum evaporator destroy the cell\s active layer.

Gaussian is very useful tool that could depend on to give first indication “energy band gap“ to design new materials in the fabrication of organic solar cells.

7.2 Recommendations for Future Work

Our research is concerned with improving the efficiency of organic solar.

Many solutions are suggested, first using glove box to build organic solar cell in ideal environment and using AFM to improve the morphology of the cell. Second by doping the n-type and p-type to bridge the bandwidth and change the alignment of the polymers, to increase the absorption coefficient.

Another solution is to build multi junction organic solar cell that make the area of one cell similar to area of two or more solar cells based on the number of junction. The multi-junction OPV cells can achieve higher efficiency [78].

Another method using Gaussian software to develop new donors and acceptors and calculate the HOMO- LUMO energy to make the energy difference between the HOMO-LUMO of the donor as lowest as possible and the difference between LUMO of donor and HOMO of acceptor as highest as possible to improve the efficiency of organic solar cell. With promising properties like high absorption coefficient, solubility, small band gap; high mobility and percolating morphology.

Another solution to improve efficiency is by adding metallic nano-particles (gold) in order to block the excitons recombination because of its plasmon effect [79].

Using ZnO (Zinc Oxide) nano-particles instead of PEDOT:PSS is another way to improve efficiency, because ZnO is an electron transport layer owing to its suitable properties such as

high electron mobility, easy fabrication process and most importantly its match of conduction band with the lowest unoccupied molecular orbital (LUMO) of almost all organic semiconductors [80, 81]. On the other hand ZnO could be used in the organic solar cell to be embedded in the active layer.

REFERENCES

1. Green, M.A., K. Emery, D.L. King, Y. Hishikawa, and W. Warta, *Solar cell efficiency tables (version 28).* Progress in Photovoltaics: Research and Applications, 2006. **14**(5): p. 455-461.
2. Li, G., V. Shrotriya, J. Huang, Y. Yao, T. Moriarty, K. Emery, and Y. Yang, *High-efficiency solution processable polymer photovoltaic cells by self-organization of polymer blends.* Nature Materials, 2005. **4**(11): p. 864-868.
3. Williams, R., *Becquerel Photovoltaic Effect in Binary Compounds.* The Journal of Chemical Physics, 1960. **32**(5): p. 1505-1514.
4. Tress, W., *Organic solar cells : theory, experiment, and device simulation*. Springer series in materials science. 2014, Cham: Springer.
5. Ibn-Mohammed, T., S.C.L. Koh, I.M. Reaney, A. Acquaye, G. Schileo, K.B. Mustapha, and R. Greenough, *Perovskite solar cells: An integrated hybrid lifecycle assessment and review in comparison with other photovoltaic technologies.* Renewable and Sustainable Energy Reviews, 2017. **80**: p. 1321-1344.
6. Green, M.A., Y. Hishikawa, E.D. Dunlop, D.H. Levi, J. Hohl-Ebinger, and A.W.Y. Ho-Baillie, *Solar cell efficiency tables (version 51).* Progress in Photovoltaics: Research and Applications, 2018. **26**(1): p. 3-12.
7. *https://www.nobelprize.org/prizes/chemistry/2000/summary/*. 2019.
8. Krebs, F.C., M. Hösel, M. Corazza, B. Roth, M.V. Madsen, S.A. Gevorgyan, R.R. Søndergaard, D. Karg, and M. Jørgensen, *Freely available OPV-The fast way to progress.* Energy Technology, 2013. **1**(7): p. 378-381.
9. Krebs, F.C., *Processing and preparation of polymer and organic solar cells.* Solar Energy Materials and Solar Cells, 2009. **93**(4): p. 393-393.
10. Bishop, C.A., *Vacuum deposition onto webs, films and foils*. Third edition ed. 2015, Amsterdam: Elsevier / William Andrew Publishing. xix, 582 pages.
11. Klauk, H., *Organic electronics : materials, manufacturing and applications*. 2006, Weinheim: Wiley-VCH. xvii, 428 p.
12. Mohammad Bagher, A., *Comparison of Organic Solar Cells and Inorganic Solar Cells.* International Journal of Renewable and Sustainable Energy, 2014. **3**(3): p. 53.
13. Hoppe, H. and N.S. Sariciftci, *Organic solar cells: An overview.* Journal of Materials Research, 2004. **19**(07): p. 1924-1945.
14. Green, M.A., K. Emery, Y. Hishikawa, W. Warta, and E.D. Dunlop, *Solar cell efficiency tables (version 41).* Progress in Photovoltaics: Research and Applications, 2013. **21**(1): p. 1-11.
15. Heliatek, *A new world record for organic solar technology with a cell efficiency of 12%.* Press Release, 2013.
16. Zhang, K., *New Conjugated Polymers Based on Benzodifuranone and Diketopyrrolopyrrole.* Thesis, 2010.
17. Bernède, J.C., A. Godoy, L. Cattin, F.R. Diaz, M. Morsli, and M.A.d. Valle, *Organic Solar Cells Performances Improvement Induced by Interface Buffer Layers.* Solar Energy, Radu D Rugescu (Ed.), 2010.
18. Choy, W.C.H. and SpringerLink (Online service), *Organic Solar Cells Materials and Device Physics*, in *Green Energy and Technology,*. 2013, Springer London : Imprint: Springer,: London. p. V, 265 p. 140 illus., 49 illus. in color.
19. Gunes, S., H. Neugebauer, and N.S. Sariciftci, *Conjugated Polymer – Based Organic Solar Cells.* American Chemical Society, 2007. **107**(4): p. 1324.
20. Facchetti, A., *Polymer donor–polymer acceptor (all-polymer) solar cells.* Materials Today, 2013. **16**(4): p. 123-132.

21. Guo, C., Y.H. Lin, M.D. Witman, K.A. Smith, C. Wang, A. Hexemer, J. Strzalka, E.D. Gomez, and R. Verduzco, *Conjugated block copolymer photovoltaics with near 3% efficiency through microphase separation.* Nano Lett, 2013. **13**(6): p. 2957-63.
22. Scharber, M.C. and N.S. Sariciftci, *Efficiency of bulk-heterojunction organic solar cells.* Prog Polym Sci, 2013. **38**(12): p. 1929-1940.
23. Nelson, J., *Polymer:fullerene bulk heterojunction solar cells.* Materials Today, 2011. **14**(10): p. 462-470.
24. Mori, S., H. Oh-oka, H. Nakao, T. Gotanda, Y. Nakano, H. Jung, A. Iida, R. Hayase, N. Shida, M. Saito, K. Todori, T. Asakura, A. Matsui, and M. Hosoya, *Organic photovoltaic module development with inverted device structure.* MRS Proceedings, 2015. **1737**.
25. Topham, P.D., A.J. Parnell, and R.C. Hiorns, *Block copolymer strategies for solar cell technology.* Journal of Polymer Science Part B: Polymer Physics, 2011. **49**(16): p. 1131-1156.
26. Gregg, B.A. and M.C. Hanna, *Comparing organic to inorganic photovoltaic cells: Theory, experiment, and simulation.* Journal of Applied Physics, 2003. **93**(6): p. 3605-3614.
27. *https://www.sigmaaldrich.com/*. 2018.
28. Jain, A. and A. Kapoor, *A new approach to study organic solar cell using Lambert W-function.* Solar Energy Materials and Solar Cells, 2005. **86**(2): p. 197-205.
29. Hamakawa, Y., *Thin film solar cells: Next generation photovoltaics and it application.* Springer Series in Photonics, 2004.
30. McEvoy, A.J., T. Markvart, and L. Castañer, *Practical handbook of photovoltaics : fundamentals and applications*. 2nd ed. 2012, Amsterdam ; London: Elsevier Academic Press. xxiv, 1244 p.
31. Scharber, M.C., D. Mühlbacher, M. Koppe, P. Denk, C. Waldauf, A.J. Heeger, and C.J. Brabec, *Design Rules for Donors in Bulk-Heterojunction Solar Cells—Towards 10 % Energy-Conversion Efficiency.* Advanced Materials, 2006. **18**(6): p. 789-794.
32. Tomas Torres, G.B., *Organic Nanomaterials: Synthesis, characterization and Devise Application.* Wiley, 2013.
33. Hussein Selman, N., *Comparison Between Perturb & Observe, Incremental Conductance and Fuzzy Logic MPPT Techniques at Different Weather Conditions.* International Journal of Innovative Research in Science, Engineering and Technology, 2016. **5**(7): p. 12556-12569.
34. Schilinsky, P., C. Waldauf, and C.J. Brabec, *Recombination and loss analysis in polythiophene based bulk heterojunction photodetectors.* Applied Physics Letters, 2002. **81**(20): p. 3885-3887.
35. Dyakonov, V., *Electrical aspects of operation of polymer–fullerene solar cells.* Thin Solid Films, 2004. **451-452**: p. 493-497.
36. Hummelen, I.R.J.P.V.D.L.L.D.V.J.C., *Effect of Temperature and Illumination on the Electrical Characteristics of Polymer–Fullerene Bulk-Heterojunction Solar Cells.* Advanced Functional Materials, 2004. **14**: p. 38-44.
37. Janssen, J.K.J.v.D.X.Y.J.L.C.W.T.B.L.A.B.S.J.C.H.R.A.J., *Relating the Morphology of Poly(p-phenylene vinylene)/Methanofullerene Blends to Solar-Cell Performance.* Advanced Functional Materials 2004. **14**: p. 425-434.
38. Hoppe, H., N. Arnold, N.S. Sariciftci, and D. Meissner, *Modeling the optical absorption within conjugated polymer/fullerene-based bulk-heterojunction organic solar cells.* Solar Energy Materials and Solar Cells, 2003. **80**(1): p. 105-113.

39. C. J. Brabec, A.C., D. Meissner, N. S. Sariciftci, M. T. Rispens, L. Sanchez, J. C. Hummelen, T. Fromherz, *The influence of materials work function on the open circuit voltage of plastic solar cells.* Thin Solid Films, 2002. **403**: p. 368-372.
40. Brabec, C.J., S.E. Shaheen, C. Winder, N.S. Sariciftci, and P. Denk, *Effect of LiF/metal electrodes on the performance of plastic solar cells.* Applied Physics Letters, 2002. **80**(7): p. 1288-1290.
41. Shaheen, S.E., C.J. Brabec, N.S. Sariciftci, F. Padinger, T. Fromherz, and J.C. Hummelen, *2.5% efficient organic plastic solar cells.* Applied Physics Letters, 2001. **78**(6): p. 841-843.
42. Marcus, T.C.E., *P3HT:PCBM Bilayer Planar Heterojunction Organic Photovoltaic Thin Film Solar Cell Efficiency Optimisation*. 2012.
43. Jäger, K.-D., O. Isabella, A.H.M. Smets, R.A.C.M.M.v. Swaaij, and M. Zeman, *Solar energy : fundamentals, technology and systems*. 2016, UIT Cambridge,: Cambridge. p. 1 online resource.
44. Rühle, S., *Tabulated values of the Shockley–Queisser limit for single junction solar cells.* Solar Energy, 2016. **130**: p. 139-147.
45. Andersen, T.R., H.F. Dam, M. Hösel, M. Helgesen, J.E. Carlé, T.T. Larsen-Olsen, S.A. Gevorgyan, J.W. Andreasen, J. Adams, N. Li, F. Machui, G.D. Spyropoulos, T. Ameri, N. Lemaître, M. Legros, A. Scheel, D. Gaiser, K. Kreul, S. Berny, O.R. Lozman, S. Nordman, M. Välimäki, M. Vilkman, R.R. Søndergaard, M. Jørgensen, C.J. Brabec, and F.C. Krebs, *Scalable, ambient atmosphere roll-to-roll manufacture of encapsulated large area, flexible organic tandem solar cell modules.* Energy & Environmental Science, 2014. **7**(9): p. 2925.
46. Cramer, C.J., *Essentials of computational chemistry : theories and models*. 2nd ed. 2004, Chichester, West Sussex, England: Wiley. xx, 596 p.
47. Lewars, E.G., *Computational chemistry : introduction to the theory and applications of molecular and quantum mechanics*. 2nd ed. 2011, Dordrecht: Springer. xvi, 664 p.
48. *https://www.chemicool.com/definition/schrodinger_equation.html*. 2018.
49. *https://www.st-andrews.ac.uk/media/school-of-chemistry/documents/Gaussian.pdf*. 2018.
50. FISCHER, C.F., *GENERAL HARTREE-FOCK PROGRAM.* Computer Physics Communications, 1987. **43**: p. 11.
51. Barth, U.v., *Basic Density-Functional Theory-an Overview.* Physica Scripta, 2004. **T109**: p. 31.
52. Bertini, I., *Inorganic and bio-inorganic chemistry*. Encyclopedia of life support systems. 2009, Oxford: Eolss Publishers.
53. *Gaussian 09, Revision A.02,* M. J. Frisch, G. W. Trucks, H. B. Schlegel, G. E. Scuseria, M. A. Robb, J. R. Cheeseman, G. Scalmani, V. Barone, G. A. Petersson, H. Nakatsuji, X. Li, M. Caricato, A. Marenich, J. Bloino, B. G. Janesko, R. Gomperts, B. Mennucci, H. P. Hratchian, J. V. Ortiz, A. F. Izmaylov, J. L. Sonnenberg, D. Williams-Young, F. Ding, F. Lipparini, F. Egidi, J. Goings, B. Peng, A. Petrone, T. Henderson, D. Ranasinghe, V. G. Zakrzewski, J. Gao, N. Rega, G. Zheng, W. Liang, M. Hada, M. Ehara, K. Toyota, R. Fukuda, J. Hasegawa, M. Ishida, T. Nakajima, Y. Honda, O. Kitao, H. Nakai, T. Vreven, K. Throssell, J. A. Montgomery, Jr., J. E. Peralta, F. Ogliaro, M. Bearpark, J. J. Heyd, E. Brothers, K. N. Kudin, V. N. Staroverov, T. Keith, R. Kobayashi, J. Normand, K. Raghavachari, A. Rendell, J. C. Burant, S. S. Iyengar, J. Tomasi, M. Cossi, J. M. Millam, M. Klene, C. Adamo, R. Cammi, J. W. Ochterski, R. L. Martin, K. Morokuma, O. Farkas, J. B. Foresman, and D. J. Fox*, Gaussian, Inc., Wallingford CT.* 2016.
54. *http://gaussian.com/*. 2018.

55. Li, Y., D. Qi, P. Song, and F. Ma, *Fullerene-Based Photoactive Layers for Heterojunction Solar Cells: Structure, Absorption Spectra and Charge Transfer Process.* Materials (Basel), 2014. **8**(1): p. 42-56.
56. Liu, X., Y. Cai, X. Huang, R. Zhang, and X. Sun, *A perylene diimide electron acceptor with a triptycene core for organic solar cells.* Journal of Materials Chemistry C, 2017. **5**(12): p. 3188-3194.
57. Yu, Q., H.-B. Xie, T. Li, F. Ma, Z. Fu, Z. Wang, C. Li, Z. Fu, D. Xia, and J. Chen, *Atmospheric chemical reaction mechanism and kinetics of 1,2-bis(2,4,6-tribromophenoxy)ethane initiated by OH radical: a computational study.* RSC Advances, 2017. **7**(16): p. 9484-9494.
58. Posudievsky, O.Y., N.V. Konoshchuk, A.G. Shkavro, V.G. Koshechko, and V.D. Pokhodenko, *Structure and electronic properties of poly(3,4-ethylenedioxythiophene) poly(styrene sulfonate) prepared under ultrasonic irradiation.* Synthetic Metals, 2014. **195**: p. 335-339.
59. Pani, R.C., B.D. Bond, G. Krishnan, and Y.G. Yingling, *Correlating fullerene diffusion with the polythiophene morphology: molecular dynamics simulations.* Soft Matter, 2013. **9**(42): p. 10048.
60. Cheng, Y.-J., C.-H. Hsieh, Y. He, C.-S. Hsu, and Y. Li, *Combination of Indene-C60 Bis-Adduct and Cross-Linked Fullerene Interlayer Leading to Highly Efficient Inverted Polymer Solar Cells.* American Chemical Society, 2010. **132**: p. 3.
61. He, Y., H.-Y. Chen, J. Hou, and Y. Li, *Indene-C60 Bisadduct A New Acceptor for High-Performance Polymer Solar Cells.* American Chemical Society, 2010. **132**: p. 1377.
62. Kymissis, I. and SpringerLink (Online service), *Organic Field Effect Transistors Theory, Fabrication and Characterization*, in *Integrated Circuits and Systems,*. 2009, Springer Science+Business Media, LLC,: Boston, MA.
63. Thompson, B.C. and J.M. Frechet, *Polymer-fullerene composite solar cells.* Angew Chem Int Ed Engl, 2008. **47**(1): p. 58-77.
64. Kim, H., W.-W. So, and S.-J. Moon, *Effect of thermal annealing on the performance of P3HT/PCBM polymer photovoltaic cells.* Journal of the Korean Physics Society, 2005. **48**: p. 5.
65. Ge, W., *An overview on P3HT:PCBM, the most efficient organic solar cell material so far.* 2009.
66. Zhao, G., Y. He, and Y. Li, *6.5% Efficiency of polymer solar cells based on poly(3-hexylthiophene) and indene-C(60) bisadduct by device optimization.* Adv Mater, 2010. **22**(39): p. 4355-8.
67. Ng, A., X. Liu, C.H. To, A.B. Djurisic, J.A. Zapien, and W.K. Chan, *Annealing of P3HT:PCBM blend film--the effect on its optical properties.* ACS Appl Mater Interfaces, 2013. **5**(10): p. 4247-59.
68. Singh, I., D. Madhwal, J. Kumar, C.S. Bhatia, P.K. Bhatnagar, and P.C. Mathur, *Effect of thermal annealing on the efficiency of poly (3-hexylthiphone):[6,6]-phenyl- C61-butyric acid methyl ester bulk heterojunction solar cells.* Journal of Nanophotonics, 2011. **5**: p. 8.
69. *https://www.tek.com/*. 2018.
70. Benanti, T.L. and D. Venkataraman, *Organic Solar Cells: An Overview Focusing on Active Layer Morphology.* Photosynthesis Research, 2006. **87**(1): p. 73-81.
71. Law, A.M., *Simulation Modeling and Analysis*. Fifth ed. 2015: McGraw-Hill Education.
72. M. Abdulkadir, A.S.S., A. H. M. Yatim, *Modeling and Simulation of a Solar Photovoltaic System, Its Dynamics and Transient Characteristics in LABVIEW.*

International Journal of Power Electronics and Drive System (IJPEDS), 2013. **3**(2): p. 8.
73. Tamrakar, V., S.C. Gupta, and Y. Sawle, *Single-Diode Pv Cell Modeling And Study Of Characteristics Of Single And Two-Diode Equivalent Circuit.* Electrical and Electronics Engineering: An International Journal (ELELIJ), 2015. **4**(3): p. 12.
74. *https://www.mathworks.com/.* 2018.
75. Raj, S., A.K. Sinha, and A.K. Panchal, *Solar cell parameters estimation from illuminated I-V characteristic using linear slope equations and Newton-Raphson technique.* Journal of Renewable and Sustainable Energy, 2013. **5**: p. 8.
76. Askarzadeh, A. and A. Rezazadeh, *Parameter identification for solar cell models using harmony search-based algorithms.* Solar Energy 2012. **86**: p. 9.
77. Wan, Q., X. Guo, Z. Wang, W. Li, B. Guo, W. Ma, M. Zhang, and Y. Li, *10.8% Efficiency Polymer Solar Cells Based on PTB7-Th and PC71BM via Binary Solvent Additives Treatment.* Advanced Functional Materials, 2016. **26**(36): p. 6635-6640.
78. Xiao, X., K. Lee, and S.R. Forrest, *Scalability of multi-junction organic solar cells for large area organic solar modules.* Applied Physics Letters, 2015. **106**: p. 4.
79. Stratakis, E. and E. Kymakis, *Nanoparticle-based plasmonic organic photovoltaic devices.* Materials Today, 2013. **16**: p. 14.
80. Ullah, I., S.K. Shah, S. Wali, K. Hayat, S.A. Khattak, and A. Khan, *Enhanced efficiency of organic solar cells by using ZnO as an electron transport layer.* Materials Research Express, 2017. **4**: p. 15.
81. Zheng, Z., O.M. Awartani, B. Gautam, D. Liu, Y. Qin, W. Li, A. Bataller, K. Gundogdu, H. Ade, and J. Hou, *Efficient Charge Transfer and Fine-Tuned Energy Level Alignment in a THF-Processed Fullerene-Free Organic Solar Cell with 11.3% Efficiency.* Adv Mater, 2017. **29**(5).

APPENDECIES

Appendix A (Data)

Solar cell sample 1 (Blend ratio 1:1)

Voltage (V)	Current (A)	Power (W)
0.00E+00	2.83E-04	0.00E+00
0.02429	2.82E-04	6.86E-06
0.04857	2.82E-04	1.37E-05
0.07286	2.82E-04	2.05E-05
0.09714	2.81E-04	2.73E-05
0.12143	2.81E-04	3.41E-05
0.14571	2.80E-04	4.09E-05
0.17	2.80E-04	4.76E-05
0.19429	2.80E-04	5.43E-05
0.21857	2.79E-04	6.10E-05
0.24286	2.79E-04	6.77E-05
0.26714	2.79E-04	7.44E-05
0.29143	2.78E-04	8.11E-05
0.31571	2.78E-04	8.77E-05
0.34	2.77E-04	9.43E-05
0.36429	2.77E-04	1.01E-04
0.38857	2.77E-04	1.07E-04
0.41286	2.76E-04	1.14E-04
0.42206	2.76E-04	1.17E-04
0.43714	2.76E-04	1.21E-04
0.46143	2.75E-04	1.27E-04
0.48571	2.75E-04	1.34E-04
0.51	2.75E-04	1.40E-04
0.53429	2.74E-04	1.47E-04
0.55857	2.74E-04	1.53E-04
0.58286	2.73E-04	1.59E-04
0.60714	2.73E-04	1.65E-04
0.63143	2.71E-04	1.71E-04
0.65571	2.69E-04	1.76E-04
0.66015	2.68E-04	1.77E-04
0.68	2.64E-04	1.79E-04
0.68831	2.60E-04	1.79E-04
0.70429	2.53E-04	1.78E-04
0.70567	2.52E-04	1.78E-04
0.71483	2.44E-04	1.74E-04

0.72857	2.33E-04	1.70E-04
0.73236	2.27E-04	1.66E-04
0.73816	2.19E-04	1.62E-04
0.7449	2.11E-04	1.57E-04
0.7527	2.03E-04	1.53E-04
0.76043	1.87E-04	1.42E-04
0.76513	1.79E-04	1.37E-04
0.77053	1.70E-04	1.31E-04
0.77714	1.62E-04	1.26E-04
0.77975	1.54E-04	1.20E-04
0.78291	1.46E-04	1.14E-04
0.78652	1.38E-04	1.09E-04
0.79064	1.30E-04	1.03E-04
0.79531	1.22E-04	9.69E-05
0.80062	1.14E-04	9.10E-05
0.80143	1.12E-04	9.01E-05
0.80615	9.74E-05	7.85E-05
0.80917	8.93E-05	7.23E-05
0.8126	8.12E-05	6.60E-05
0.81647	7.31E-05	5.97E-05
0.82084	6.49E-05	5.33E-05
0.82571	5.69E-05	4.70E-05
0.82574	5.68E-05	4.69E-05
0.83037	4.06E-05	3.37E-05
0.83624	2.44E-05	2.04E-05
0.83974	1.62E-05	1.36E-05
0.84367	8.12E-06	6.85E-06
0.84808	0.00E+00	0.00E+00

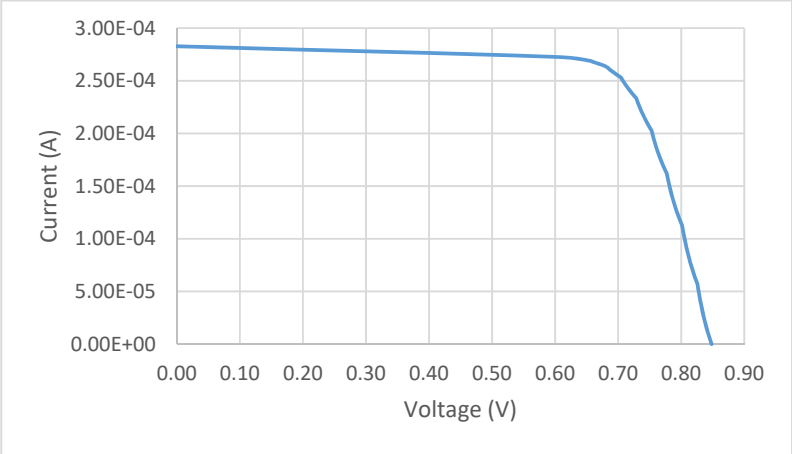

Figure 1: IV curve of solar cell with 1:1 blend ratio

Solar cell sample 2 (Blend ratio 2:1)

Voltage (V)	Current (A)	Power (W)
0.00E+00	3.47E-04	0.00E+00
3.13E-04	3.46E-04	1.08E-07
0.00259	3.36E-04	8.71E-07
0.00276	3.36E-04	9.26E-07
0.00518	3.26E-04	1.69E-06
0.0052	3.26E-04	1.69E-06
0.00764	3.16E-04	2.41E-06
0.00777	3.15E-04	2.45E-06
0.01009	3.06E-04	3.09E-06
0.01037	3.05E-04	3.16E-06
0.01254	2.96E-04	3.71E-06
0.01296	2.94E-04	3.82E-06
0.01499	2.86E-04	4.29E-06
0.01555	2.84E-04	4.42E-06
0.01745	2.76E-04	4.82E-06
0.01814	2.74E-04	4.96E-06
0.0199	2.67E-04	5.30E-06
0.02073	2.63E-04	5.46E-06
0.02236	2.57E-04	5.74E-06
0.02332	2.53E-04	5.90E-06
0.02483	2.47E-04	6.13E-06
0.02591	2.42E-04	6.28E-06
0.02729	2.37E-04	6.47E-06
0.0285	2.32E-04	6.61E-06
0.02976	2.27E-04	6.76E-06
0.0311	2.22E-04	6.90E-06
0.03224	2.17E-04	7.00E-06
0.03369	2.11E-04	7.12E-06
0.03472	2.07E-04	7.20E-06
0.03628	2.01E-04	7.30E-06
0.03721	1.97E-04	7.35E-06
0.03887	1.91E-04	7.42E-06
0.0397	1.88E-04	7.45E-06
0.04146	1.81E-04	7.49E-06
0.0422	1.78E-04	7.50E-06
0.04405	1.70E-04	7.51E-06
0.0447	1.68E-04	7.50E-06
0.04664	1.60E-04	7.47E-06
0.04721	1.58E-04	7.46E-06
0.04923	1.50E-04	7.39E-06

0.04974	1.48E-04	7.37E-06
0.05183	1.40E-04	7.25E-06
0.05227	1.38E-04	7.22E-06
0.05482	1.28E-04	7.04E-06
0.05701	1.20E-04	6.83E-06
0.0596	1.10E-04	6.55E-06
0.05995	1.09E-04	6.51E-06
0.06219	1.00E-04	6.22E-06
0.06478	9.02E-05	5.84E-06
0.06514	8.89E-05	5.79E-06
0.06777	7.90E-05	5.35E-06
0.06997	7.08E-05	4.95E-06
0.07042	6.91E-05	4.87E-06
0.07256	6.12E-05	4.44E-06
0.07515	5.17E-05	3.89E-06
0.07774	4.24E-05	3.29E-06
0.07855	3.95E-05	3.10E-06
0.08033	3.31E-05	2.66E-06
0.08134	2.96E-05	2.41E-06
0.08292	2.41E-05	1.99E-06
0.08417	1.97E-05	1.66E-06
0.08551	1.51E-05	1.29E-06
0.08706	9.87E-06	8.59E-07
0.0881	6.33E-06	5.58E-07
0.09001	0.00E+00	0.00E+00

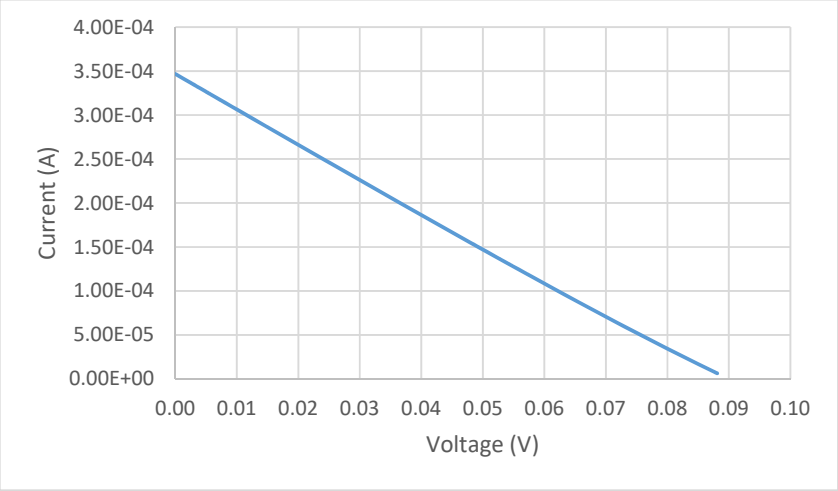

Figure 2: IV curve of solar cell with 2:1 blend ratio

Solar cell sample 3 (Blend ratio 3:1)

Voltage (V)	Current (A)	Power (W)
0.00E+00	5.23E-05	0.00E+00
4.02E-16	5.23E-05	2.11E-20
0.01305	5.19E-05	6.77E-07
0.02611	5.15E-05	1.34E-06
0.03916	5.10E-05	2.00E-06
0.05221	5.06E-05	2.64E-06
0.06527	5.02E-05	3.28E-06
0.07483	4.99E-05	3.73E-06
0.07832	4.98E-05	3.90E-06
0.09137	4.93E-05	4.51E-06
0.10443	4.89E-05	5.11E-06
0.11748	4.85E-05	5.70E-06
0.13053	4.81E-05	6.28E-06
0.14359	4.77E-05	6.84E-06
0.14964	4.75E-05	7.10E-06
0.15664	4.72E-05	7.40E-06
0.16969	4.68E-05	7.94E-06
0.18275	4.64E-05	8.48E-06
0.1958	4.60E-05	9.00E-06
0.20885	4.55E-05	9.51E-06
0.22191	4.51E-05	1.00E-05
0.22428	4.50E-05	1.01E-05
0.23496	4.47E-05	1.05E-05
0.24802	4.43E-05	1.10E-05
0.26107	4.38E-05	1.14E-05
0.27412	4.34E-05	1.19E-05
0.28718	4.29E-05	1.23E-05
0.29602	4.26E-05	1.26E-05
0.30023	4.25E-05	1.27E-05
0.31328	4.20E-05	1.31E-05
0.32634	4.14E-05	1.35E-05
0.33939	4.08E-05	1.38E-05
0.34883	4.02E-05	1.40E-05
0.35244	4.00E-05	1.41E-05
0.3655	3.89E-05	1.42E-05
0.37629	3.78E-05	1.42E-05
0.37855	3.75E-05	1.42E-05
0.3916	3.54E-05	1.39E-05
0.39199	3.53E-05	1.39E-05
0.40196	3.29E-05	1.32E-05

0.40466	3.23E-05	1.31E-05
0.40929	3.05E-05	1.25E-05
0.41564	2.81E-05	1.17E-05
0.41771	2.73E-05	1.14E-05
0.42038	2.56E-05	1.08E-05
0.42435	2.32E-05	9.85E-06
0.42832	2.08E-05	8.90E-06
0.43076	1.93E-05	8.31E-06
0.4317	1.84E-05	7.93E-06
0.43415	1.59E-05	6.92E-06
0.43659	1.35E-05	5.90E-06
0.43904	1.11E-05	4.87E-06
0.44149	8.67E-06	3.83E-06
0.44382	6.36E-06	2.82E-06
0.44389	6.24E-06	2.77E-06
0.44538	3.82E-06	1.70E-06
0.44688	1.40E-06	6.23E-07
0.44837	0.00E+00	0.00E+00

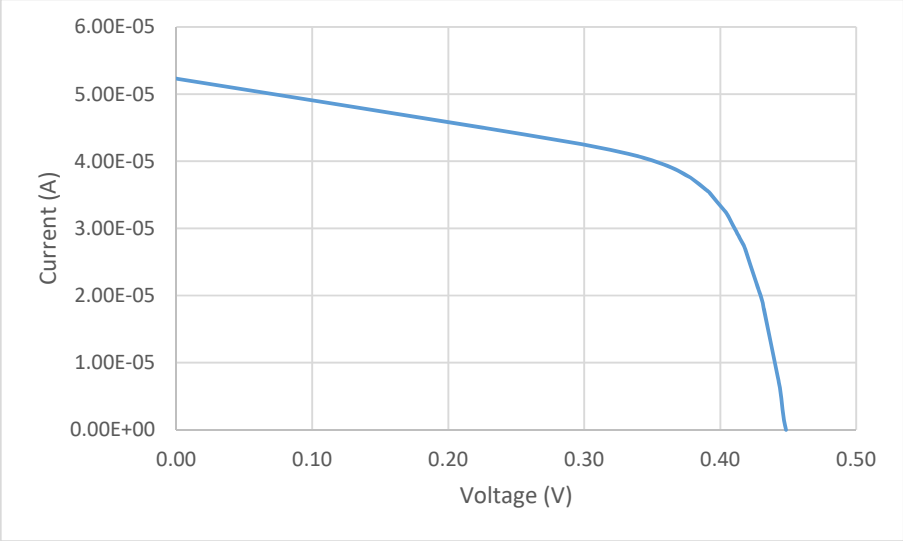

Figure 3: IV curve of solar cell with 3:1 blend ratio

Solar cell sample 4 (Blend ratio 1:2)

Voltage (V)	Current (A)	Power (W)
0	2.24E-06	0.00E+00
0.00778	2.22E-06	1.72E-08
0.01315	2.20E-06	2.89E-08
0.0263	2.15E-06	5.64E-08
0.03944	2.10E-06	8.27E-08
0.04466	2.08E-06	9.28E-08
0.05259	2.05E-06	1.08E-07
0.06574	2.00E-06	1.31E-07
0.07889	1.95E-06	1.53E-07
0.08041	1.94E-06	1.56E-07
0.09204	1.89E-06	1.74E-07
0.10519	1.84E-06	1.93E-07
0.11426	1.80E-06	2.06E-07
0.11833	1.78E-06	2.11E-07
0.13148	1.73E-06	2.27E-07
0.14463	1.67E-06	2.41E-07
0.14607	1.66E-06	2.43E-07
0.15778	1.61E-06	2.54E-07
0.17093	1.55E-06	2.64E-07
0.17536	1.53E-06	2.67E-07
0.18408	1.48E-06	2.73E-07
0.19722	1.41E-06	2.79E-07
0.2028	1.39E-06	2.81E-07
0.21037	1.35E-06	2.83E-07
0.22352	1.28E-06	2.85E-07
0.22868	1.25E-06	2.86E-07
0.23667	1.20E-06	2.85E-07
0.24982	1.13E-06	2.82E-07
0.25339	1.11E-06	2.81E-07
0.26297	1.05E-06	2.77E-07
0.27611	9.80E-07	2.71E-07
0.27735	9.73E-07	2.70E-07
0.28926	8.96E-07	2.59E-07
0.30022	8.35E-07	2.51E-07
0.30241	8.21E-07	2.48E-07
0.31556	7.35E-07	2.32E-07
0.32222	6.97E-07	2.24E-07
0.32871	6.54E-07	2.15E-07
0.34186	5.73E-07	1.96E-07
0.3443	5.58E-07	1.92E-07

0.355	4.84E-07	1.72E-07
0.36588	4.20E-07	1.54E-07
0.36815	4.05E-07	1.49E-07
0.3813	3.15E-07	1.20E-07
0.3867	2.82E-07	1.09E-07
0.39445	2.28E-07	8.98E-08
0.4076	1.48E-07	6.02E-08
0.40816	1.44E-07	5.89E-08
0.42075	5.23E-08	2.20E-08
0.42827	6.10E-09	2.61E-09
0.43389	0.00E+00	0.00E+00

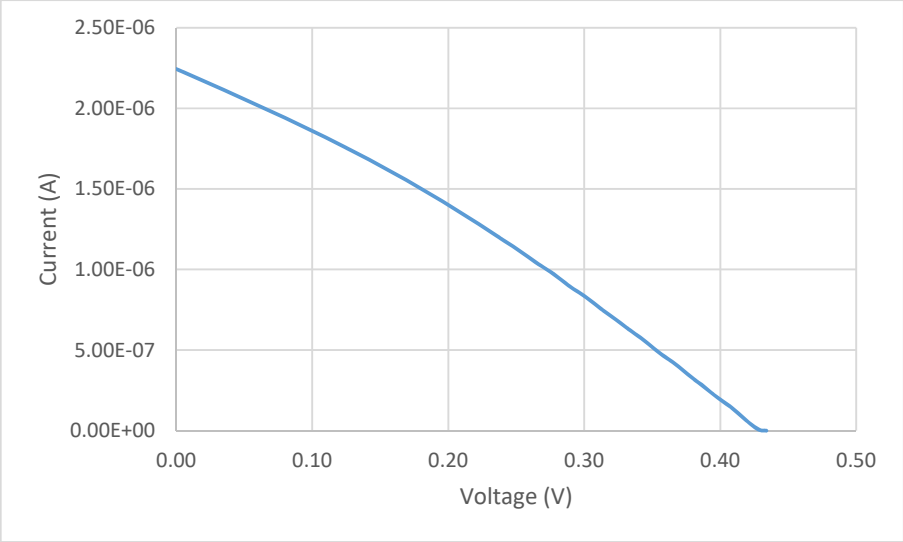

Figure 4: IV curve of solar cell with 1:2 blend ratio

Solar cell sample 5 (Blend ratio 1:3)

Voltage (V)	Current (A)	Power (W)
0.00E+00	3.46E-04	0.00E+00
0.00259	3.36E-04	8.71E-07
0.00276	3.36E-04	9.26E-07
0.00518	3.26E-04	1.69E-06
0.0052	3.26E-04	1.69E-06
0.00764	3.16E-04	2.41E-06
0.00777	3.15E-04	2.45E-06
0.01009	3.06E-04	3.09E-06
0.01037	3.05E-04	3.16E-06
0.01254	2.96E-04	3.71E-06
0.01296	2.94E-04	3.82E-06
0.01499	2.86E-04	4.29E-06
0.01555	2.84E-04	4.42E-06
0.01745	2.76E-04	4.82E-06
0.01814	2.74E-04	4.96E-06
0.0199	2.67E-04	5.30E-06
0.02073	2.63E-04	5.46E-06
0.02236	2.57E-04	5.74E-06
0.02332	2.53E-04	5.90E-06
0.02483	2.47E-04	6.13E-06
0.02591	2.42E-04	6.28E-06
0.02729	2.37E-04	6.47E-06
0.0285	2.32E-04	6.61E-06
0.02976	2.27E-04	6.76E-06
0.0311	2.22E-04	6.90E-06
0.03224	2.17E-04	7.00E-06
0.03369	2.11E-04	7.12E-06
0.03472	2.07E-04	7.20E-06
0.03628	2.01E-04	7.30E-06
0.03721	1.97E-04	7.35E-06
0.03887	1.91E-04	7.42E-06
0.0397	1.88E-04	7.45E-06
0.04146	1.81E-04	7.49E-06
0.0422	1.78E-04	7.50E-06
0.04405	1.70E-04	7.51E-06
0.0447	1.68E-04	7.50E-06
0.04664	1.60E-04	7.47E-06
0.04721	1.58E-04	7.46E-06
0.04923	1.50E-04	7.39E-06
0.04974	1.48E-04	7.37E-06

0.05227	1.38E-04	7.22E-06
0.05482	1.28E-04	7.04E-06
0.05737	1.18E-04	6.80E-06
0.0596	1.10E-04	6.55E-06
0.05995	1.09E-04	6.51E-06
0.06253	9.87E-05	6.17E-06
0.06478	9.02E-05	5.84E-06
0.06514	8.89E-05	5.79E-06
0.06997	7.08E-05	4.95E-06
0.07042	6.91E-05	4.87E-06
0.07256	6.12E-05	4.44E-06
0.07515	5.17E-05	3.89E-06
0.07581	4.94E-05	3.74E-06
0.07855	3.95E-05	3.10E-06
0.08033	3.31E-05	2.66E-06
0.08134	2.96E-05	2.41E-06
0.08292	2.41E-05	1.99E-06
0.08417	1.97E-05	1.66E-06
0.08551	1.51E-05	1.29E-06
0.08706	9.87E-06	8.59E-07
0.0881	6.33E-06	5.58E-07
0.09001	0.00E+00	0.00E+00

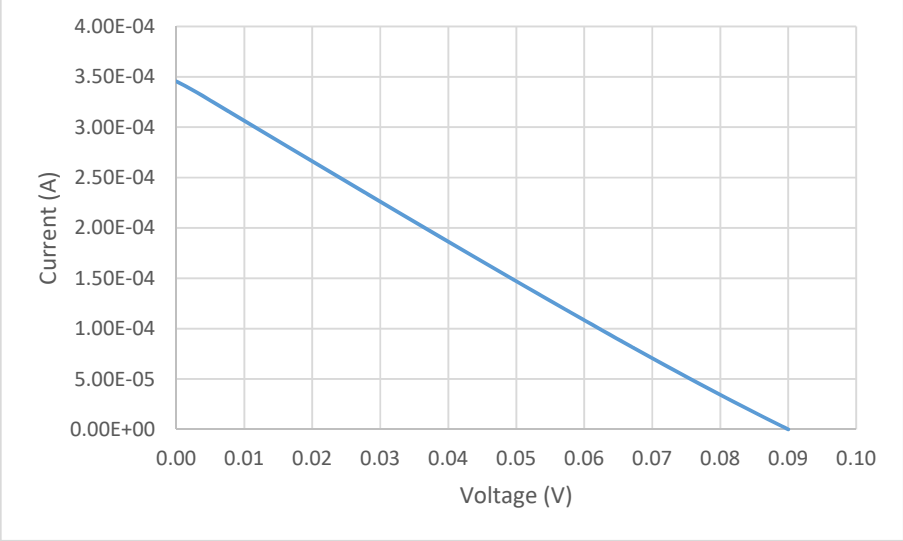

Figure 5: IV curve of solar cell with 1:3 blend ratio

Appendix B (Photos of the Practical Part of Thesis “Experiment”)

A. Spin coater building.

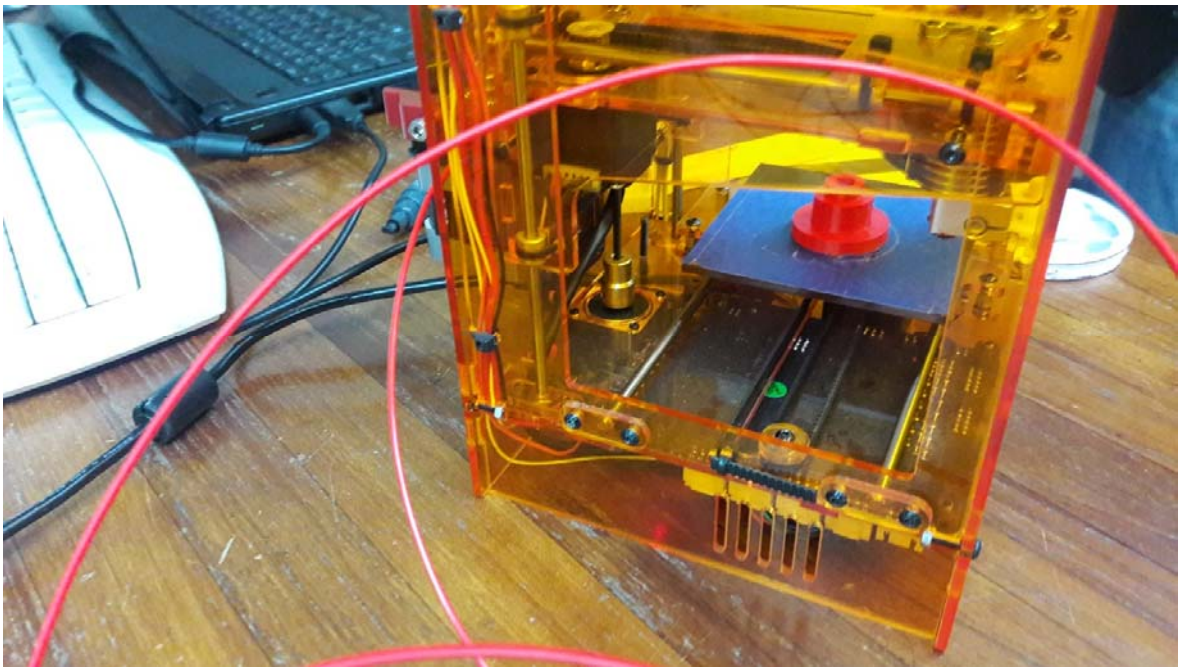

Figure A.1: Building spin coater using 3D printer

Figure A.2: The built spin coater

B. ITO cleaning.

Figure B.1: Etching ITO using Zn

Figure B.2: ITO washing

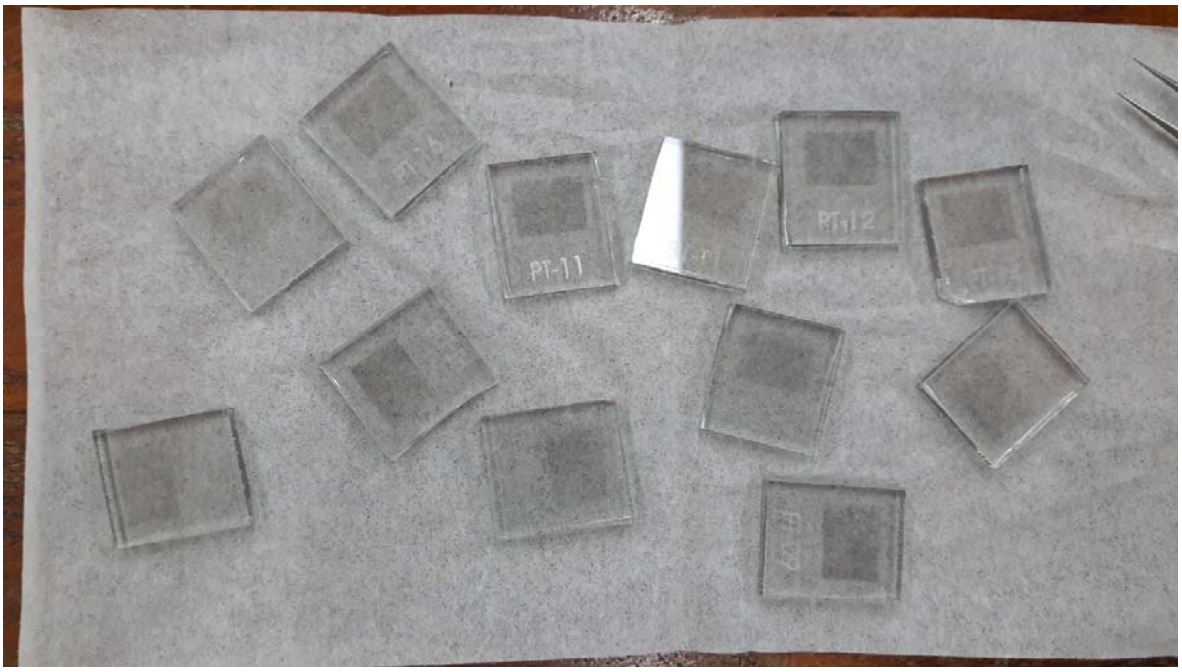

Figure B.3: ITO after cleaning

C. P3HT-ICBA.


Figure C.1: P3HT

Figure C.2: ICBA

Figure C.3: weighting P3HT and ICBA

D. (P3HT:ICBA) Blends.

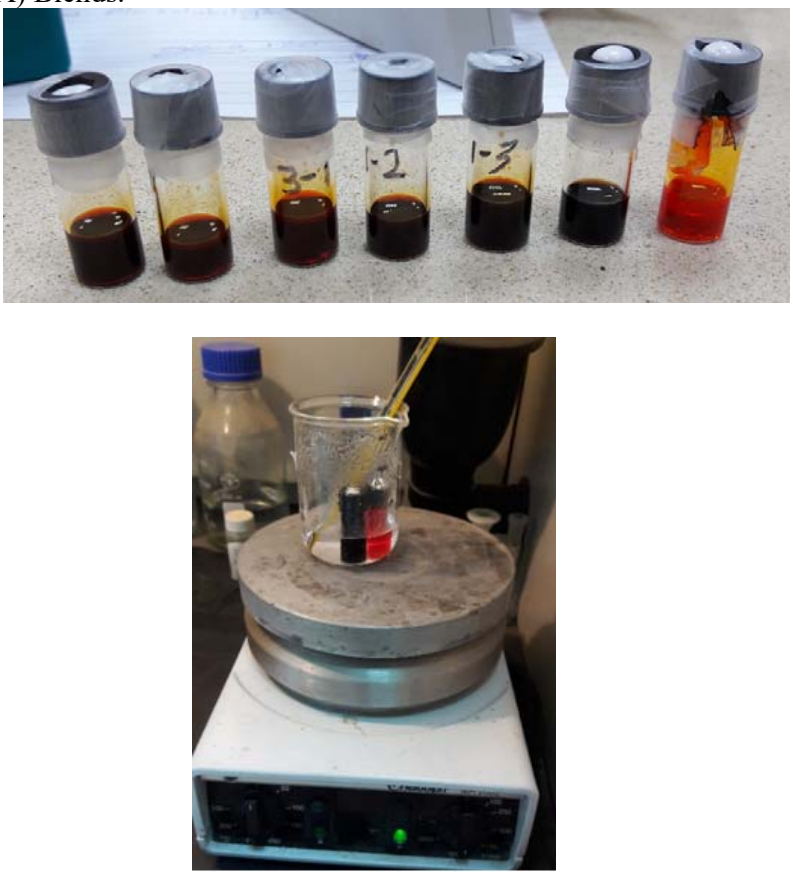

Figure D.1: Blends preparation

E. PEDOT:PSS.

Figure E.1: filtering PEDOT:PSS

F. ITO draying with N_2 and UV.

Figure F.1: Drying ITO

Figure F.1: ITO

G. First electrodes.

Figure G.1: side electrodes on ITO

H. Coating and annealing.

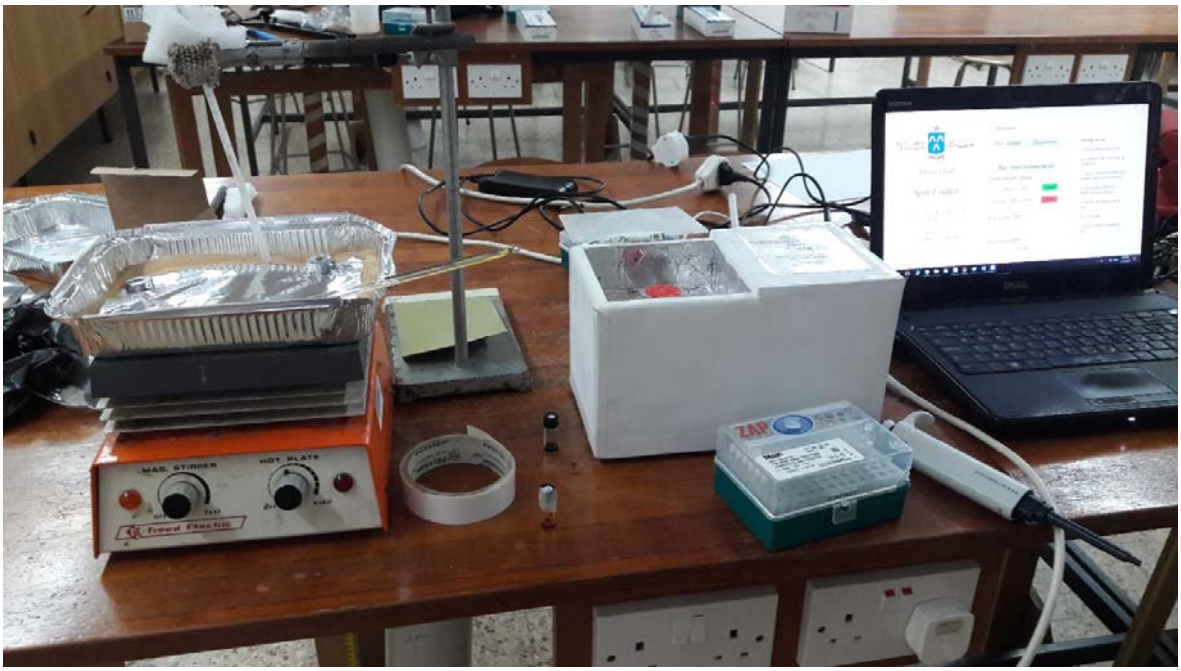

Figure H.1: Coating and annealing the active layer

Figure H.2: The active layer on ITO

I. Thermal vacuum evaporator.

Figure I.1: Evaporation the top electrode

J. Testing.


Figure J.1: Prepared OPV

Figure J.2: Testing OPV (IV test)

Appendix C (Nelder–Mead method)

Nelder-Mead simplex algorithm

The Nelder–Mead method or downhill simplex method or amoeba method is a commonly applied numerical method used to find the minimum or maximum of an objective function in a multidimensional space. It is applied to nonlinear optimization problems for which derivatives may not be known. However, the Nelder–Mead technique is a heuristic search method that can converge to non-stationary points on problems that can be solved by alternative methods.

The Nelder–Mead technique was proposed by John Nelder and Roger Mead (1965) as a development of the method of Spendley et al.

The method uses the concept of a simplex, which is a special polytope of $n + 1$ vertices in n dimensions. Examples of simplices include a line segment on a line, a triangle on a plane, a tetrahedron in three-dimensional space and so forth.

The method approximates a local optimum of a problem with n variables when the objective function varies smoothly and is unimodal. Typical implementations minimize functions, and we maximize $f(x)$ by minimizing $-f(x)$.

The Nelder–Mead method requires, in the original variant, no more than two evaluations per iteration except for the shrink operation, which is attractive compared to some other direct-search optimization methods. However, the overall number of iterations to proposed optimum may be high.

Nelder–Mead in n dimensions maintains a set of $n+1$ test points arranged as a simplex. It then extrapolates the behavior of the objective function measured at each test point, in order to find a new test point and to replace one of the old test points with the new one, and so the technique progresses. The simplest approach is to replace the worst point with a point reflected through the centroid of the remaining n points. If this point is better than the best current point, then we can try stretching exponentially out along this line. On the other hand, if this new point isn't

much better than the previous value, then we are stepping across a valley, so we shrink the simplex towards a better point. An intuitive explanation of the algorithm is presented in:

The downhill simplex method now takes a series of steps, most steps just moving the point of the simplex where the function is largest ("highest point") through the opposite face of the simplex to a lower point. These steps are called reflections, and they are constructed to conserve the volume of the simplex (and hence maintain its nondegeneracy). When it can do so, the method expands the simplex in one or another direction to take larger steps. When it reaches a "valley floor," the method contracts itself in the transverse direction and tries to ooze down the valley. If there is a situation where the simplex is trying to "pass through the eye of a needle," it contracts itself in all directions, pulling itself in around its lowest (best) point.

Unlike modern optimization methods, the Nelder–Mead heuristic can converge to a non-stationary point unless the problem satisfies stronger conditions than are necessary for modern methods. Modern improvements over the Nelder–Mead heuristic have been known since 1979.

Many variations exist depending on the actual nature of the problem being solved. A common variant uses a constant-size, small simplex that roughly follows the gradient direction (which gives steepest descent). Visualize a small triangle on an elevation map flip-flopping its way down a valley to a local bottom. This method is also known as the Flexible Polyhedron Method.

The approximates the procedure in the original Nelder-Mead paper

We are trying to minimize the function $f(x)$, where $x \in R$. Our current test points are $x_1, \ldots, x_{n+1}$.

1. Order according to the values at the vertices:

$f(x_1) \leq f(x_2) \leq \cdots \leq f(x_{n+1})$. Check if method should stop.

3. Calculate x_0 , the centroid of all points except x_{n+1}.

3. Reflection

Compute reflected point $x_r = x_0 + \alpha\ (x_0 - x_{n+1})$ with $\alpha > 0$.

If the reflected point is better than the second worst, but not better than the best, i.e.

$f(x_1) \leq f(x_r) \leq f(x_{n+1})$then obtain a new simplex by replacing the worst point x_{n+1} with the reflected point x_r, and go to step 1.

4. Expansion

If the reflected point is the best point so far, $f(x_r) < f(x_1)$,

then compute the expanded point $x_e = x_0 + \gamma\ (x_r - x_0)$ with $\gamma > 1$.

If the expanded point is better than the reflected point, , $f(x_e) < f(x_r)$,

then obtain a new simplex by replacing the worst point x_{n+1} with the expanded point x_e and go to step 1;

else obtain a new simplex by replacing the worst point x_{n+1} with the reflected point x_r and go to step 1.

5. Contraction

Here it is certain that $f(x_r) \geq f(x_n)$. (Note that x_n is second or "next" to highest.)

Compute contracted point $x_c = x_0 + \rho\ (x_{n+1} - x_0)$ with $0 < \rho \leq 0.5$.

If the contracted point is better than the worst point, i.e. $f(x_c) < f(x_{n+1})$,

then obtain a new simplex by replacing the worst point $x_{n+1}$with the contracted point x_c and go to step 1;

6. Shrink

Replace all points except the best (x_1) *with*

$x_i = x_1 + \sigma (x_i - x_1)$ and go to step 1.

Note: α , γ, ρ and σ are respectively the reflection, expansion, contraction and shrink coefficients. Standard values are $\alpha = 1$, $\gamma = 2$, $\rho = 1 / 2$ and $\sigma = 1 / 2$.

For the **reflection**, since x_{n+1} is the vertex with the higher associated value among the vertices, we can expect to find a lower value at the reflection of x_{n+1} in the opposite face formed by all vertices x_i except x_{n+1}.

For the **expansion**, if the reflection point x_r is the new minimum along the vertices, we can expect to find interesting values along the direction from x_0 to x_r.

Concerning the **contraction**, if $f(x_r) > f(x_n)$, we can expect that a better value will be inside the simplex formed by all the vertices x_i.

Finally, the **shrink** handles the rare case that contracting away from the largest point increases *f*, something that cannot happen sufficiently close to a non-singular minimum. In that case we contract towards the lowest point in the expectation of finding a simpler landscape. However, Nash [1] notes that finite-precision arithmetic can sometimes fail to actually shrink the simplex, and implemented a check that the size is actually reduced.

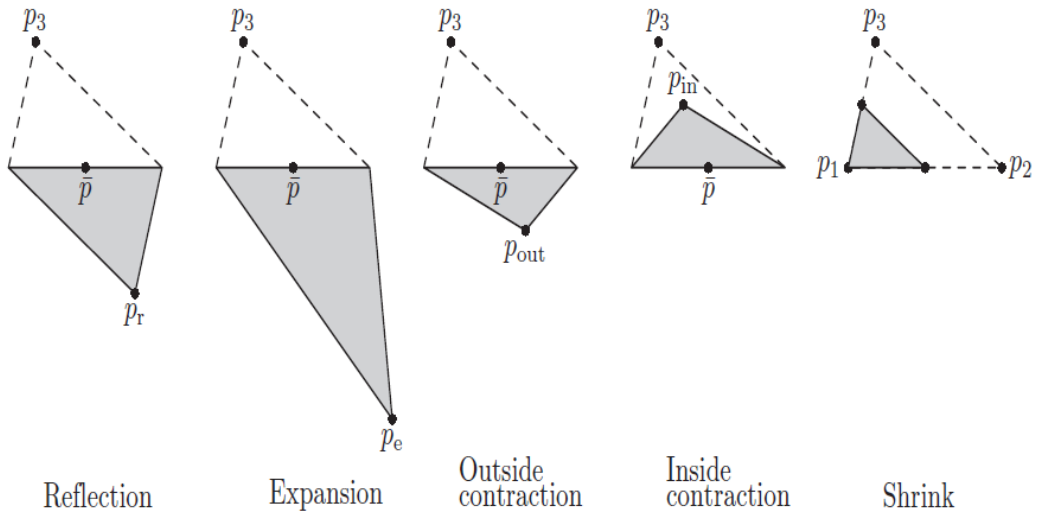

Figure 1: How Nelder–Mead method Initial simplex

Initial simplex

The initial simplex is important. Indeed, a too small initial simplex can lead to a local search, onsequently the NM can get more easily stuck. So this simplex should depend on the nature of the problem. However, the original paper suggested a simplex where an initial point is given as x_1 , with the others generated with a fixed step along each dimension in turn. Thus the method is sensitive to scaling of the variables that make up x.

Termination

Criteria are needed to break the iterative cycle. Nelder and Mead used the sample standard deviation of the function values of the current simplex. If these fall below some tolerance, then the cycle is stopped and the lowest point in the simplex returned as a proposed optimum. Note that a very "flat" function may have almost equal function values over a large domain, so that the solution will be sensitive to the tolerance. Nash adds the test for shrinkage as another termination criterion. Note that programs terminate, while iterations may converge.